LEBANESE AMERICAN UNIVERSITY

Effects of Deck Transverse Cracks on the Temperature Distribution in Composite Bridges

By

Omar Youssef El Masri

A thesis submitted in partial fulfillment of the requirements

For the degree of Master of Science in Civil and Environmental Engineering

School of Engineering

May 2014

LAU
الجامعة اللبنانية الأميركية
Lebanese American University

Lebanese American University

School of Engineering, Byblos Campus

THESIS APPROVAL FORM

Student Name: Omar El Masri I.D. #: 200702400

Thesis Title : Effects of Deck Transverse Cracks on the Temperature Distribution in Composite Bridges

Program: Civil Engineering

Department: Civil Engineering

School: Engineering

The undersigned certify that they have examined the final electronic copy of this thesis and approved it in Partial Fulfillment of the requirements for the degree of:

Master of Science in the major of Civil and Environmental Engineering

Thesis Advisor's Name Camille Issa Signature Signatures Redacted Date 5/6/2014

Co- Advisor Name Caesar Abi Shdid Signature Signatures Redacted Date 5/6/2014

Committee Member's Name Mazen Tabbara Signature Signatures Redacted Date 5/6/2014

THESIS COPYRIGHT RELEASE FORM

LEBANESE AMERICAN UNIVERSITY NON-EXCLUSIVE DISTRIBUTION LICENSE

By signing and submitting this license, you (the author(s) or copyright owner) grants to Lebanese American University (LAU) the non-exclusive right to reproduce, translate (as defined below), and/or distribute your submission (including the abstract) worldwide in print and electronic format and in any medium, including but not limited to audio or video. You agree that LAU may, without changing the content, translate the submission to any medium or format for the purpose of preservation. You also agree that LAU may keep more than one copy of this submission for purposes of security, backup and preservation. You represent that the submission is your original work, and that you have the right to grant the rights contained in this license. You also represent that your submission does not, to the best of your knowledge, infringe upon anyone's copyright. If the submission contains material for which you do not hold copyright, you represent that you have obtained the unrestricted permission of the copyright owner to grant LAU the rights required by this license, and that such third-party owned material is clearly identified and acknowledged within the text or content of the submission. IF THE SUBMISSION IS BASED UPON WORK THAT HAS BEEN SPONSORED OR SUPPORTED BY AN AGENCY OR ORGANIZATION OTHER THAN LAU, YOU REPRESENT THAT YOU HAVE FULFILLED ANY RIGHT OF REVIEW OR OTHER OBLIGATIONS REQUIRED BY SUCH CONTRACT OR AGREEMENT. LAU will clearly identify your name(s) as the author(s) or owner(s) of the submission, and will not make any alteration, other than as allowed by this license, to your submission.

Name: Omar El Masri

Signature:  Date: May 23, 2014

PLAGIARISM POLICY COMPLIANCE STATEMENT

I certify that I have read and understood LAU's Plagiarism Policy. I understand that failure to comply with this Policy can lead to academic and disciplinary actions against me.
This work is substantially my own, and to the extent that any part of this work is not my own I have indicated that by acknowledging its sources.

Name: Omar El Masri

Signature:  Date: May 23, 2014

Dedication

To my beloved family

ACKNOWLEDGMENTS

I wish to thank Dr. Caesar Abi Shdid, my thesis advisor, for his substantial efforts and continuous guidance throughout the course of this study. His dedication, commitment, and support made this work fruitful and possible. I would also wish to thank my co-advisor Dr. Camille Issa for his guidance and support throughout my undergraduate and graduate studies at LAU. Appreciation is also extended to my committee member, Dr. Mazen Tabbara, for his guidance during my studies at LAU.

Finally, I wish to express my gratitude, appreciation, and love to my parents and siblings. Their support, patience, and love made it possible to be here today. Special thanks go to my aunt who supported and encouraged me in every step I took. Her words and confidence in me kept me working.

Effects of Deck Transverse Cracks on the Temperature Distribution in Composite Bridges

Omar Youssef El Masri

Abstract

Thermally induced stresses in composite steel-concrete bridges are higher than those experienced by their concrete and steel cousins due to dissimilarity in material properties. These thermal stresses are relatively high when compared to service load stresses, leading to significant damage that manifest itself in terms of crack development in the concrete deck. This in turns leads to the corrosion of the steel reinforcement, steel superstructure, along with the deterioration of the concrete through water seepage. The various bridge design codes emphasize the importance of thermal stresses by providing designers with suggested thermal gradients that account for the temperature differential in bridges. However, previous studies have failed to account for the pre-existing construction transverse cracks in the concrete deck and their effect on the temperature distribution in composite bridges.

In this study, a three-dimensional finite element model was developed to investigate the temperature distribution in a selected case study bridge. The model is a realistic depiction of an existing bridge with pre-existing transverse deck cracks and actual environmental boundary conditions for a selected geographical region. The results of a thermo-elastic analysis show that the AASHTO LRFD Bridge Design Specification is overly conservative and overestimates the vertical temperature gradient for the studied bridge. The AASHTO and other models found in

existing literature seem to ignore the nonlinear thermal gradient for composite bridges, which produces a nonlinear strain component that can be critical for the bridge design and cannot be treated in a trivial manner. In addition, the pre-service deck transverse cracks appear to have a considerable effect on both, the vertical and the longitudinal temperature distributions in composite steel-concrete bridges, and hence require further assessment.

Keywords: Composite bridges, Thermal profile, Finite Elements, Numerical Analysis, Transverse deck cracking.

Table of Contents

List of Tables

List of Figures

Chapter One
Introduction

1.1 INTRODUCTION

Bridges are subjected to continuously changing diurnal environmental conditions that lead to continuous heat gain and lose with their surroundings. The thermal gradient that develops within a bridge cross section is affected by four basic heat transfer phenomena: a- convection at the surfaces, b- irradiation, c- solar radiation, and d- conduction within the bridge. While the solar radiation intensity has the highest effect on changing the bridge temperature, the thermal gradient is largely affected by the thermal diffusivity of the constituent materials which affects the rate of heat conduction within the bridge. It is the difference in this thermal diffusivity that makes the thermal stresses in composite steel-concrete bridges particularly high, due to the large temperature differential that exists in the thermal gradient of the bridge. Previous studies on the vertical temperature distribution in composite bridges have indicated a uniform temperature distribution in the steel girder and a linear temperature distribution in the concrete deck (Kennedy & Soliman, 1987).

The non-uniform temperature distribution within a bridge cross section leads to non-uniform thermal stresses. These stresses are known to be relatively high when compared to service load stresses, leading to considerable damage in the concrete deck. The major damage attributed to thermal stresses is developing deck cracks that lead to the corrosion of the steel reinforcement by allowing the water to seep into the concrete. However, and despite its importance, limited studies have been dedicated

to investigating the temperature distribution in composite bridges (Zuk, 1961; Imbsen et al., 1985; Fu, Ng, & Cheung, 1990).

Bridge design codes assert the importance of accounting for thermal stresses in bridge design by providing designers with proposed thermal gradients to use that describe the vertical temperature distribution in various types of bridges (AASHTO, 2012). However, previous studies—on which the proposed AASHTO gradient is based—have failed to take into account the effect of pre-existing concrete deck transverse construction cracks on the temperature distribution within the deck. These cracks are found to develop directly after the concrete deck casting and before the opening of the bridge for traffic (Ramey et al., 1997).

1.2 AIM AND OBJECTIVES

The aim of this study is to investigate the effect of air leakage through transverse deck cracks on the temperature distribution in composite steel-concrete bridges.

The following objectives should be met to achieve this aim:

- Conduct literature review on the existing thermal profiles, parameters affecting the thermal profile, and bridge deck cracking.
- Develop a three-dimensional numerical model based on Finite Element Analysis to accurately simulate the thermal behavior of composite bridges under different environmental conditions.
- Use the developed model to analyze the effect of transverse cracks on the temperature distribution in composite steel-concrete bridges.

- Assess current thermal profiles for accuracy of representation of actual conditions, and recommend whether the developed model will affect the stress distribution—and consequently the design—of composite bridges.

1.3 SIGNIFICANCE TO THE FIELD

Thermal stresses are significant when compared to service load stresses, particularly in composite steel-concrete bridges, and are therefore taken into account by bridge engineers during the design process. Current thermal profiles that are prescribed for composite bridges, and that result in such thermal stresses, take into account various geometrical and environmental factors, but fall short of considering cracks in the concrete deck. Such cracks develop early in the construction process and result in air leakage through the deck thus significantly affecting the thermal profile of the bridge. The significance of this study lies in developing a new, more accurate thermal profile for composite bridges that takes into account the effect of transverse cracks on the temperature distribution in composite bridges. Through a three-dimensional finite element model that models these pre-existing cracks in the concrete deck, this work will enhance the understanding of air leakage through the cracks and the overall thermal behavior of composite bridges.

1.4 ORGANIZATION OF THESIS

The thesis is divided into five chapters. After Chapter 1 (Introduction), Chapter 2 reviews the existing literature of studies that have been conducted on the thermal profile of composite bridges, parameters affecting the thermal profile, and bridge deck cracking. The methodology used in selecting the bridge location and calculating the various heat transfer components is provided in Chapter 3 along with a

description of the 3D finite element thermal model. In Chapter 4, the results of the FE model thermo-elastic analysis are presented, analyzed, and compared with previous thermal gradient models. Furthermore, the effects of the deck transverse cracks on the temperature distribution within the bridge are investigated. Finally, Chapter 5 draws conclusions on the main findings and provides recommendations for future studies.

Chapter Two
Review of the Literature

2.1 INTRODUCTION

Composite steel-concrete bridges experience thermal stresses higher than those experienced by their concrete or steel cousins due to dissimilarity in material properties (Fu, Ng, & Cheung, 1990). These thermal stresses are of higher magnitude when compared to live and dead load stresses, leading to significant damage that manifest itself in terms of crack development in the concrete deck. This in turn leads to the corrosion of the steel reinforcement, steel superstructure, along with the deterioration of the concrete through water seepage (Kennedy & Soliman, 1987). Despite its importance, few studies have been dedicated to composite steel-concrete bridges compared to a vast literature addressing temperature effects on concrete bridges (Giussani, 2009). Of these studies dedicated to composite bridges, all focused on either developing thermal profiles of typical two-dimensional cross sections, or studying the parameters affecting such profiles. However, none of these studies take into consideration the effect of the already existing cracks in the concrete deck, even though they are known to appear early during the construction phase of the bridge (Ramey et al., 1997).

This literature review addresses three areas related to thermal stresses in composite bridges. The first section addresses research related to the development of thermal profiles over a bridge cross section. The second section focuses on research studies that address the various parameters that affect the thermal profile in

composite bridges. Finally, the third section discusses research related to bridge deck cracking.

2.2 BODY OF THE REVIEW

2.2.1 Thermal Profile

Few researchers have studied the effect of thermal stresses on composite bridges. Analytical, numerical, and experimental investigations have led to the development of various thermal profiles that have been adopted by different codes around the world. Zuk (1961) developed theoretical equations to calculate the longitudinal and transverse stresses in composite bridges under different conditions of temperature and shrinkage. He also developed equations for the shears and moments at the surface interface between the slab and the supporting steel beams in order to demonstrate the effect of such stresses. These equations were developed for four (4) different cases of temperature distribution; however, a uniform temperature for the steel beam is adopted in all cases due to its high thermal conductivity and its ability to adjust its temperature quickly to that of the surrounding environment. It is good to note that in formulating the equations, Zuk assumed that the entire shear force is concentrated near the ends of the beam as shown in Figure 2-1.

Zuk's equations were applied to an actual bridge in Virginia, and the associated thermal stresses and deflections for the four different cases of temperature distribution were shown to be too large to ignore as shown in Figure 2-2.

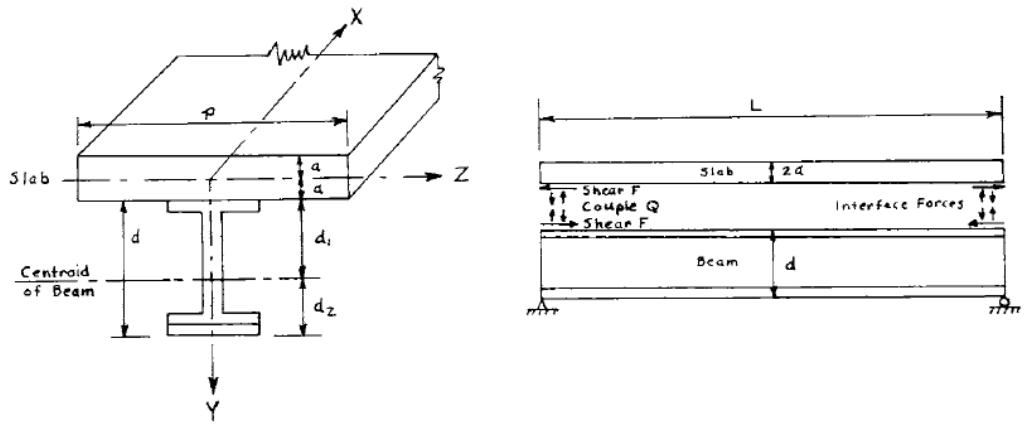

Figure 2-1 Composite beam (left); separated slab and beam with interface forces (right) (Zuk, 1961)

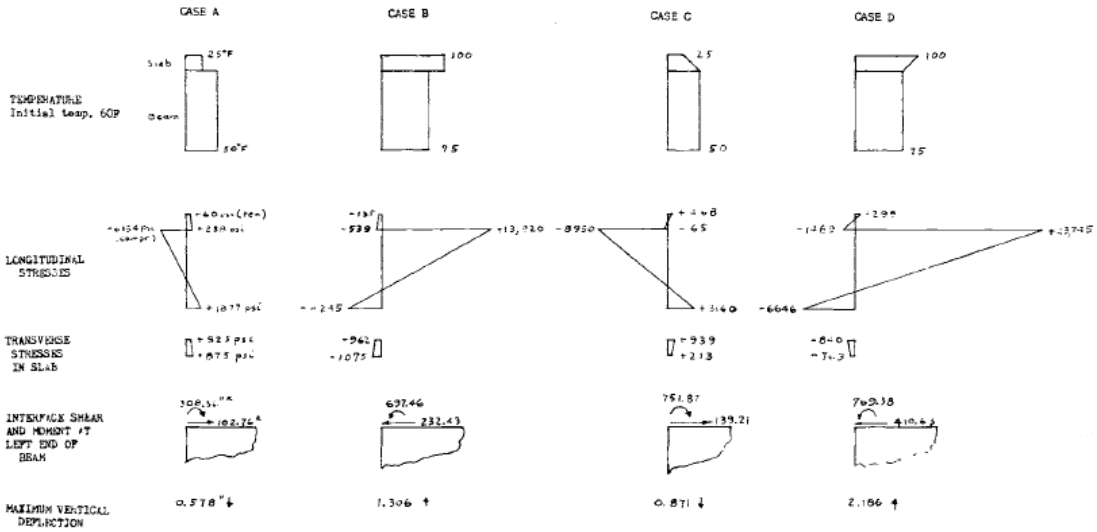

Figure 2-2 Comparative composite beam behavior (Zuk, 1961)

The study concluded that despite the fact that some of the high thermal stresses might be canceled by the application of service dead and live load stresses, they should not be discounted because of the presence of vibrating impact stresses that might be either positive or negative (Zuk, 1961).

In a later study, Berwanger (1983) developed through analytical and experimental investigations a numerical procedure that uses two-dimensional finite element analysis to precisely predict the transient temperature in the cross sections of composite bridges. A finite element thermo-elastic analysis was used to determine

the stresses and deformations that resulted from the effects of transient temperatures. The investigation consisted of cooling a model composite bridge by covering it with ice for 77 minutes. The air temperature gradually reduced from 25.8 ˚C to 22.1˚C, and then a finite element model was created to simulate the experimental conditions.

The predicted temperatures representing the temperatures measured in the bride model were verified through statistical analyses. Results showed a slower response for the concrete slab with a very rapid increase in thermal moments to reach a maximum value within 6 minutes; however, lower temperatures were reached in the steel beam. The study concluded that a linear temperature profile could be used satisfactorily to represent the temperature in the transverse cross section. The study also stresses that possible existing cracks in the concrete deck were ignored.

Thermal gradients used in developing the thermal profile in composite bridges differ from one code to another. Imbsen et al. (1985) evaluated and assessed the thermal effects on bridge superstructures based on different codes: New Zealand, England, Ontario, and those recommended by the Post Tensioning Institute (PTI). The study presented two case studies on actual bridges: the Columbia River Bridger (a cast-in-place pre-stressed segmental box girder), and the Miller Creek Bridge (precast, prestressed segments and box girder). The different thermal gradients used for the two case studies corresponding to the different codes are presented in Figure 2-3.

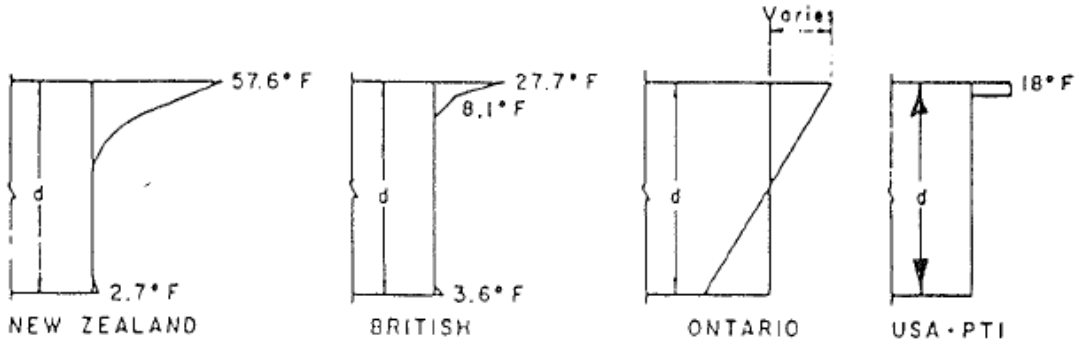

Figure 2-3 Thermal gradients used for case studies (Imbsen et al., 1985)

The study shows that thermal stresses do not initiate cracks in the concrete slab, but they do contribute to the cracking problem. It was also concluded that the stress pattern induced by thermal gradients are generally similar for different bridges but change in magnitude. Many of the findings and recommendations of this study were included in the following revision of the American Association for State Highway and Transportation Officials (AASHTO) code: Thermal Effects in Concrete Bridge Superstructures (1989) (Imbsen et al., 1985).

Other studies have led to various thermal profiles and vertical temperature distribution to be prescribed for composite bridges. Kennedy and Soliman (1987) synthesized the various theoretical and experimental studies that had been conducted on composite concrete slab on steel beam bridges. Based on their survey, they proposed a simple one dimensional vertical temperature distribution within the section of composite concrete deck slab on steel beam bridges. The distribution they proposed is uniform through the depth of the steel beam and is linear through the concrete deck as shown in Figure 2-4. This proposed distribution leads to simple formulation of thermal stresses in simple and continuous spans (Kennedy & Soliman, 1987).

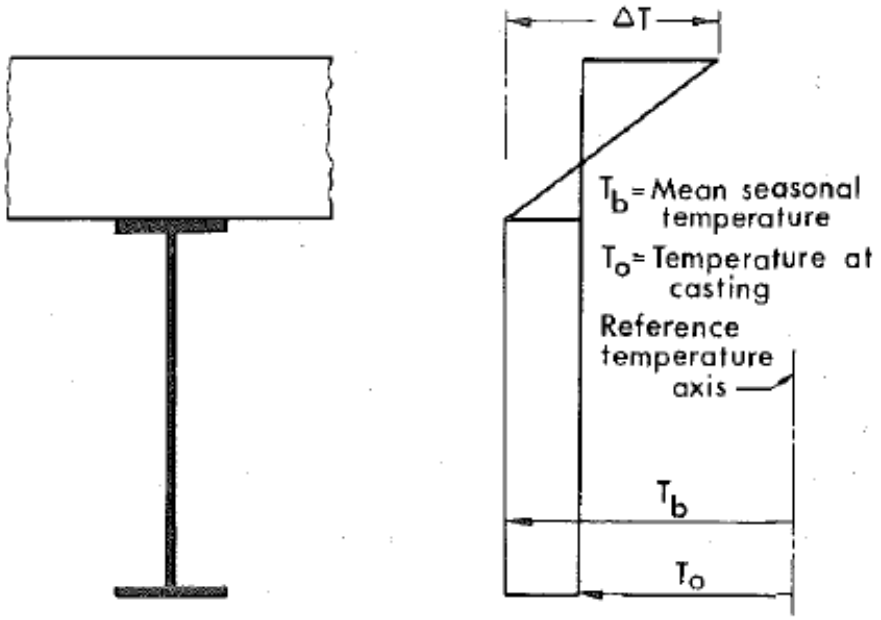

Figure 2-4 Proposed Linear-Uniform Vertical Temperature Distribution (Kennedy & Soliman, 1987)

A study by Fu, Ng, and Cheung (1990) concluded that a steady-state thermal condition never exists within a bridge structure, and that the time dependency of the ambient air temperature and solar radiation would dictate a transient analysis. A more recent thermal profile was proposed by Chen (2008) based on numerical analysis using two-dimensional finite element analysis (FEA). The proposed vertical temperature distributions for heating and cooling are shown in Figures 2-5 and 2-6.

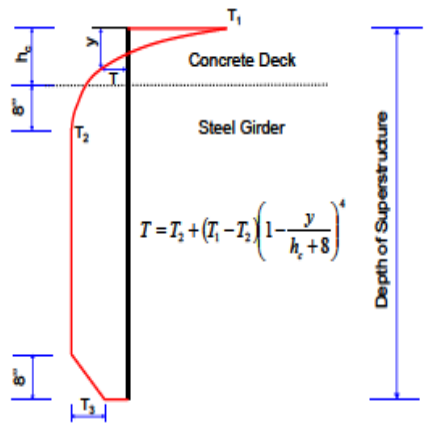

Figure 2-5 Vertical Temperature Distribution for Heating (Chen, 2008)

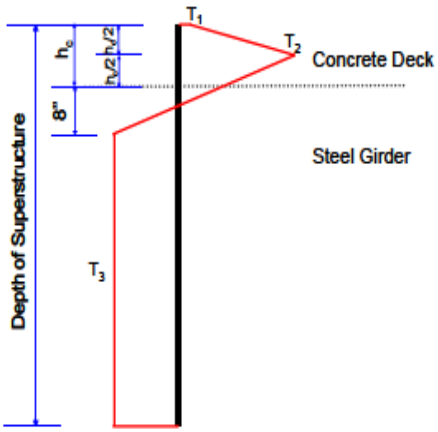

Figure 2-6 Vertical Temperature Distribution for Cooling (Chen, 2008)

2.2.2 Parameters Affecting the Thermal Profile

Thermal profiles of composite bridges are highly affected by the geometrical, material, and environmental parameters of the bridge cross section and its surrounding area. Dilger et al. (1983) performed parametric studies on composite box girder bridges in order to discover the effect of each parameter and the maximum temperature difference that can be reached between the concrete and the steel. The authors suggested the following conditions where the temperature difference is the highest:

1) Extreme variation in the ambient temperature
2) Winter and spring conditions
3) A dark surface of the steel box
4) Snow or ice cover on top of the bridge
5) High solar radiation intensity
6) A wind velocity of zero.
7) Small or negligible overhang cantilever
8) Large steel box.

The occurrence of all the previous conditions simultaneously at one site could lead to a temperature difference of as much as 70 ˚C between the concrete and the steel. Yet, many of these conditions can be reduced through for example panting the steel box with a bright color and extending the cantilever (Dilger et al., 1983).

Emanuel and Taylor (1985) conducted a computer-based study on composite bridges to investigate the relationship between uniform, linear, and non-linear components of thermally-induced stresses on the one hand and varying span lengths, number of spans, and support conditions on the other hand. The study concluded that

the three components of thermally induced stresses are independent of the span length. The study also found that even though the deflection induced by thermal loading was dependent on the span length, induced moments and stresses were not (Emanuel & Taylor, 1985).

Bridge decks with overhangs present a problem for predicting the daily temperature in a cross section due to the shading effect that they will have on the steel girders—an effect that will vary between geographical locations, and throughout the time of the day and the day of the year. To have a realistic vertical thermal profile within the bridge, one must therefore take into consideration the length of the cantilever, the characteristics of the shaded part, and the pattern of the shading due to the distinct positions that the sun occupies in the sky at various time intervals during the day/year. An analytical parametric study was conducted by Fu, Ng, and Cheung (1990) on composite bridges to find out the effects of shading. The study analyzed three different types of composite bridge structures while examining the effect of such variables as the slab overhang and convection coefficient. Various overhang to girder depth ratio were tested (0.25, 0.5, 0.75, and 1.0) while maintaining the same geographic and material properties. Other parameters that were tested included the variation in ambient air temperature, the solar radiation, and the heat transfer coefficient. The study also concluded the shading on the girders from the slab overhang to be the most influential factor on the vertical thermal distribution (Fu, Ng, & Cheung, 1990).

A different investigation confirmed the previous theoretical findings through temperature measurements on experimental bridge scaled models placed on the roof of a building as well as on an existing steel bridge in Hong Kong. The field study was conducted on a steel plate deck supported by two I-beam sections. The major

factors that affected the temperature distribution over the cross section were the solar radiations and the shade air temperature. However, temperature differences of only 2-3 ˚C occurred in the longitudinal or transverse directions, but they are negligible when compared with the temperature gradient across the depth, which is more than 15 ˚C on most summer days. The study concluded that a one-dimensional heat transfer model in bridges, on which most codes are based, was sufficiently accurate (Tong, Tham, & Au, 2002).

The most recent study done on the parameters affecting temperature variations in composite bridges was conducted in 2009. Giussani (2009) analytically investigated the effects of static loads, shrinkage, and thermal gradients on continuous and simply supported composite bridges using sectional and structural analysis. The concrete cracking that can be caused by diurnal and seasonal temperature was also included in the study. The author concluded that self-equilibrated stresses have to be added along with the ones induced by concrete shrinkage to the regular stresses obtained by dead and live loads, even in the case of simply supported beams. Additionally, stresses in the concrete slab in the service stage were recommended to be closely evaluated during the design since cracking due to tensile stresses might occur; however, the stresses in the steel beam at that stage were concluded to be insignificant (Giussani, 2009).

2.2.3 Bridge Deck Cracking

Cracks occur in concrete bridge decks in different forms: transverse cracks, longitudinal cracks, and map cracks. A crack is usually created when the stress in the concrete deck exceeds the allowable tensile strength of the concrete.

Transverse cracks are cracks that run perpendicular to the girders of the superstructure and earlier studies have found them to be the predominant form of cracking in the reinforced concrete bridge decks (Ramey et al., 1997; Ramey & Wright, 1994). The location of these cracks is in general at the top surface of the bridge deck or above the transverse reinforcements. Transverse cracks tend to be of full depth and occur at regular intervals of 3 to 10 feet apart along the bridge length (PCA 1970; Cheng & Johnston, 1985; Kosel & Michols, 1985), in both the positive and negative moment regions of the bridge (Krauss & Rogalla, 1996). The widths of the cracks have been reported in the range of 0.004 to 0.020 in. These cracks have been observed along the entire length of bridges with a steel superstructure, in both simple and continuous span construction. They have been also observed more in cases where stay-in-place steel forms were used instead of removable plywood forms. Ramey et al (1997) noted that transverse cracks occur early during the construction process typically after the casting of the concrete, and before the bridge has been placed in service.

Longitudinal cracks are cracks that run parallel to the girders of the superstructure. These cracks appear in different types of bridges above the longitudinal reinforcing steel on top of the bridge deck or above the edges of the girders in the superstructure. Curtis and White (2007) noted that the path of the longitudinal cracking usually follows the path of the steel girders. They also noted that these cracks are produced by the differential movements along the girders. These differential movements are believed to be created by the rotation of the girders about their longitudinal axis. Frosch (2007) found that longitudinal cracking occurs, in general, above the edge of the girders.

Pattern or map cracking, as the name implies, are random cracks and run in various directions. This is a common form of cracking and might occur in all types of concrete bridge decks. Map cracking might occur for several reasons; for instance, they might occur due to placing of wet concrete on dry precast concrete beams. They initiate at the bottom surface of the concrete deck, and then propagate in a vertical direction until they reach the top surface (Curtis & White, 2007).

2.3 SUMMARY

To ensure the service behavior of composite steel-concrete bridges, it is imperative to take into account the thermal stresses during the bridge design by accurately predicting the thermal profile within the bridge superstructure. Few researchers attempted to investigate the thermal behavior of composite steel-concrete bridges compared to the vast literature that exists on their concrete cousins. The research studies reviewed in this chapter suggest that the temperature distribution is uniform in the steel girder and linear in the concrete deck. Another area that was reviewed is the parameters affecting the thermal profiles in composite bridges. The major factors that have influence on the temperature distribution over the cross section are the deck overhangs and the solar radiations. Additionally, a review of the various types of cracks in bridge decks was presented.

Although in the existing research has suggested thermal profiles to be used for predicting the thermal stresses in composite bridges, the studies neglected the presence of cracks in the decks and their effect on the thermal profile, although such cracks are known to exist from an early construction stage. This current study will contribute to the existing research literature by studying the effect of air leakage

through transverse cracks on the temperature distribution in composite steel-concrete bridges.

Chapter Three
Methodology

3.1 INTRODUCTION

Composite steel-concrete bridges are exposed to high thermal stresses due to the large temperature differential that exists between the concrete deck and the steel girders. Limited studies have attempted to examine the effect of these stresses on the behavior of composite bridges. Among these studies, none has attempted to study the effect of air leakage through the pre-existing transverse deck cracks on the temperature distribution in composite slab-on-girder bridges.

In this Chapter, the various steps and methodology followed to build a Finite Element (FE) model capable of predicting the transient temperature profile in composite bridges is presented. These steps are described in detail in the following sections. They include the selection of an appropriate location for the bridge model, the selection on an existing composite bridge as a case study for the simulation, the determination and calculation of the different thermal variables acting on the bridge, and finally a description of the developed FE model.

3.2 MODEL LOCATION

The City of Fargo in North Dakota, with its extremely cold winters and very warm summers, has been selected as an appropriate location for this study. This particular choice is made because such extreme climate highlights the vast thermal differentials that can develop in composite bridges, as well as the stack effect of air leakage

through the deck cracks. The detailed information of the selected location is provided below.

- Location: The weather station located at Hector International Airport in Fargo, North Dakota (Figure 3-1)
- Latitude: 46˚, 52’, 38”.
- Longitude: 96˚, 47’, 22”.
- Elevation: 900 ft. above sea level.
- Weather: Long, cold, windy, and snowy winters and warm summers.
- Days chosen: the two days with the highest and lowest solar radiation intensities in 2010 that are: June 4 and December 23.
- Simulation duration: 24 hours for each selected day using actual weather conditions as explained in Section 3.6.5.
- Environmental conditions: Actual ambient temperature, wind speed, and solar radiation intensity for the two selected days.
- Bridge orientation: E-W direction.

Figure 3-1 Hector International Airport, Fargo, North Dakota

3.3 TIME DOMAIN

It should be noted that for any thermal stress calculations, two cases of temperature conditions have to be considered in order to estimate the critical stresses for design. The first case is in the summer when the deck is hotter than the steel beams, and the second case is in the winter. These thermal conditions have been shown to cause considerable longitudinal and transverse stresses in the composite bridge, and some of these stresses can exceed the ultimate tensile strength of the concrete (Kennedy & Soliman, 1987).

The time domain chosen for this study consists of two 24-hour time spans occurring over two separate days: one day in December (December 23), and one day in June (June 4). The selection was based on the lowest and highest radiation intensity days of the year, respectively, for Fargo, ND. It has been shown that the solar radiation has the highest influence on the thermal gradients in bridges (Tong, Tham, & Au, 2002).

3.4 BRIDGE PROPERTIES

3.4.1 Bridge Description

Colquits River Bridge has been selected as a case study for this this investigation due to its perfectly symmetrical cross section. The bridge, which is a part of Trans-Canada Highway, is located near Victoria in British Columbia, Canada. The bridge length is 270 ft. divided into five spans of varying lengths. The total deck width is 39 ft. distributed over six steel girders (W33x141) spaced at 6.5 ft. on center and supporting a 7.08 in. deep reinforced concrete deck. This bridge has undergone extensive experimental testing since 1992 in order to determine its dynamic

characteristics. The cross section of the bridge is shown in Figure 3-2, and the material properties that are used in the model are summarized in Table 3-1.

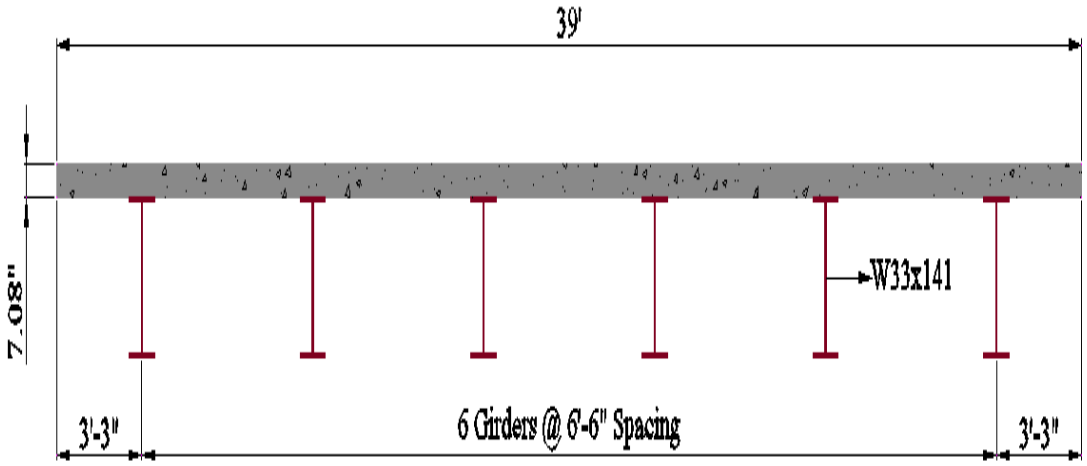

Figure 3- 2 Cross Section of Colquits River Bridge

Table 3- 1 Colquits River Bridge Material Properties

Bridge Component	Unit Weight (lb/ft^3)	Modulus of Elasticity (Ksi)	Poisson's Ratio	Grade	Compressive Strength (Ksi)
Concrete Deck	150	3834	0.2	NA	4
Steel Girders	490	29000	0.3	ASTM A992	NA

3.4.2 Bridge Model

Given the bridge cross-sectional symmetry with respect to the longitudinal axis, only a portion of the bridge cross section is needed to develop the thermal profile for the full cross section. A cross section that includes an exterior girder and one adjacent interior girder is used to develop the full three-dimensional (3D) FE model in order to minimize the computation time needed to run a transient simulation. The total width of this section including concrete deck overhang is 13 ft.

As was described in Chapter 2, post-construction and pre-service transverse cracks in concrete decks have been reported to have a minimum spacing of 3 ft. Hence, the bridge was modeled to start at the face of one crack, include two additional transverse cracks, and end at the face of the fourth transverse crack. The width of these cracks was modeled as observed experimentally to be 0.02 in., and to extend the full depth of the concrete deck over the entire cross section. The total length of the bridge model is thus 9 ft. Figure 3-3 shows a top view of the bridge model with magnified crack size for illustration purposes, while Figure 3-4 offers a 3D view of the modeled bridge in the commercial FE software package Abaqus®.

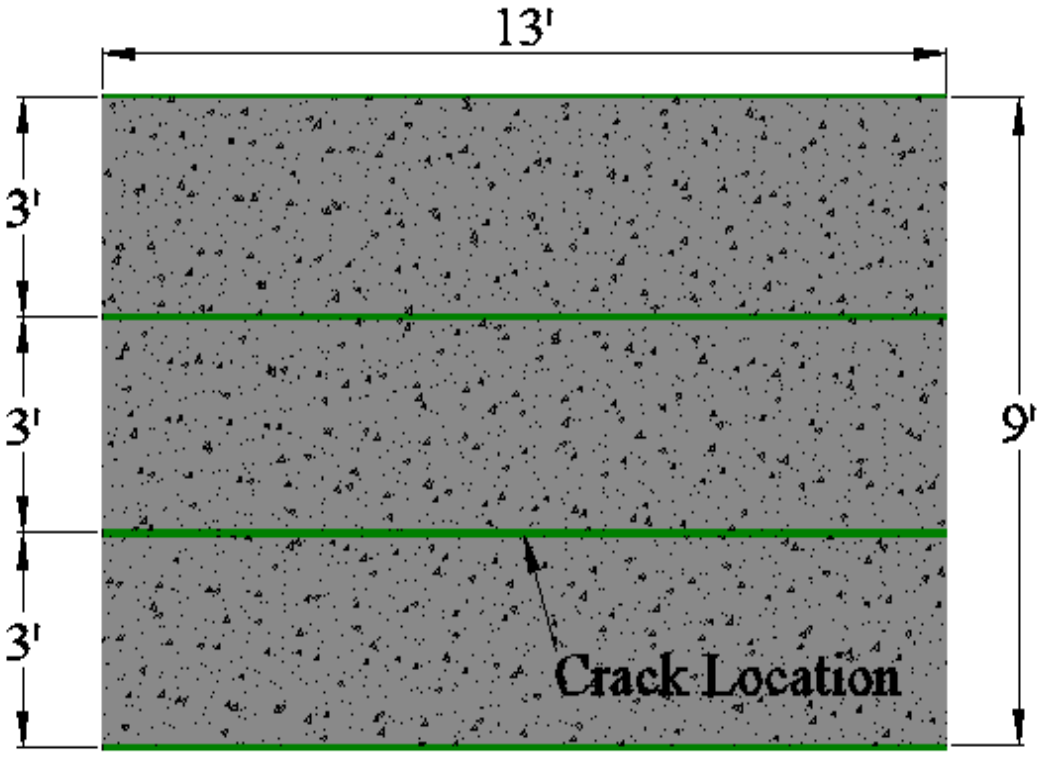

Figure 3-3 Top View of the Bridge Model

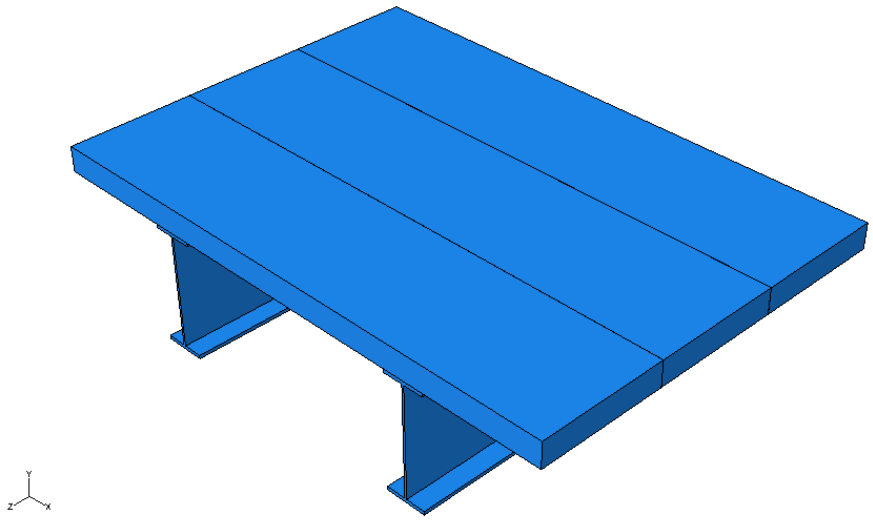

Figure 3-4 Developed 3D Bridge Model Using Abaqus

3.5 Environmental Variables and Heat Flow Conditions

Any bridge is exposed to various environmental conditions that lead to heat energy exchange between its surfaces and the surrounding. This exchange is the main culprit behind the unsteady thermal state within the bridge cross section. The different heat transfer components acting on the boundaries of a bridge are: conduction, convection, and solar radiation and irradiation. However, heat transfer at the exterior surfaces of the bridge is primarily due to radiation and convection, while the heat transfer by conduction can be neglected in comparison to these two (Noda et al., 2000). The various components of the heat transfer process are visually depicted in Figure 3-5.

3.5.1 Heat Transfer

The heat transfer at any arbitrary point within a bridge is governed by the nonlinear partial differential equation (PDE) shown in Equation 3-1.

$$\rho c \frac{\partial T}{\partial t} = K\left(\frac{\partial^2 T}{\partial x^2} + \frac{\partial^2 T}{\partial y^2} + \frac{\partial^2 T}{\partial z^2}\right) \quad (3\text{-}1)$$

Where K is the thermal conductivity, Btu/(h ft ˚F); ρ is the density, lb/ ft^3; c is the specific heat, Btu/(lb ˚F); t is the time, h; and T is the temperature at any selected point, ˚F.

3.5.2 Boundary Conditions

The boundary conditions shown in Figure 3-5 may be presented in terms of heat flux as shown in Equation 3-2.

$$q = q_c + q_r + q_s \tag{3-2}$$

Where q is rate of energy transfer, Btu/(h ft^2); q_c is the convection; q_r is the thermal irradiation, and q_s is the solar radiation.

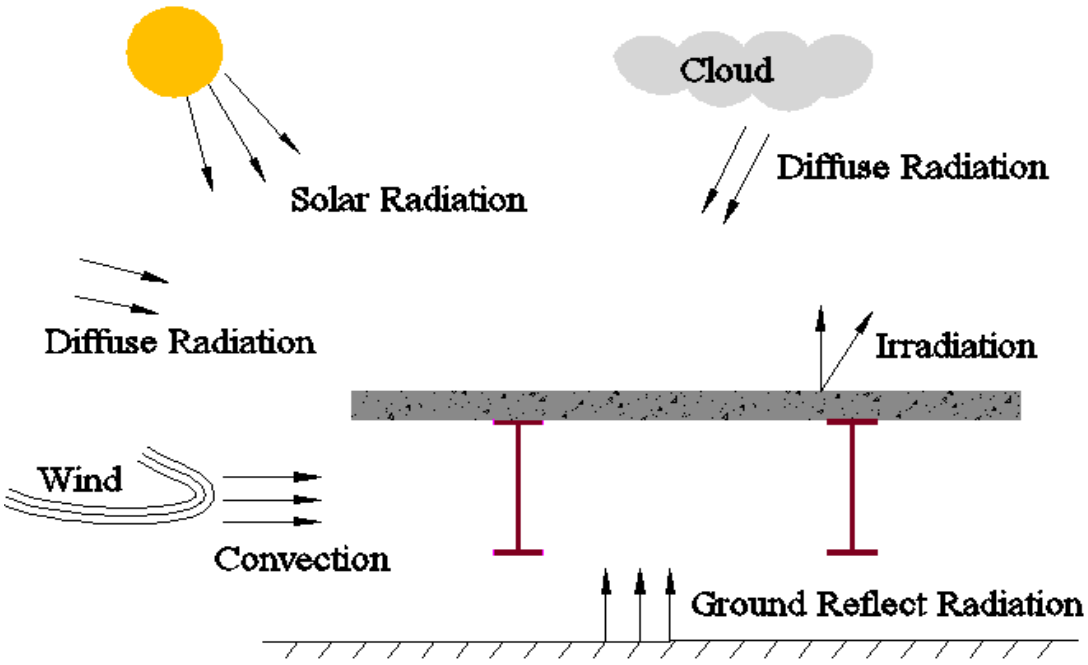

Figure 3-5 Heat Transfer Process in a Bridge Exposed to Environment

3.5.2.1 Convection

Convection is mainly the result of temperature difference between the bridge surfaces and the ambient temperature causing a gain or a loss of heat. The convection component of the heat flux equation, q_c, is calculated using Equation 3-3.

$$q_c = h_c(T - T_a) \tag{3-3}$$

Where h_c is the convection heat transfer coefficient, Btu/(h ft^2 ˚F); T is the temperature of the surface, ˚F; and T_a is the ambient temperature, ˚F.

The convective heat transfer coefficient is affected by various parameters such as the wind speed, surface roughness, and the geometrical configuration of the structure (Emanuel & Hulsey, 1978). It can be calculated using the empirical formula suggested by Ibrahim (1995) and shown in Equation 3-4.

$$h_c = \begin{cases} 4.67 + 3.83u & for\ top\ surfaces \\ 2.17 + 3.83u & for\ soffit\ surfaces \\ 3.67 + 3.83u & for\ steel\ webs\ and\ slab\ outer\ surfaces \end{cases} \tag{3-4}$$

Where u is the wind speed in m/s and h_c is in w/m^2.

The air temperature and the wind speed data for the two chosen days were obtained for the Hector International Airport in Fargo, ND from the National Climatic Data Center (NCDC, www.ncdc.noaa.gov).

3.5.2.2 Irradiation

Irradiation is caused by long wave radiation between the bridge surface and the surrounding atmosphere thus inducing a nonlinear boundary condition. The irradiation component in the heat flux equation, q_r, is calculated using Equation 3-5.

$$q_r = \varepsilon F(T^4 - T_a^4) \tag{3-5}$$

Where F is the Stefan-Boltzmann constant equals to 0.174x10^{-8} btu/(ft^2 hr ˚R^4); T is the temperature of the surface; T_a is the ambient temperature; and ε is the emissivity of the surface. The emissivity value for concrete and rusty steel and iron is reported by ASHRAE (1959) to be between 0.85 and 0.95.

3.5.2.3 Solar Radiation

Solar radiation is the energy received by the bridge surface through radiant energy emitted by the sun. The heat radiation component of the heat flux equation, q_s, is calculated using Equation 3-6.

$$q_s = aI_t \tag{3-6}$$

Where a is the absorptivity for solar radiation; and I_t is the total hourly solar radiation on a bridge surface, Btu/ft^2. The absorptivity value for concrete and rusty steel and iron is reported by ASHRAE (1959) to be between 0.65 and 0.80.

The hourly total solar radiation I_t on a bridge surface contains three components: beam radiation, diffused radiation, and ground-reflected radiation. Duffie and Beckman (1991) provided an expression to compute $I_t$as shown in Equation 3-7.

$$I_t = I_b \frac{\cos\theta}{\cos\theta_z} + I_d\left(\frac{1+\cos\beta}{2}\right) + I\rho\left(\frac{1-\cos\beta}{2}\right) \tag{3-7}$$

Where I_t is the total solar radiation; I_b is the beam solar radiation on a horizontal surface; I_d is the diffuse radiation on a horizontal surface; I is the total radiation on a horizontal surface ($I_b + I_d$); θ is the angle of incidence; θ_z is the zenith angle; β is the slope of the surface; ρ is the diffused ground reflection and is equal to 0.2.

The expression to determine $\cos\theta$ is shown in Equation3-8.

$$\begin{aligned}\cos\theta = {} & sin\delta \sin\emptyset \cos\beta - sin\delta \cos\emptyset \sin\beta \cos\gamma + \\ & \cos\delta \cos\emptyset \cos\beta \cos\omega + \cos\delta \sin\emptyset \sin\beta \cos\gamma \cos\omega + \\ & \cos\delta \sin\beta \sin\gamma \sin\omega\end{aligned} \tag{3-8}$$

Where $\emptyset$ is the surface latitude; δ is the declination; γ the surface azimuth angle; ω is hour angle.

The hourly solar radiation data at the selected location for the two chosen days, including the beam and diffused components I_b and I_d, were obtained from the National Renewable Energy Laboratory (NREL, www.nrel.gov). Tables 3-2 and 3-3 summarize the materials properties and the solar properties used in the computations respectively.

Table 3-2 Material Properties of the Bridge Model

Physical Properties	Concrete Deck	Steel Girders
Modulus of Elasticity (Ksi)	3834	29000
Unit Weight (lb/ft^3)	150	490
Specific Heat (BTU/lb.˚F)	0.23	0.122
Thermal Conductivity (BTU/hr.in.˚F)	0.0625	2.22
Solar Absorptivity	0.8	0.8
Emissivity	0.9	0.9

Table 3-3 Solar Properties

Symbol	Definition	Value	Comments
β	Slope	0˚	Horizontal Surfaces
		90˚	Vertical Surfaces
ρ	Diffuse Ground Reflection	0.2	
θ_z	Zenith Angle	Varies	Time Dependent
$\emptyset$	Latitute	46.925˚	
δ	Declination	22.47˚	June 4,2010
		-23.43˚	December 23,2010
γ	Surface Azimuth Angle	0˚	(E-W) orientation
ω	Hour Angle	Varies	Time Dependent
θ	Angle of Incidence	Varies	Time Dependent
γ_s	Sun Azimuth Angle	Varies	Time Dependent
θ_a	Solar altitude	Varies	Time Dependent

3.5.2.4 Shading Effect

As shown in Figure 3-6, the web of the exterior girder may be shaded by the concrete deck overhang. This shading can be partial, complete, or non-existent depending on the time of the day, the sun azimuth angle, and the solar altitude. When the web surface is shaded, the sun beams radiation does not reach its surface, but the diffuse radiation does not get affected.

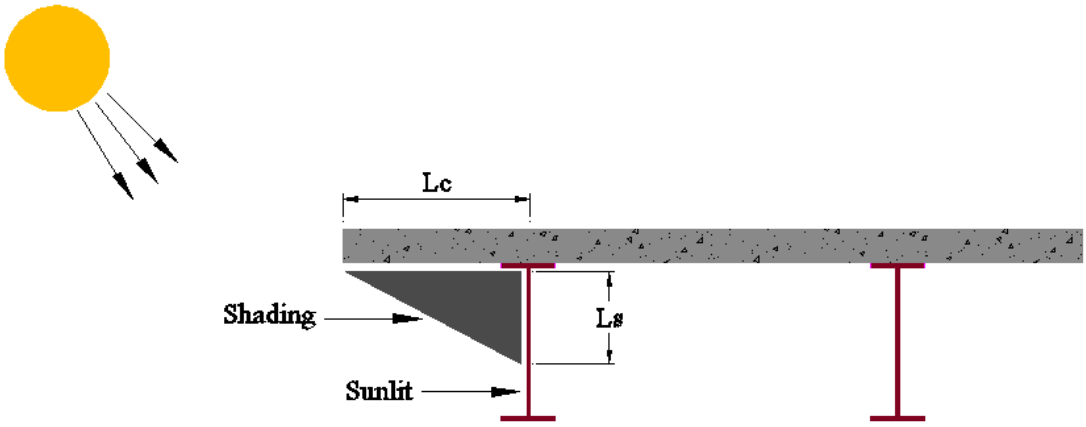

Figure 3-6 Shading Effect

The hourly height of the shade created by the deck overhang on the web of the exterior girder is given by the following expression (Elbadry and Ghali, 1983):

$$L_s = L_c \frac{\tan \theta_a}{\sin(90 + \gamma - \gamma_s) \sin \delta - \cos \beta \tan \theta_a} \quad (3\text{-}9)$$

Where L_c is the length of the overhang slab in inches; θ_a is the solar altitude angle in degrees; γ is the surface azimuth angle in degrees; γ_s is the sun azimuth angle in degrees.

The hourly solar altitude angle and sun azimuth angle were obtained from the National Renewable Energy Laboratory (NREL, www.nrel.gov) for the chosen bridge location and on the two selected days in June and Decemebr. This data was used in conjunction with Equation 3-9 to obtain the shading length on the web surface of the exterior steel girder.

3.6 FINITE ELEMENT MODEL OF THE BRIDGE

The commercial finite element software package Abaqus v.6.9 (Abaqus, 2009) was used to develop the 3D FE model for conducting the transient thermal analysis. The techniques used to create the model are described in this section.

3.6.1 Three Dimensional Model

Numerous studies are found in the literature that have conducted one- and two-dimensional finite element analyses to study the thermal behavior of composite bridges, assuming that the temperature remains constant along the length, and sometimes the transverse width, of the bridge (Fu et al., 1990; Moorty & Roeder, 1990). The 2D model is widely accepted as an accurate approach for conducting transient heat transfer simulation in composite bridges. However, such 1D and 2D models fall short of being able to model the thermal effect of transverse cracks that have been repeatedly reported to exist prior to the bridge being put into service. A 3D model is used in this study to better reflect the effect of the transverse cracks on the temperature distribution within the bride cross section.

The 3D FE model constructed included two girders—an exterior girder and an adjacent girder—and four transverse cracks as described in Section 3.4.2. The developed 3D model shown in Figure 3-7 has a total length of 9 ft. and total width of 13 ft. The material properties listed in Table 3-2 were used in modeling the mesh elements.

3.6.2 Element Types

Both the concrete deck and the steel girder were modeled using homogenous solid elements. For heat transfer analysis, DC3D8 element of Abaqus was assigned to all

sections. DC3D8 is a 3D 8-node linear hexahedral heat transfer mesh element with temperature as a single degree of freedom at each node (Abaqus, 2009).

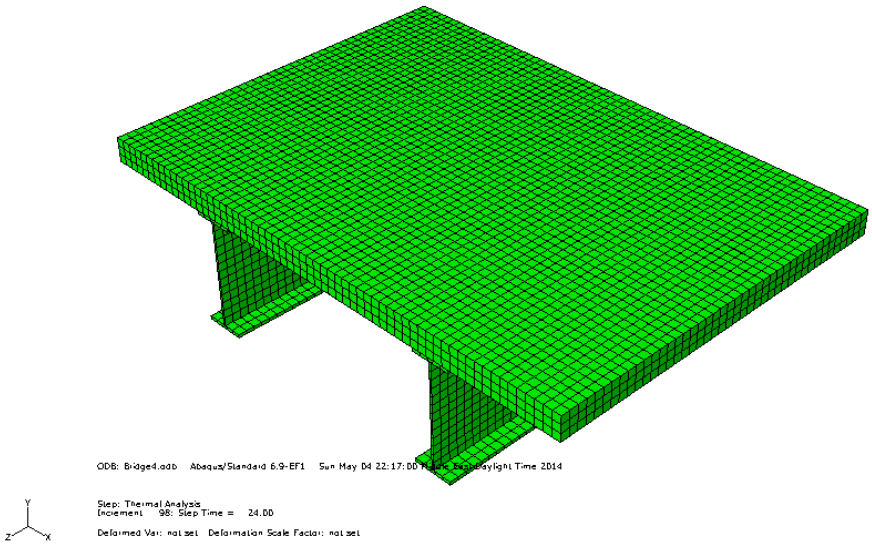

Figure 3-7 Three-Dimensional Abaqus Finite Element Model

3.6.3 Mesh Size

A good quality mesh is essential for obtaining a good solution and avoiding simulation errors. A mesh with poor element quality, high levels of element skewness, low orthogonality, and other issues adversely affects the accuracy and stability of the numerical solution.

In meshing the FE model, close attention is given to critical factors beside the regular general mesh quality considerations. Particularly important is the element size, especially within deck cracks in order to insure the meshing of all airflow paths. Proper contact between the fluid in the cracks and the inner crack surfaces is also essential to the accuracy of the solution. Proper tessellation of the mesh to avoid having a missing mesh or mesh gaps in thin sections. This is most critical in corner joints between the deck and the girders.

In order to determine whether the number of mesh elements in the model is sufficiently large to obtain accurate results, the mesh was refined until no significant difference in the simulation results ~~was~~ could be observed. The concrete deck was first divided vertically into ~~eight~~ three elements having a size ~~0.89~~2.36 inches and then refined into ~~three~~ eight elements having a size of ~~2.36~~0.89 inches for comparison purposes. If no significant difference between the analysis results is obtained, then the larger mesh can be adequate for the model. The 3D FE model for the 2.36 inches elements contains a total of 16,092 nodes with associated 10,318 mesh elements as illustrated in Figure 3-8.

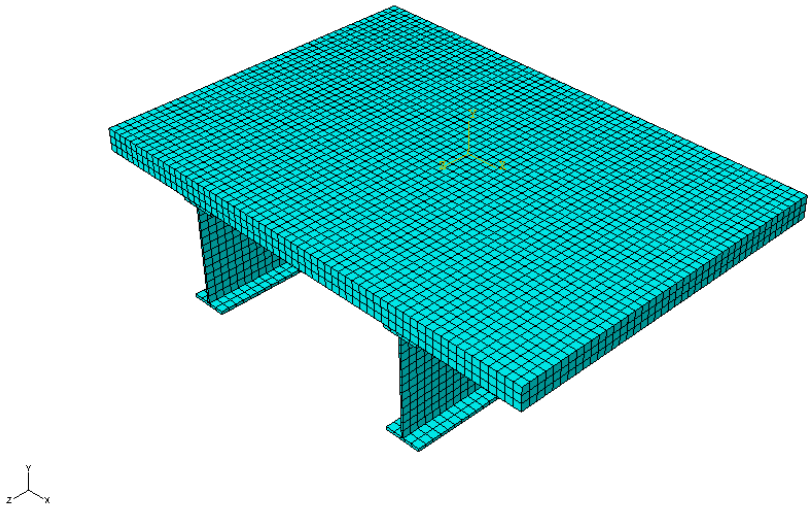

Figure 3-8 Meshed 3D FE Model (2.36 inches concrete deck elements)

3.6.4 Crack Modeling

The transverse cracks in the concrete deck are modeled as open fluid space in the concrete deck. As previously shown in Chapter 2, existing literature suggest that transverse cracks tend to penetrate the full depth of the bridge deck, with a typical spacing of 3 feet and maximum width of 0.02 inches. The 9 ft. bridge section was therefore modeled with the concrete deck forming three solid elements of 3 feet length each with a fluid separation of 0.02 in between each element.

To account for the effect of cracks on the temperature of the concrete deck and the air leakage inside the cracks due to the stack effect, convection and surface irradiation interaction properties were assigned to the two surfaces of the crack. Heat transfer is also allowed between the two crack surfaces through the material conduction properties. Solar radiation was not accounted for on the crack surfaces due its small width and the inability of the radiations to reach such surfaces as shading is provided by the adjacent surface.

3.6.5 Time Step

Transient heat transfer analysis is time dependent. The total simulation time domain spanned over two separate 24-hours durations that represent two full days that start at 0:00 and end at 24:00. A time step of 1 hour was used given that little change of temperature and radiation will occur within one hour. Additionally, the ambient temperature and the wind speed obtained from the National Climatic Data Center (NCDC, www.ncdc.noaa.gov) are provided on an hourly basis. Each time step was divided into 4 increments to account for the transition of temperature between the time steps.

Previous studies have indicated that initial temperature appears to have very little effect on the temperature difference within a bridge deck (Emanuel & Taylor, 1985; Fu, Ng, & Cheung, 1990). Given this fact, no temperature was assigned to the model at time step 0; this means that the model temperature was initially set to zero.

3.6.6 Interactions

To ensure a full composite action between the concrete deck and the steel girders, a "Tie" interaction was used at the contact surface between the two components. This approach ensures a hard pressure overclosure between the two surfaces (Abaqus,

2009) and hence permits the heat to transfer through conduction. This property was used by Klein (2006) and provided effective results.

Surface irradiation to the surrounding fluid was modeled as a time dependent surface property covering the whole model with uniform emissivity distribution and hourly ambient temperature data. The absolute zero temperature, the temperature at which a thermodynamic system has the lowest energy, was set to -459.67 ˚F corresponding to the zero Rankine temperature.

Three different sets of convection heat fluxes were calculated and implemented on the FE model. The three components are for the top surfaces, soffit surfaces, and side surfaces—including the cracks' surfaces as explained in sections 3.5.2.1 and 3.6.4. The calculated and implemented convection data is provided in Appendix A.

3.6.7 Loads

The only load applied to the bridge in a heat transfer analysis is a surface heat flux simulating the solar radiations on the various surfaces of the bridge. The calculated solar intensities, in accordance with Sections 3.5.2.3 and 3.5.2.4, are divided into four heat flux components: 1- on the top surface of the concrete deck, 2- on the bottom surfaces of the concrete deck and the steel girders, 3- on the surfaces of the interior web and the inner surface of the exterior web, and 4- on the outer surface of the exterior web. These thermal loads are implemented in the FE model as time step dependent. Appendix A provides the calculated solar radiations for each component for the two selected days.

3.6 SUMMARY

The methodology used in this study was presented, including the chosen location of the model and the selected bridge section and properties. Also presented were the various heat transfer phenomena occurring within the bridge model or acting as boundary conditions. These included conduction, convection, solar radiation, and surface irradiation. Finally, the techniques used to build an accurate 3D FE model of the bridge were presented, including the transverse deck cracks and steel-concrete composite action.

Chapter Four
Analysis of Results

4.1 INTRODUCTION

Thermal stresses in composites bridges are relatively high when compared to service load stresses. Such thermal stresses are known to cause various types of damage in bridges such as magnifying the development of concrete deck cracks which leads to the corrosion of the steel reinforcements and the steel girders. The various bridge design codes emphasize this importance by providing designers with provisions to follow that account for the differential temperature distribution in bridges. However, previous studies have failed to account for the existence of construction transverse cracks and their effect on the thermal profile of composite bridges.

This chapter presents the results of a 3D finite element model simulation that investigates the temperature distribution in a selected case study bridge by including the pre-service transverse deck cracks and actual environmental boundary conditions. Discussion will include analysis of the results; studying the temperature distribution in the bridge and comparing it to the AASHTO provisions; analyzing the effect of the transverse cracks on temperature distribution within the bridge; and drawing preliminary conclusions.

4.2 THERMAL ANALYSIS SIMULATION

4.2.1 Advantages of the Used FE Model

The 3D FE model developed in this study has numerous advantages over similar models that have been used in other studies available in the literature. The first advantage lies in the approach adopted in selecting the two days for the simulation as the ones with the highest and lowest solar radiation intensities, given that solar radiation has been shown to have the highest influence on the thermal profile (Tong, Tham, & Au, 2002). Previous studies assumed that the two days for the simulation that represent the extreme thermal cases of the year are those with the highest and lowest ambient temperature, where these temperatures were calculated based on existing empirical expressions (Emanuel & Taylor, 1985). The second advantage of the FE model used in this study lies in the fact that actual ambient temperature and wind speed data for the actual location of the case study bridge, as shown in Figures 4-1 and 4-2, were used and implemented in the FE model; rather than data calculated using empirical equations.

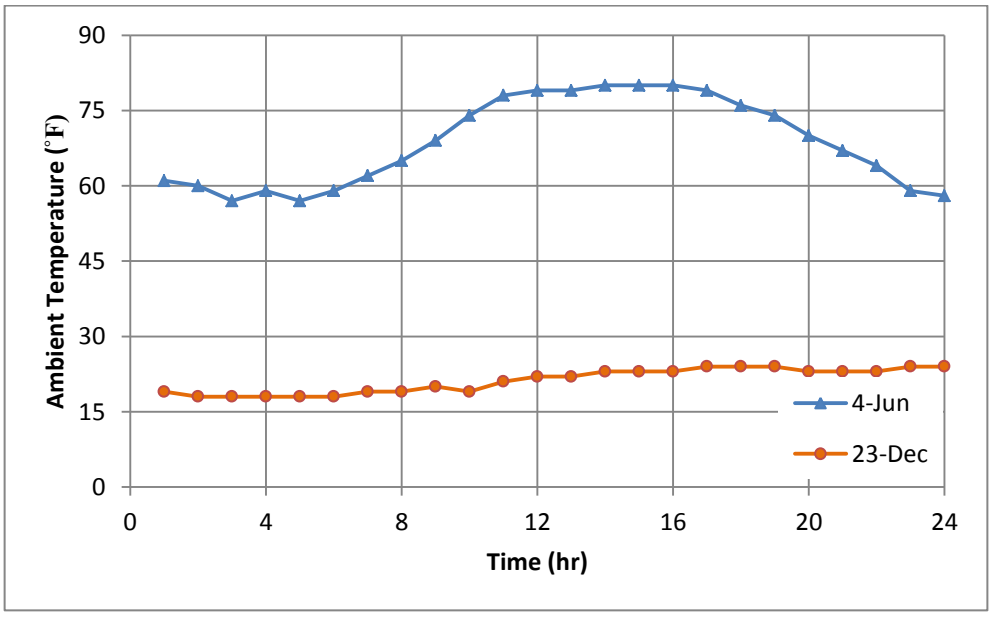

Figure 4-1 Hourly Ambient Temperature

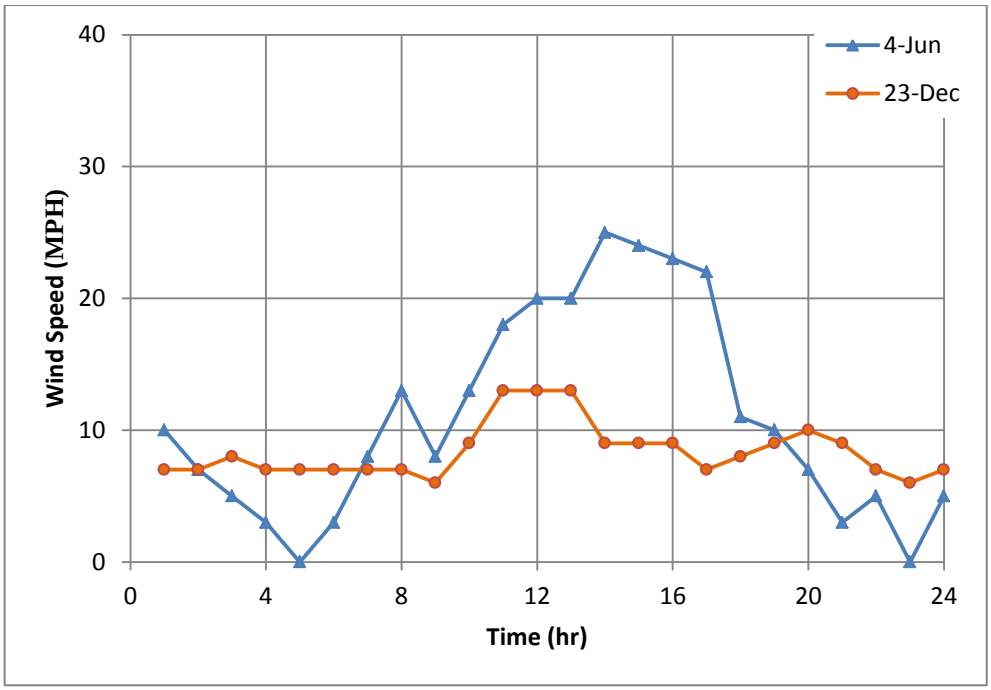

Figure 4-2 Hourly Wind Speed

Previous studies conducted on the thermal behavior of composite bridges have used an average assumed solar constant to compute an average solar radiation value on the bridge surfaces (Dilger et al., 1983; Fu, Ng, & Cheung, 1990). The third advantage of the FE model used in this study thus lies in the methodology adopted in obtaining actual solar radiation for the specific location of the case study bridge and distributing it on each surface of the bridge section as discussed in Sections 3.5.2.3 and 3.6.7. Such actual measured data takes into account the actual altitude of the bridge above the sea level, and how that affects the solar angles.

The fourth advantage of the FE model used in this study lies in its realistic depiction of: an existing bridge layout, an actual chosen geographic location, and most importantly the inclusion of actual construction deck transverse cracks.

4.2.2 Mesh ~~Comparison~~Size Sensitivity Analysis

As discussed in Section 3.6.3, a sensitivity analysis ~~has been~~was conducted in order to determine the effect of the mesh size on the temperature profile obtained within

the bridge. The results obtained from the model with a mesh size of 0.89 inches, as shown in Figure 4-3, were compared to those obtained from the model with a mesh size of 2.39 inches. The difference in the temperature between the two models did not exceed 1˚F at any point within the bridge and at any time throughout the two simulated days. It is therefore concluded that dividing the concrete deck vertically into three elements is sufficient enough to produce accurate temperature results.

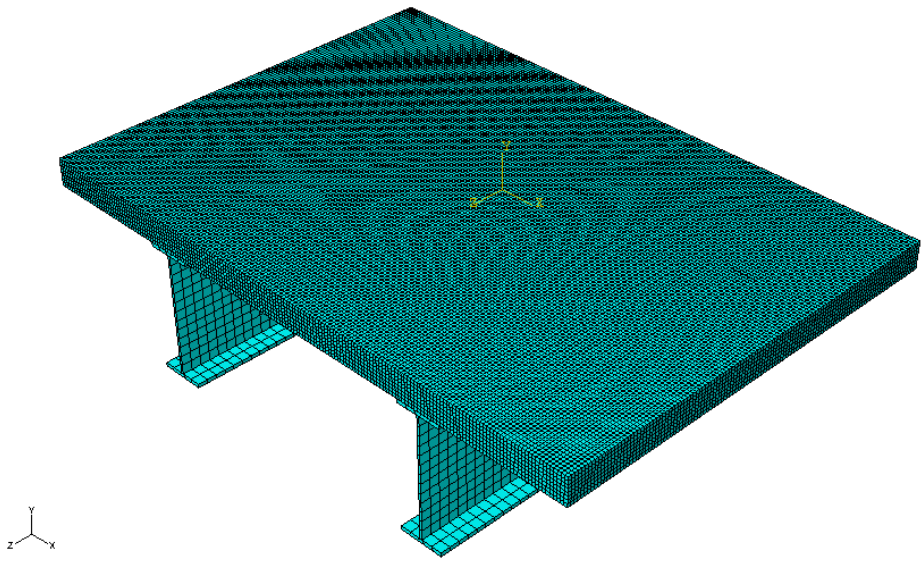

Figure 4-3 Meshed 3D FE Model (0.89 inches concrete deck elements)

4.2.3 Finite Element Model Results

Transient heat analysis is time dependent; therefore, the temperature for each node within the FE model of the bridge was updated at each time step, and a thermo-elastic analysis was conducted. The 3D FE model makes it easier to visualize the distribution of temperature in the bridge, as can be seen from Figure 4-4, and subsequently analyzing the effect of the concrete deck transverse cracks on the temperature profile.

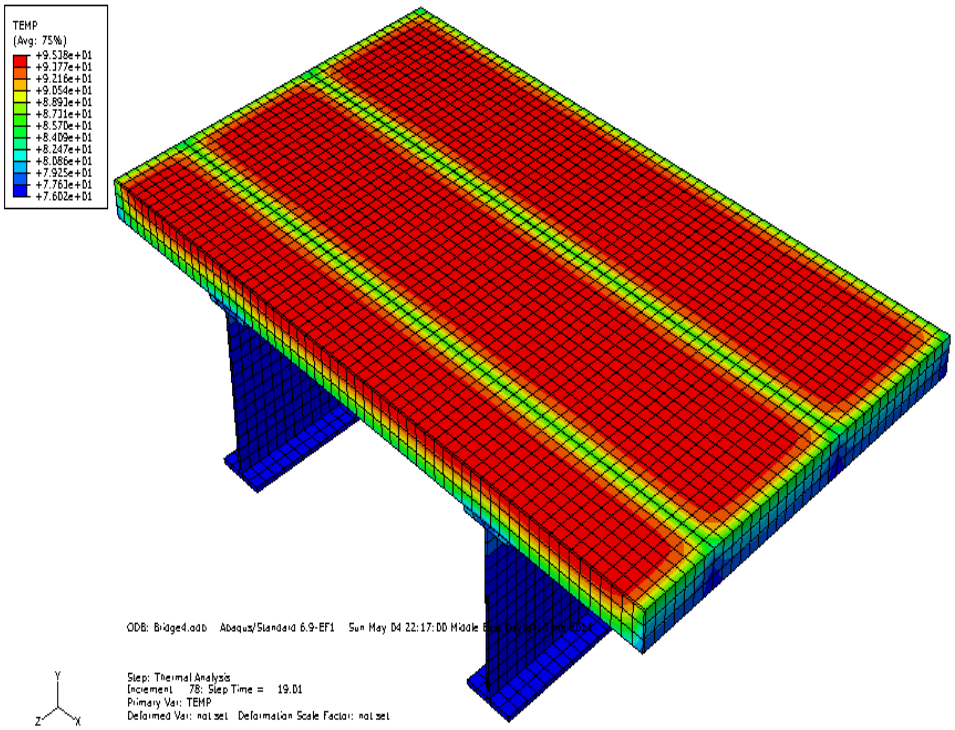

Figure 4-4 Temperature Distribution (19:00; June 4, 2010)

The vertical temperature distribution, similar to the one of Figure 4-6, was obtained at four distinct critical positions as illustrated in Figure 4-5. These positions are:

- Position I: In the middle between the two cracks, for the exterior girder
- Position II: At the surface of the crack, for the exterior girder
- Position III: In the middle between the two cracks, for the interior girder
- Position IV: At the surface of the crack, for the interior girder

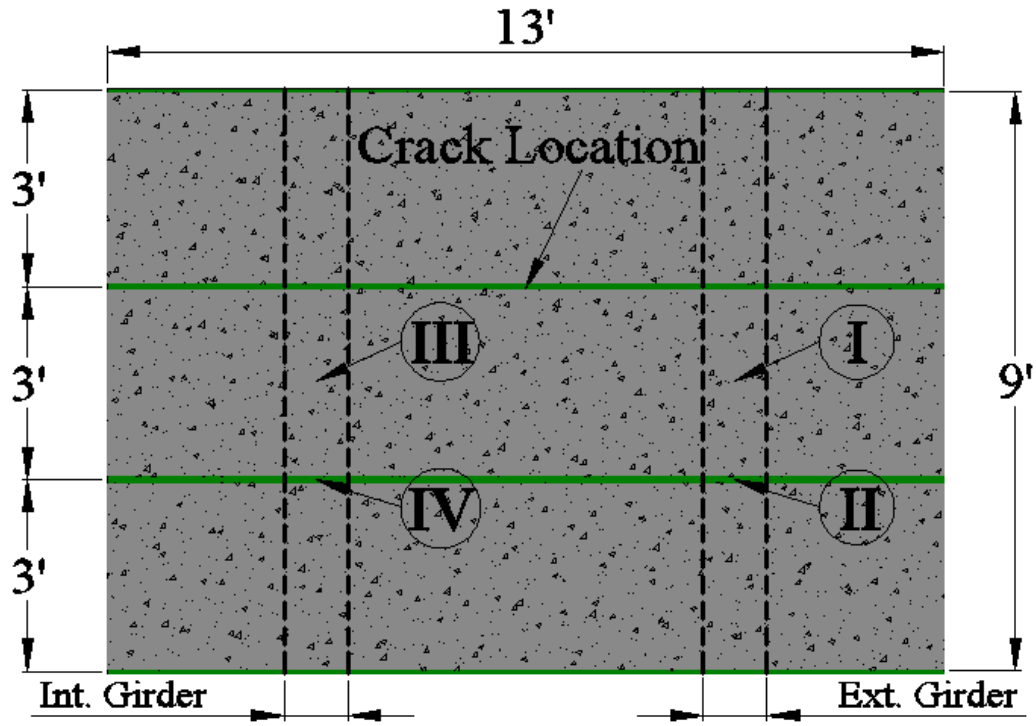

Figure 4-5 Positions of Analyzed Vertical Temperature Distribution

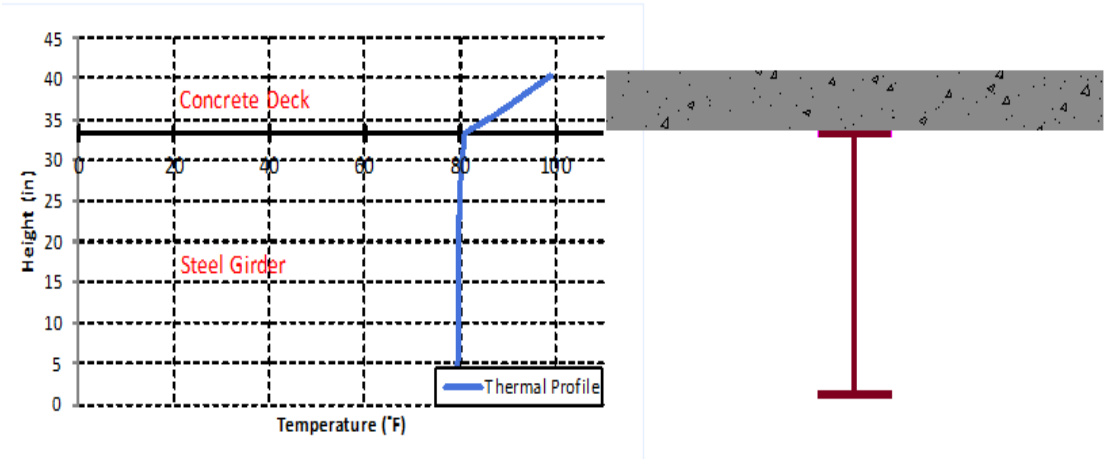

Figure 4-6 Vertical Temperature Distribution at Position I (18:00; June 4, 2010)

4.3 INITIAL INTERPRETATIONS

4.3.1 Exterior vs. Interior Girder

An initial comparison of the vertical temperature distributions between the bridge sections at the exterior and interior girders revealed similar results between Positions

I and III on the one hand, and Positions II and IV on the other hand. This similarity in the temperature profile was valid for both simulated days on June 4 and December 23. A maximum temperature differential of 0.8 ˚F was reached between the two girders at 8:00 on June 4, 2010. This small difference is due to the sun beams radiations reaching to exterior steel web soon after sunrise. However, the shading effect on the exterior girder provided by the deck overhang for the remainder of the day results in the same temperature distribution for the two girders. The full calculations of the shading length are provided in Appendix A. These results show that for the current deck overhang shading properties, the exterior girder was shaded most of the time and thus leading to a maximum temperature differential between the concrete deck the steel girder. The deck overhang shading properties include an overhang to depth ratio of roughly 1, the location of the bridge, the time of the year, and the bridge orientation.

The vertical temperature distribution for each position at 8:00 on June 4, 2010 is provided in Figures 4-7 to 4-10. Based on aforementioned observation of temperature profile similarity, the results of the interior girder will be neglected in favor of considering only the vertical temperature distribution of the bridge section at Positions I and II of the exterior girder. It is these results that will be displayed, analyzed, and discussed in this Chapter.

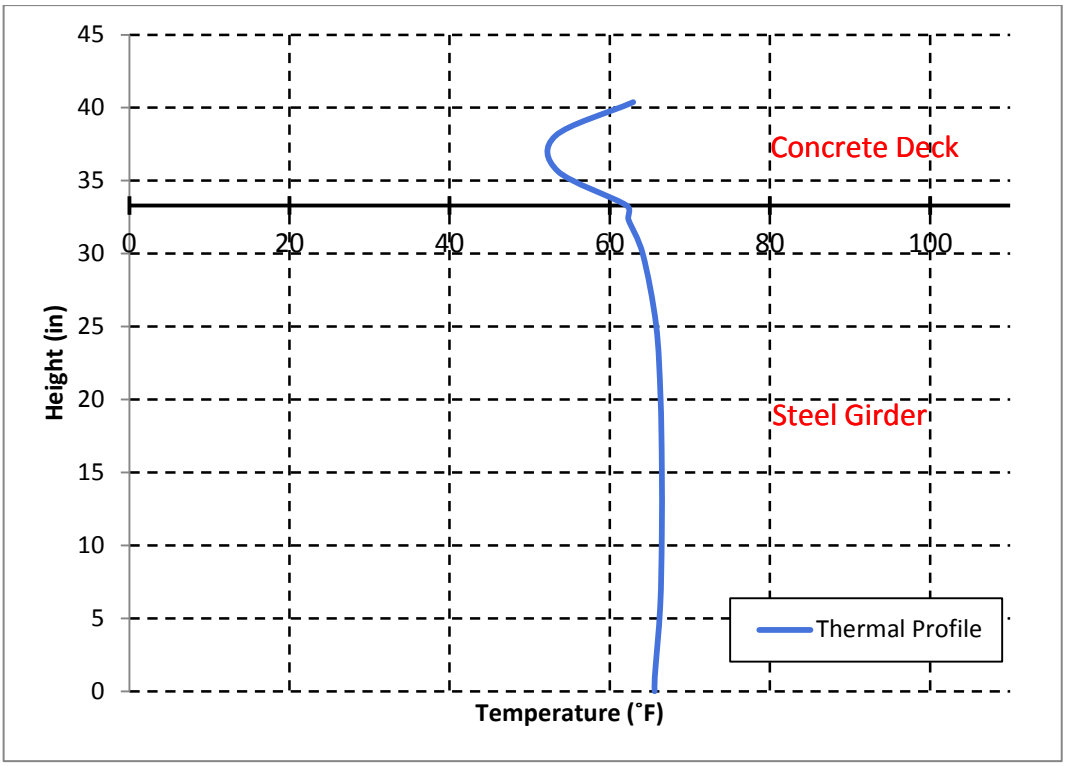

Figure 4-7 Vertical Temperature Distribution at Position I (8:00; June 4, 2010)

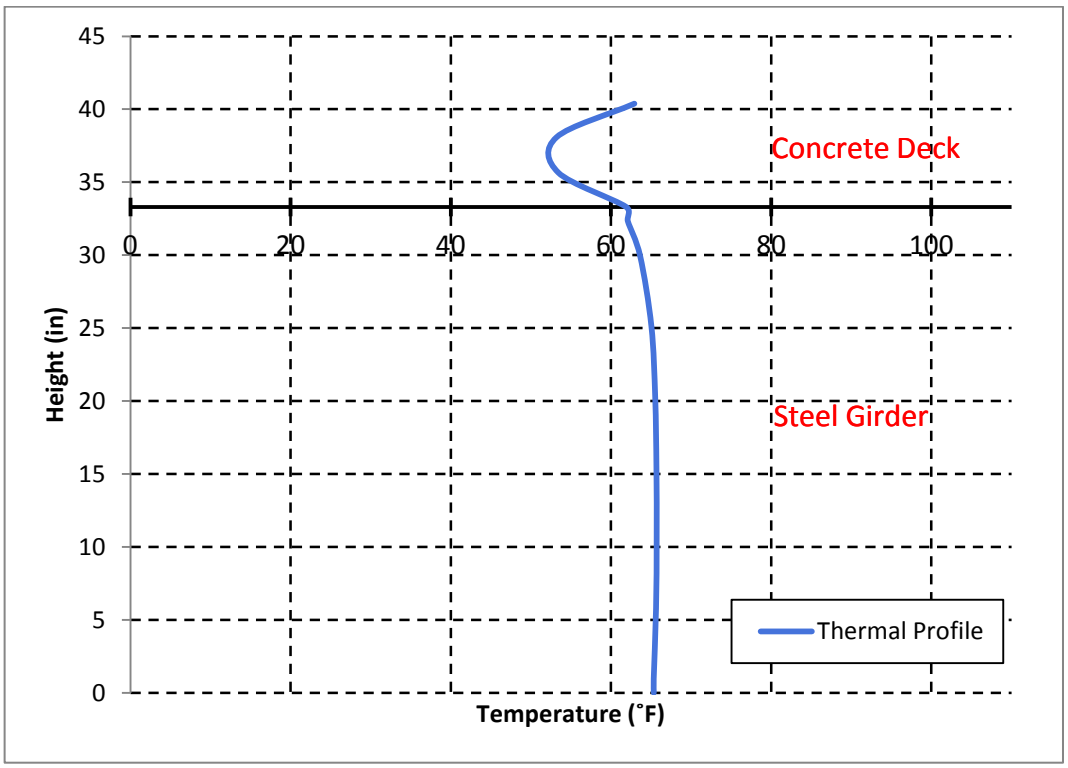

Figure 4-8 Vertical Temperature Distribution at Position III (8:00; June 4, 2010)

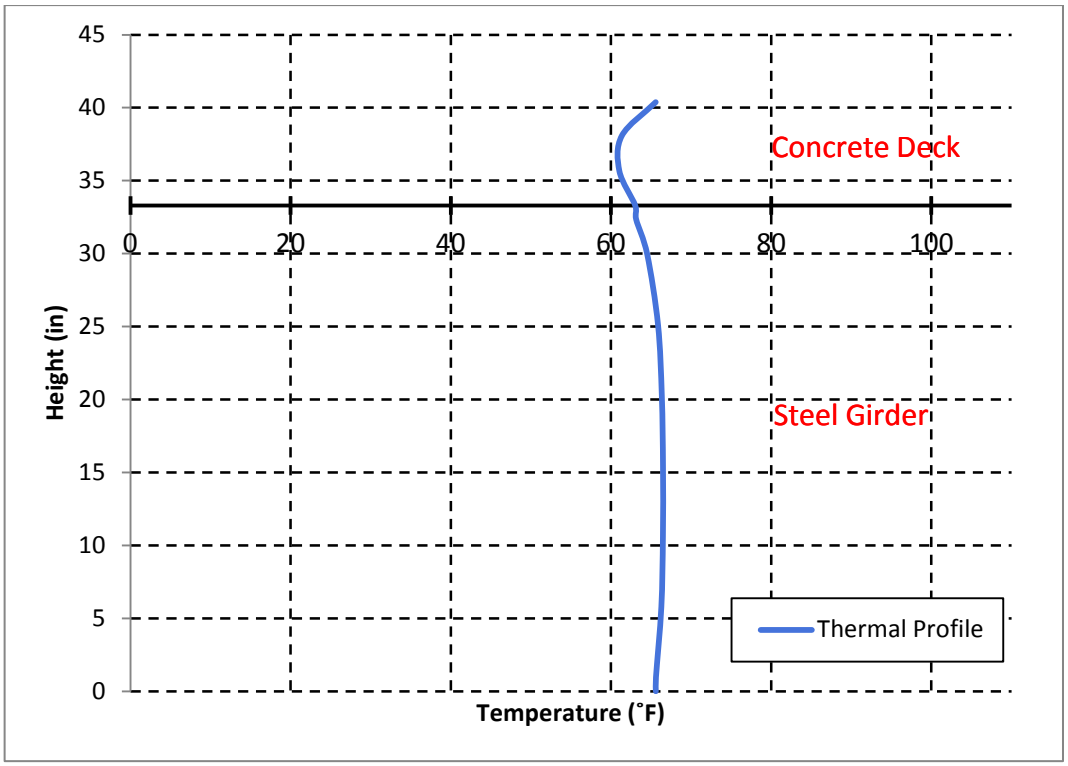

Figure 4-9 Vertical Temperature Distribution at Position II (8:00; June 4, 2010)

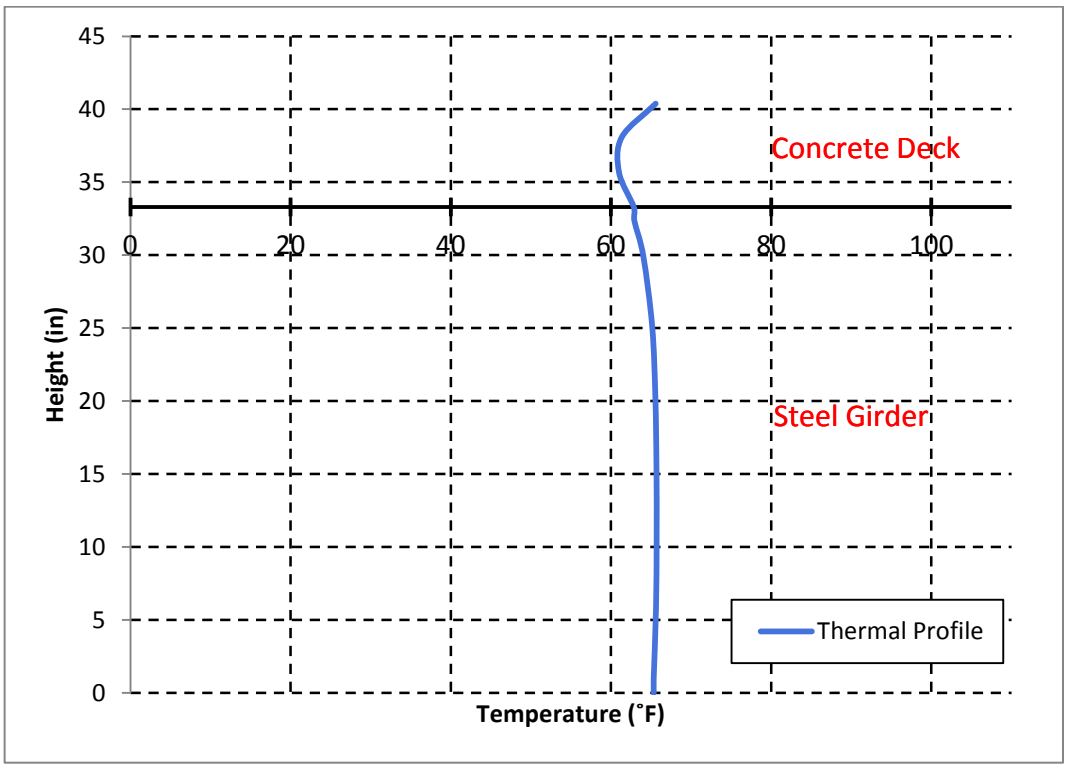

Figure 4-10 Vertical Temperature Distribution at Position IV (8:00; June 4, 2010)

4.3.2 Effect of Initial Temperature Assumption

The model initial temperature was set to zero; this means that no temperature was assigned to the FE model at time step 0. This assumption has been validated in previous studies in which it was reported that the initial temperature does not affect the distribution of temperature within the bridge (Emanuel & Taylor, 1985; Fu, Ng, & Cheung, 1990). When comparing the vertical temperature distributions at time 0:00 and time 24:00, it is apparent that a large temperature change occurred in the concrete deck. The main reason behind this change is the initial temperature assumption. In fact, the heating process of the concrete when the solar radiations are absent is much lower than that of steel due to the very low conductivity of concrete material. The analysis of the FE model results confirm that the concrete needed five hours to converge to a steady temperature differential during the cooling process. Therefore, the results of the first four hours will be discarded from the remainder of the analysis. This leads to the conclusion that initial bridge temperature has insignificant effect only when the bridge is exposed to solar radiation. A comparison sample showing three thermal profiles at position I is provided in Figure 4-11.

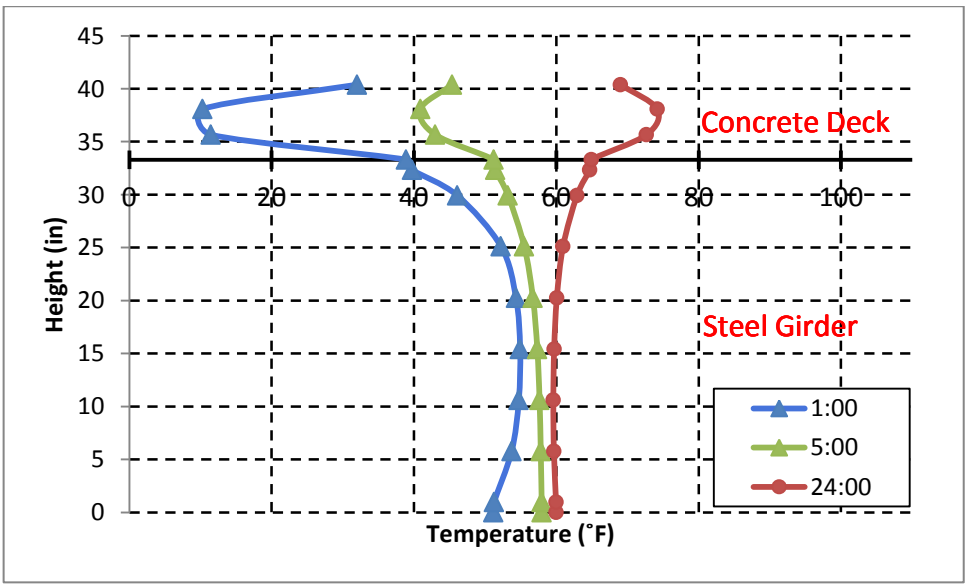

Figure 4-11 Vertical Temperature Distribution at Position I (June 4, 2010)

4.4 ANALYSIS OF THE TEMPERATURE DISTRIBUTION

4.4.1 Maximum Temperature in the Concrete Deck

The absolute maximum temperature in the concrete deck is expected to be reached near the end of the heating process in the afternoon before sunset, at which time the bridge starts to cool. This maximum effective temperature is critical for calculating the bridge thermal stresses resulting from the various components of thermal strains (uniform, linear, and non-linear). On June 4, the temperature in the concrete deck reached a maximum value of 101.4 ˚F at 15:00 at position I (midway between the two cracks). This temperature was recorded at the top surface of the concrete deck as can be seen from Figure 4-12. At this same time, the temperature at position II (at the crack surface) reached a maximum value of 92.7 ˚F at the top end of the crack. This difference of 8.7 ˚F in the maximum temperature between Positions I and II is caused by the air leakage through the cracks. Figures 4-13 and 4-14 provide the vertical temperature distribution at these two locations.

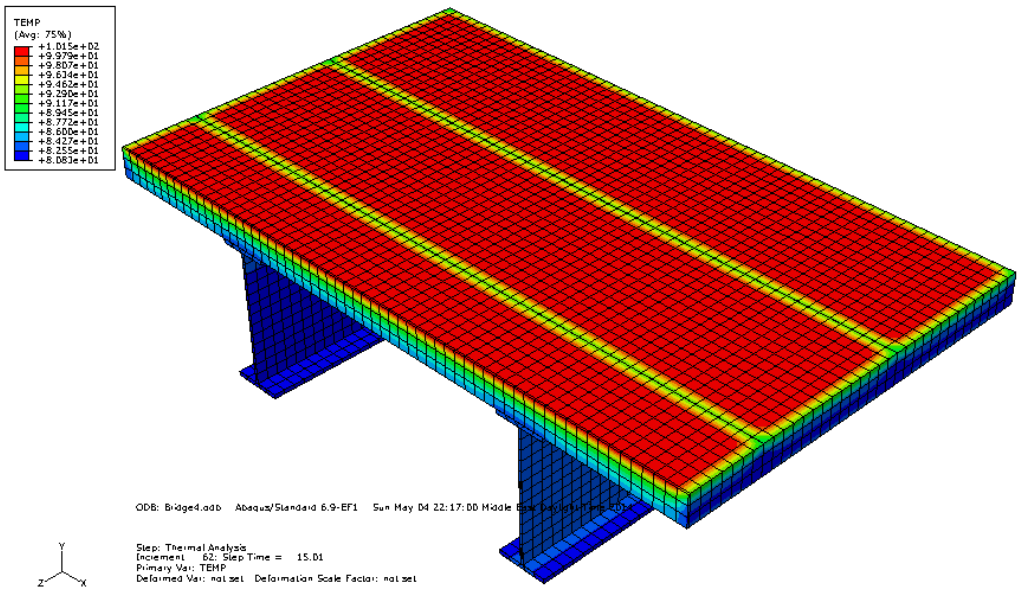

Figure 4-12 Temperature Distribution (15:00; June 4, 2010)

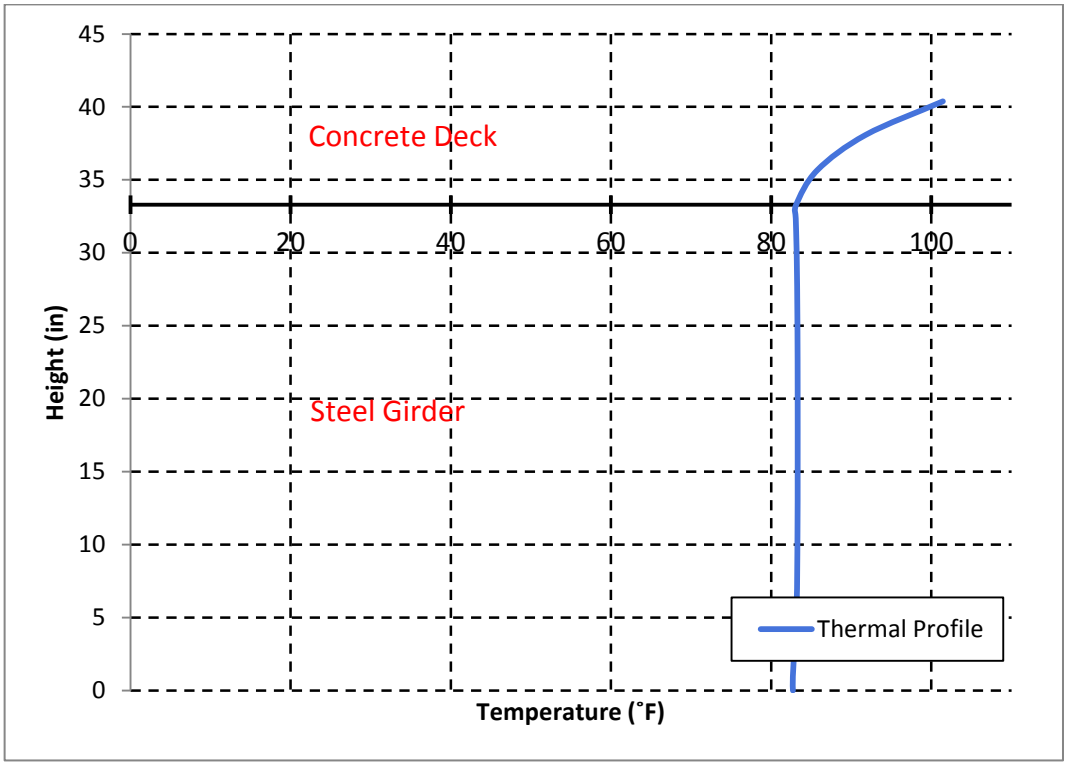

Figure 4-13 Vertical Temperature Distribution at Position I (15:00; June 4, 2010)

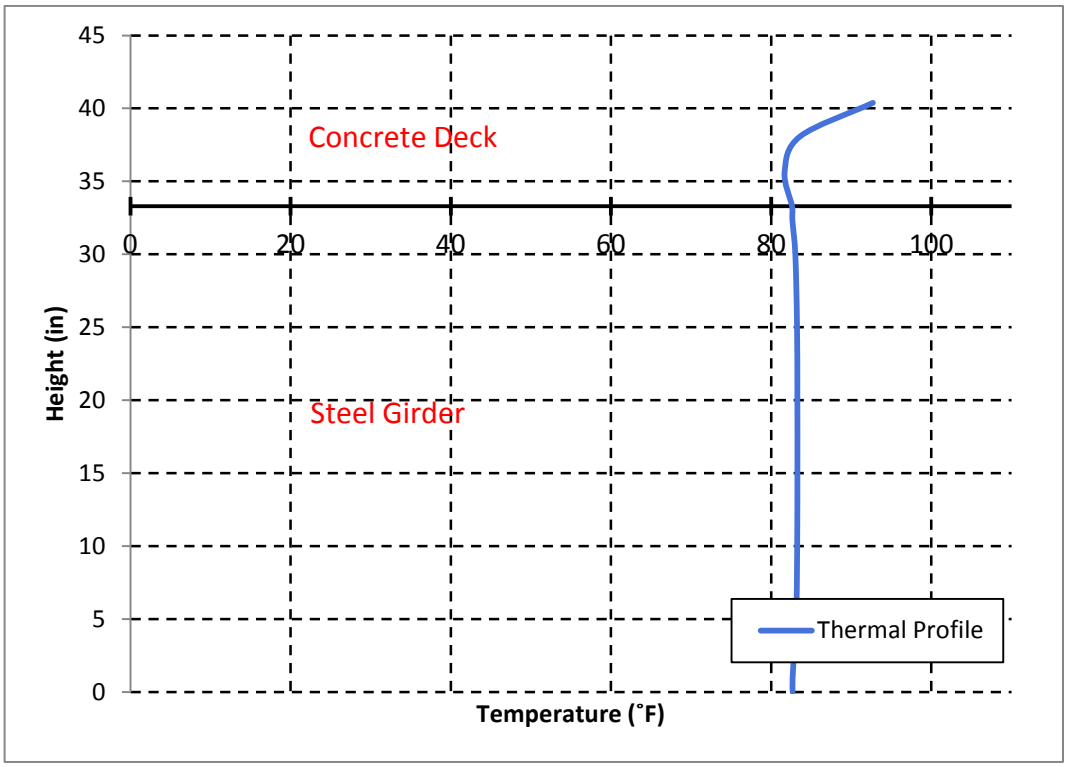

Figure 4-14 Vertical Temperature Distribution at Position II (15:00; June 4, 2010)

It is also worth noting that due to solar radiations reflected from the ground, the temperature at the bottom surface of the concrete deck tends to be slightly cooler right over the two steel girders than the regions between the two girders and on the overhang. This phenomenon can also be seen by inspecting Figure 4-12.

On December 23, the temperature in the concrete deck reached a peak value of 24.5 ˚F at 15:00 at position I. This temperature occurred at the top surface of the concrete deck as shown in the thermal profile in Figure 4-15. The corresponding peak temperature at the top of the crack (Position II) was 24.2 ˚F with a difference from position I of only 0.3 ˚F. In winter, when the lowest ambient temperature and solar radiation are recorded, the deck transverse cracks do not seem to affect the maximum temperature in the concrete deck. Also affecting this low temperature differential between Positions I and II is the low wind speed that is reported for December 23.

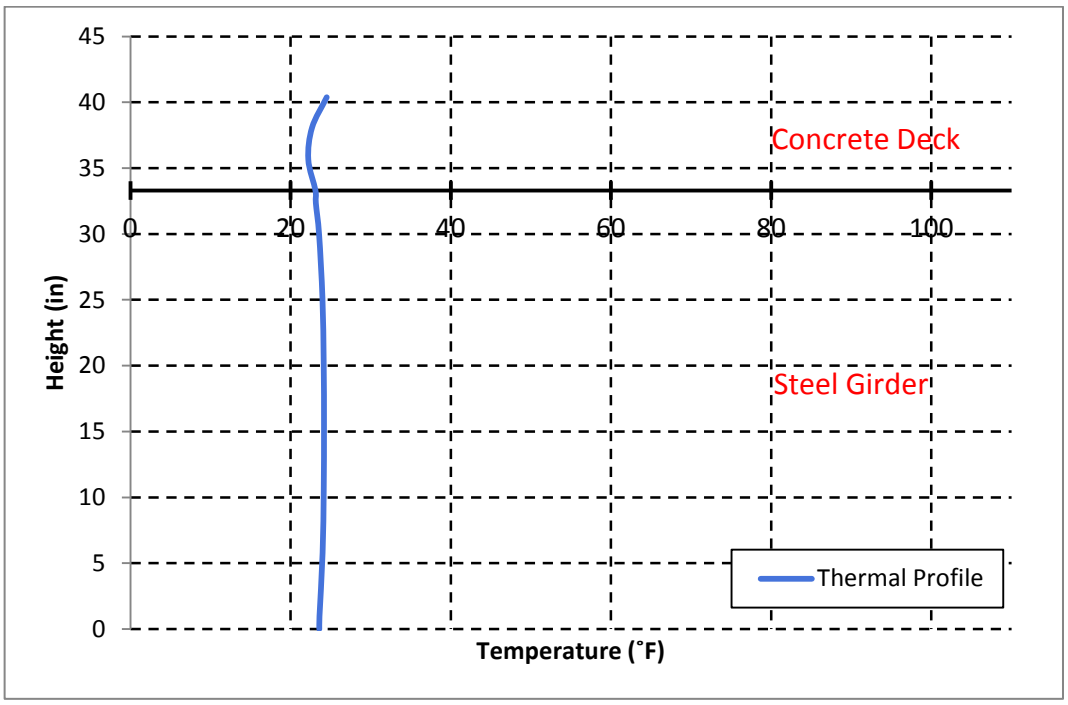

Figure 4-15 Vertical Temperature Distribution at Position I (15:00; December 23, 2010)

4.4.2 Maximum Temperature in the Steel Girder

The absolute maximum temperature in the steel girder is also expected to be reached in the exterior girder sometime in the afternoon. This temperature will significantly affect the thermal stresses corresponding to the various types of thermal strains in the bridge.

On June 4, the temperature in the steel girder reached a maximum value of 83.4 ˚F at 14:00 in the middle of the steel web. The maximum temperature on December 23 peaked at only 24.2 ˚F at 15:00 in the middle of the steel web as shown in Figure 4-16.

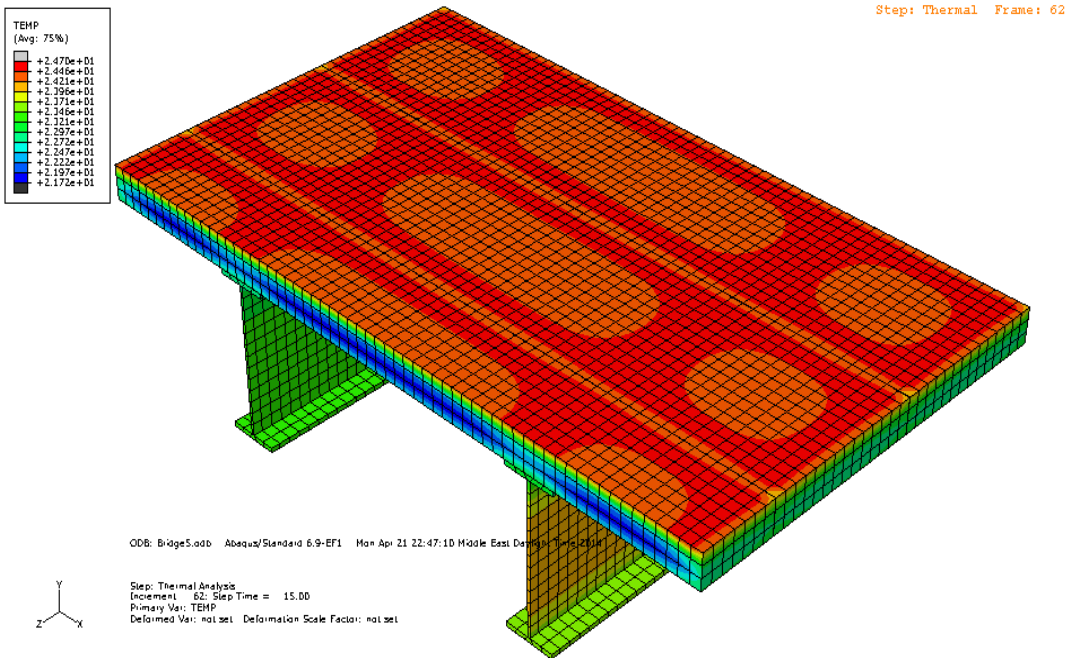

Figure 4-16 Temperature Distribution (15:00; December 23, 2010)

4.4.3 Vertical Temperature Distribution

Thermally induced stresses in bridges, resulting from the temperature gradient within the bridge cross-section and from the support restraints or inadequate or

malfunctioning support and expansion devices, are an important factor to be carefully considered by designers and not treated in a trivial manner. Different methods for the calculation of thermal stresses exist for various types of structures; however, all these methods depend on a precise estimation of the temperature distribution.

Results of the FE model show that the vertical temperature distribution in the web of the steel girder looks almost uniform for the two selected days in June and December. This temperature gradient is expected and agrees with all previous studies on the thermal behavior of composite bridges (Kennedy & Soliman, 1987).

In June (June 4), the maximum vertical temperature differential between the steel girder and the concrete deck occurred at 18:00 and reached a maximum value of 19.8 ˚F, as shown in Figure 4-17, at Position I in the middle of the deck between the two cracks. The corresponding vertical temperature difference at Position II was only 10.8 ˚F. However, it is interesting to note that the absolute maximum temperature differential was reached at 11:00 inside the concrete deck, and this is due to the low thermal diffusivity of concrete. This difference between the top surface and the mid-depth of the concrete deck reached a value of 20.2 ˚F. In fact, the top and bottom surfaces of the concrete deck are exposed to direct and ground reflected solar radiations at 11:00 during the heating process. These radiations, in conjunction with the low thermal diffusivity of concrete, lead to a lower temperature at mid-depth of the deck as shown in Figure 4-18.

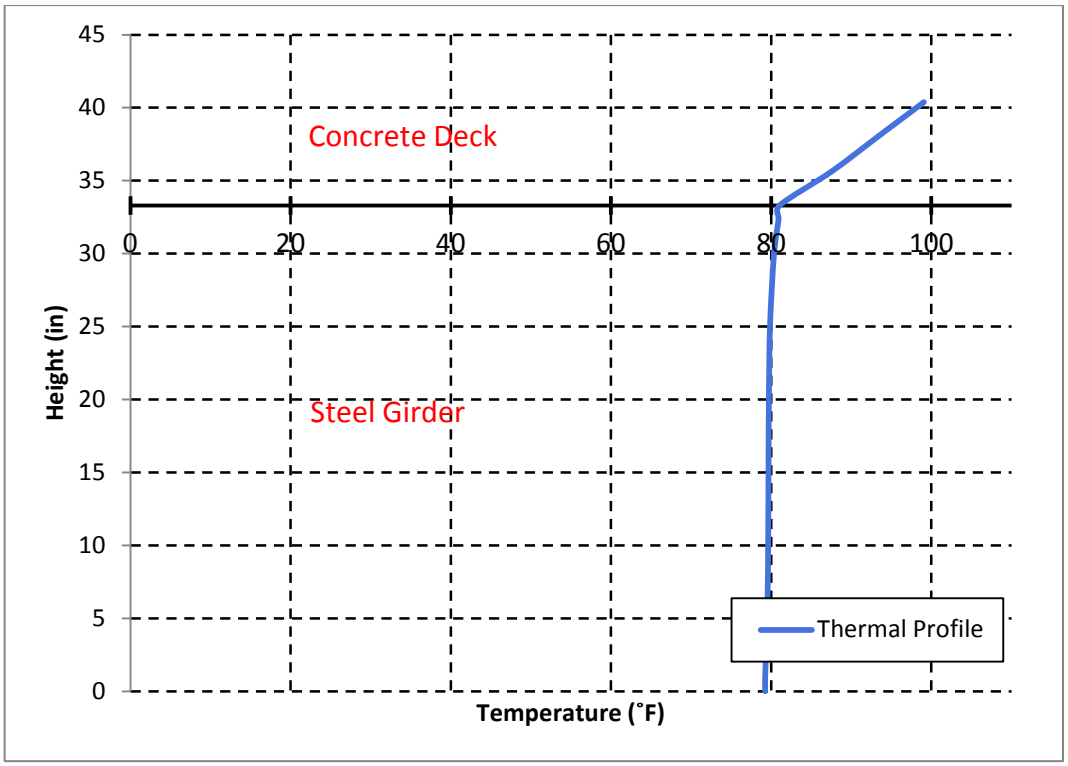

Figure 4-17 Vertical Temperature Distribution at Position I (18:00; June 4, 2010)

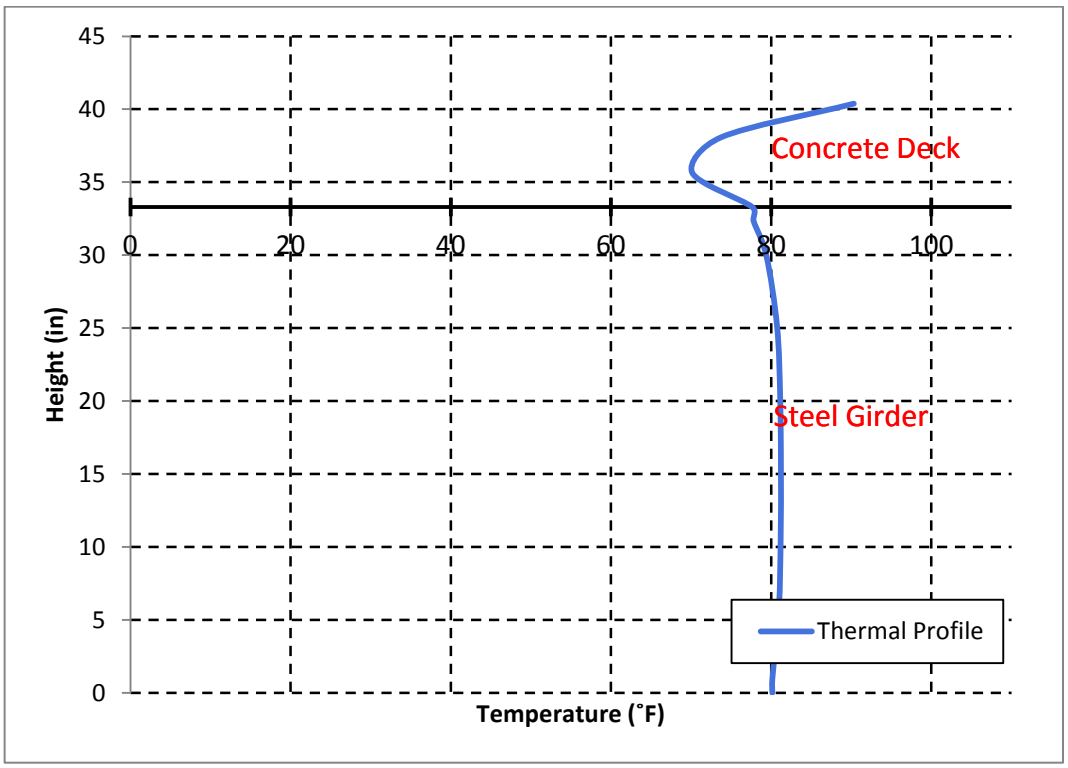

Figure 4-18 Vertical Temperature Distribution at Position I (11:00; June 4, 2010)

After sunset, the thermal profile in the concrete deck, provided in Figure 4-20, shows that the concrete is the warmest at mid-depth of the deck during the cooling process. This happens due to both top and bottom surfaces of the deck losing heat to the surrounding by convection faster than the concrete at mid-depth.

In December (December 23), the vertical temperature distribution is almost uniform for the entire day due to low ambient temperature and solar radiation. The maximum negative differential temperature between the steel girder and the concrete deck reached a value of 3.6 ˚F at 7:00 at Position I, as shown in Figure 4-21. This negative thermal gradient is due to the start of the heating process after the sunrise. After sunset (after 17:00), the temperature distribution in the bridge reached almost a steady state with a maximum vertical temperature difference of 0.6 ˚F. Therefore, the cooling process had negligible effects on the thermal gradient in December under normal environmental conditions.

For estimating the accuracy of the FE model in capturing the temperature using linear heat transfer elements, the heat flux is plotted at the time of maximum temperature differential, which is at 18:00 on June 4, as shown in Figure 4-19.

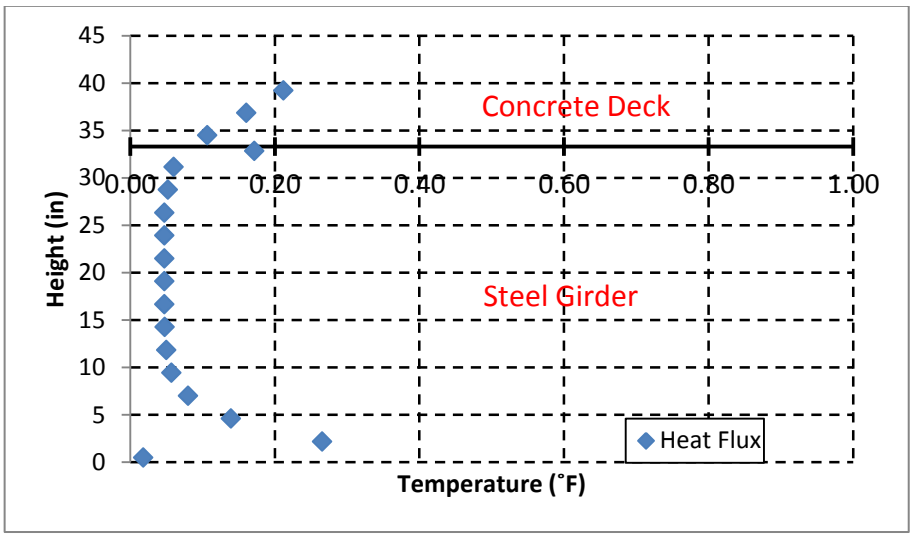

Figure 4-19 Heat Flux at Position I (18:00; June 4, 2010)

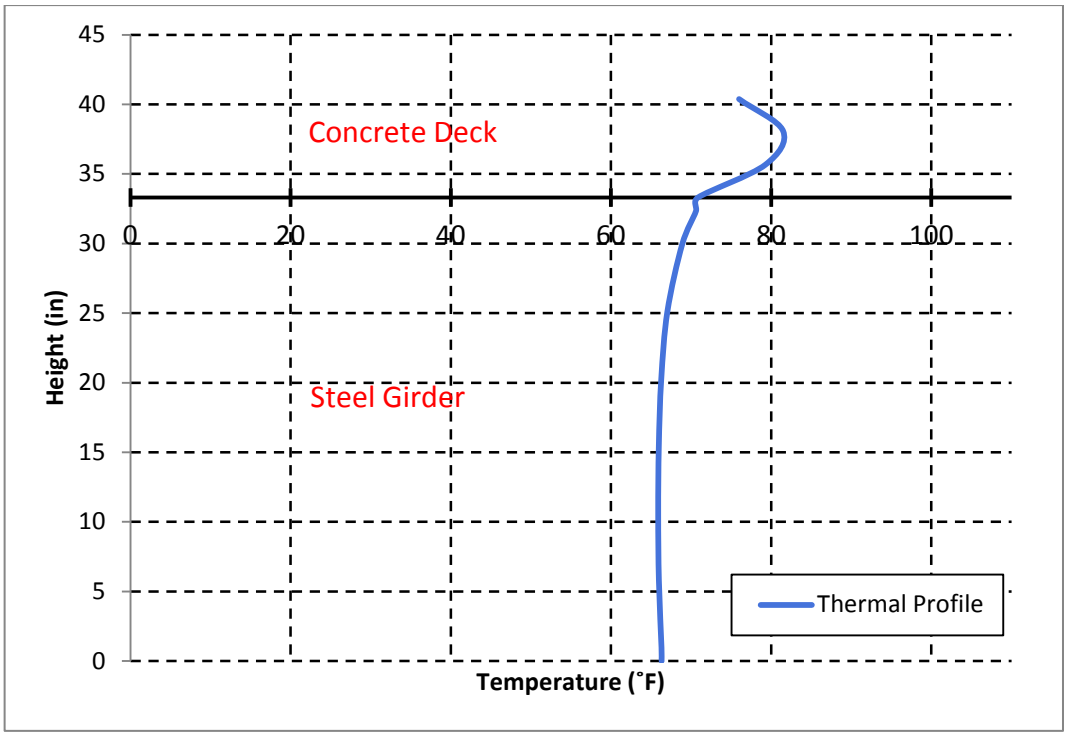

Figure 4-20 Vertical Temperature Distribution at Position I (22:00; June 4, 2010)

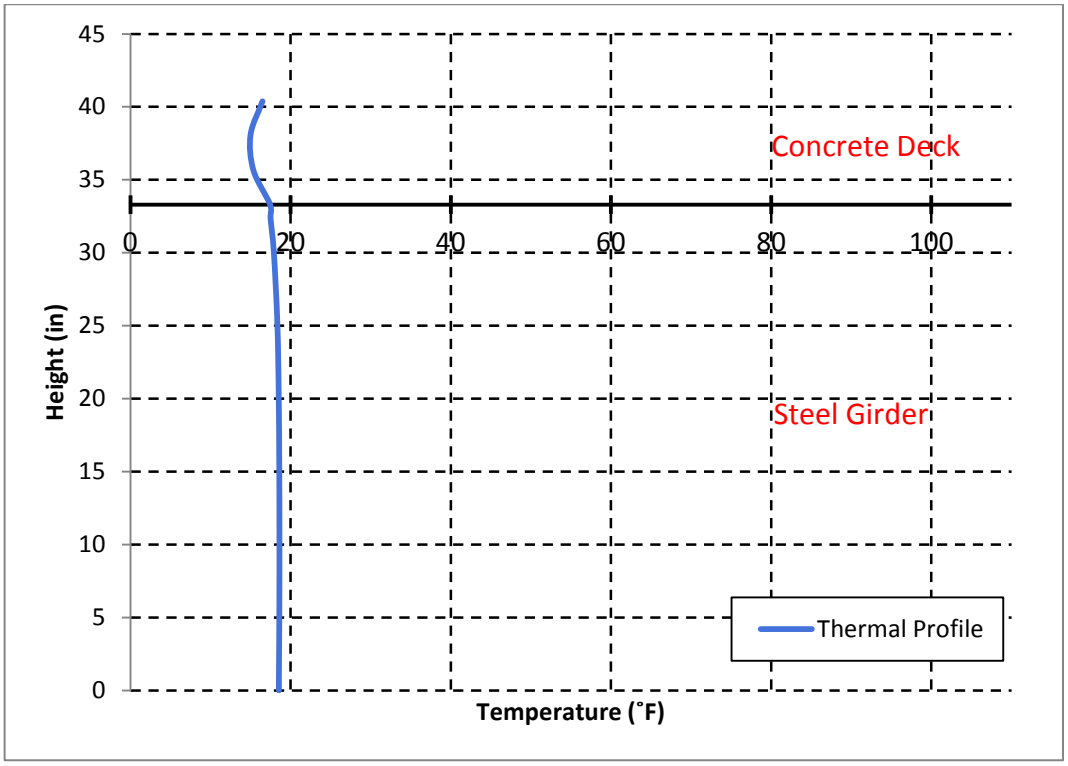

Figure 4-21 Vertical Temperature Distribution at Position I (7:00; December 23, 2010)

It is worth noting that the maximum recommended value for temperature differential during the summer by Kennedy and Soliman (1987) is 40 ˚F. However,

this recommendation is for the Middle Atlantic States and Southern Ontario, which does not include North Dakota. Table 4-1 shows the maximum temperature differentials for Positions I and II throughout the two selected days in June and December. The vertical temperature distributions for each hour are provided in Appendix B.

Table 4-1 Temperature Differentials for the FE model

	Maximum Temperature Difference (˚F)			
	4-Jun		23-Dec	
Time	Position I	Position II	Position I	Position II
1.00[1]	44.6	19.1	13.2	6.4
2.00[1]	37.1	13.8	11.6	4.8
3.00[1]	27.4	9.8	9.1	3.2
4.00[1]	21.5	7.9	6.9	2.3
5.00	17.0	6.9	5.3	1.6
6.00	14.6	6.1	4.0	1.2
7.00	14.3	5.8	3.6	1.1
8.00	13.3	5.4	3.0	0.9
9.00	13.8	8.2	3.0	1.0
10.00	18.1	10.6	2.1	0.8
11.00	20.2[2]	11.2	2.7	1.2
12.00	20.2[2]	11.6	3.2	1.6
13.00	19.7	12.3	2.7	1.4
14.00	18.1	11.3	2.7	1.6
15.00	18.7	11.0	2.3	1.4

16.00	18.8	10.5	1.5	0.9
17.00	17.9	9.3	0.9	0.5
18.00	19.8	10.8	0.6	0.3
19.00	18.3	9.6	0.3	0.3
20.00	16.8	7.3	0.3	0.2
21.00	16.4	6.3	0.5	0.2
22.00	15.6	6.1	0.4	0.2
23.00	15.1	6.7	0.3	0.2
24.00	14.6	6.1	0.5	0.2

[1] Discarded Data

[2] Occurs at mid-depth of the concrete deck

4.4.4 Comparison with Other Models

The AASTO LRFD Bridge Design Specification (2012) provides provision for the vertical temperature gradient in composite bridges. AASHTO LRFD (2012) recommends that the vertical temperature distribution be uniform in the steel girders and linear in the superimposed concrete deck. This recommendation is based on a modification of the thermal gradient proposed by Imbsen et al. (1985). The temperature differential in the concrete deck is based on the map of solar radiation zones in the United States as shown in Figure 4-22. Based on this map, the city of Fargo, ND, is located in zone 2.

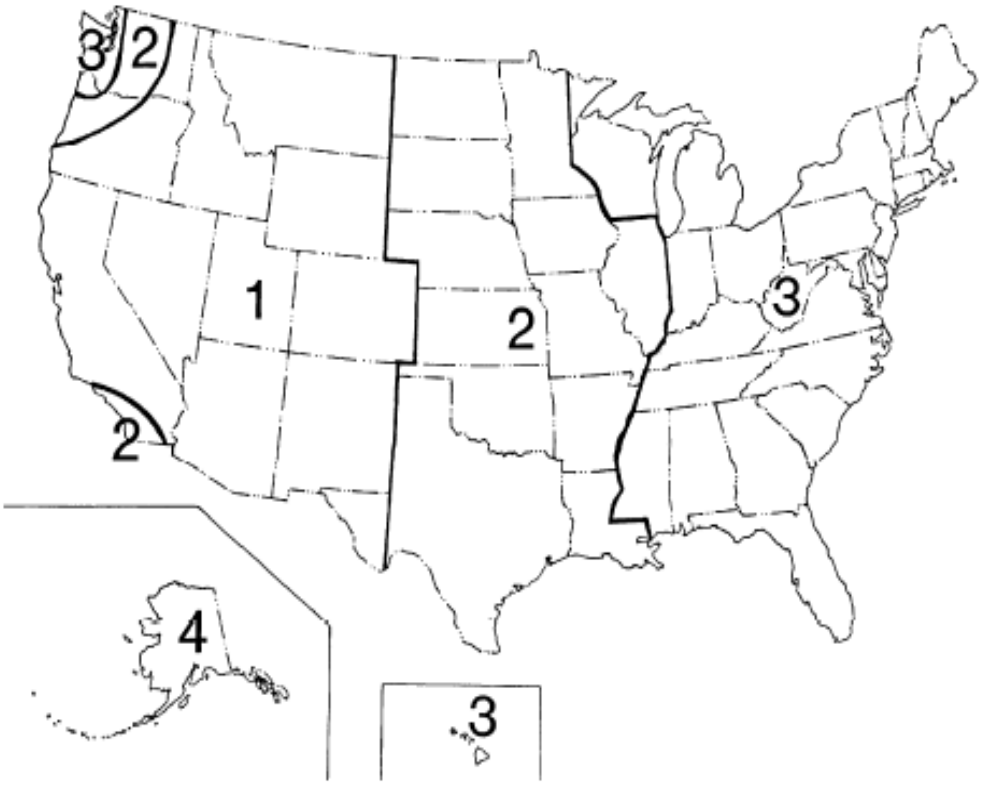

Figure 4-22 Solar Radiation Zones for the United Stated (AASHTO, 2012)

For zone 2, the AASHTO LRFD Bridge Design Specification (2012) recommends a maximum positive vertical temperature differential of 34 ˚F between the top and bottom surfaces of the concrete deck. The AASHTO temperature gradient is compared to that obtained using the thermo-elastic analysis of the FE model in June, as shown in Figures 4-23 and 4-24.

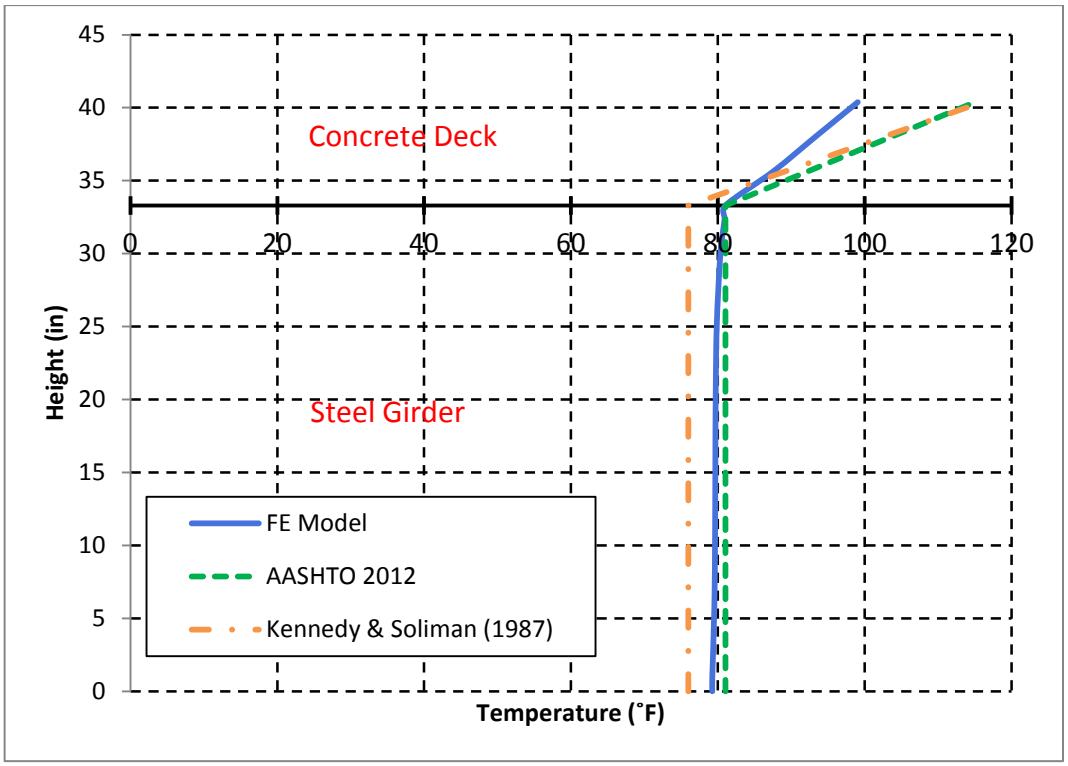

Figure 4-23 Vertical Temperature Distribution at Position I (18:00; June 4, 2010)

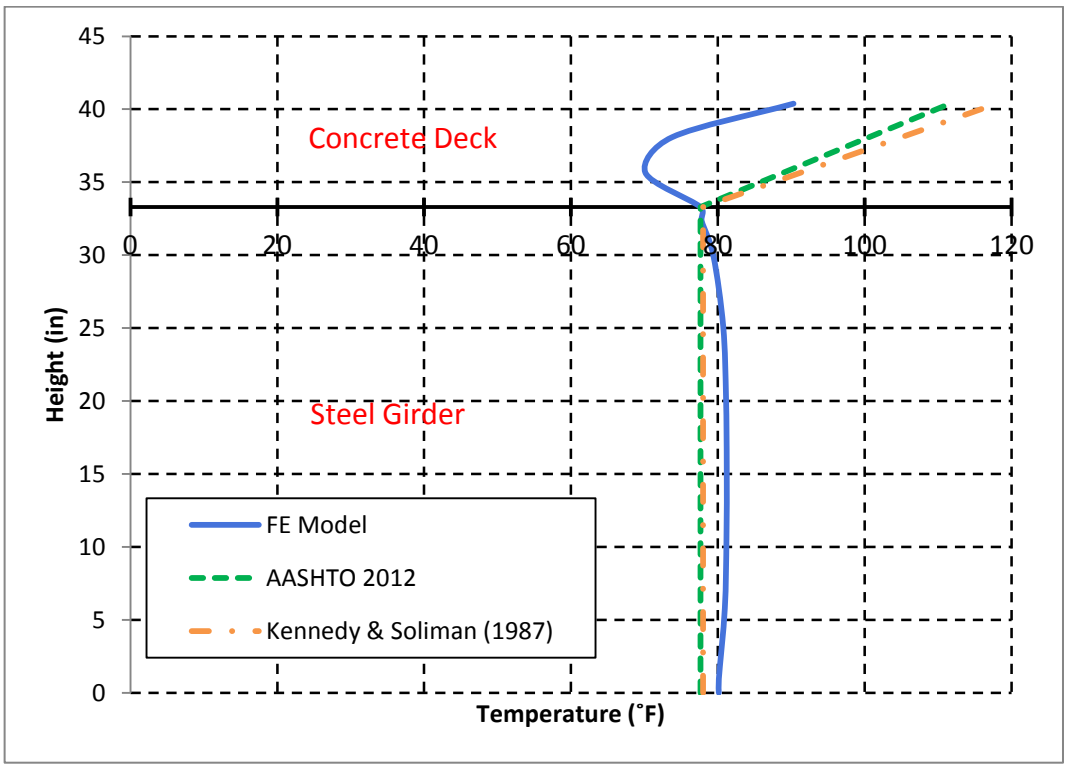

Figure 4-24 Vertical Temperature Distribution at Position I (11:00; June 4, 2010)

In Figure 4-23, the maximum temperature differential between the concrete deck and the steel girder of the FE model is compared to that proposed by the AASHTO code. The shape of the obtained vertical temperature distribution is very similar to the one proposed by AASHTO; however, the AASHTO specification provides a maximum temperature differential of 14.2 ˚F higher than the one obtained in the FE model. This very conservative approximation adopted by AASHTO leads to considerable error in assessing the thermal stresses in composite steel-concrete bridges.

In Figure 4-24, the vertical temperature distribution proposed by AASHTO is plotted against, and compared to that obtained using the thermo-elastic analysis of the FE model. This comparison is conducted at 11:00, at which time that maximum temperature differential within the thermal gradient occurred between the top and mid-depth surfaces of the concrete deck during the heating process of the bridge. The relative error between the two maximum temperature differentials in both profiles is 13.8 ˚F. It should be noted that the vertical temperature distribution in the concrete deck obtained using the finite element thermo-elastic analysis was nonlinear when compared with the linear distribution proposed by AASHTO. In fact, the vertical temperature distribution in the concrete deck was close to being linear only in the afternoon between 14:00 and 19:00, and nonlinear for the remainder of the day. This nonlinearity in the temperature distribution will produce a nonlinear thermal strain component and its effects on the design of the bridge require further investigation.

The linear-uniform vertical temperature distribution proposed by Kennedy and Soliman (1987) is also incorporated in Figures 4-23 and 4-24 for illustration purposes. The maximum temperature differential between the concrete deck and the

steel girder is suggested to be 40 ˚F during the summer season for the Middle Atlantic States and Southern Ontario.

It is therefore evident that the vertical thermal gradient proposed by AASHTO is conservative in the concrete deck due to several reasons. These reasons include:

- AASHTO provisions do not include a thermal gradient for the cooling process of the bridge.
- There is no distinction whether an asphaltic overlay on the deck is present or not.
- The depth of the concrete deck is not correlated to the maximum temperature differential.
- The thermal profile is based on a one dimensional conduction analysis, and thus the solar radiation reflected from the ground is ignored. This reflected radiation decrease the temperature differential through heating the bottom surface of the concrete deck.
- The overhang-to-depth ratio is not taken into consideration, this ratio has a high effect on the maximum temperature differential of the critical exterior beam through the shading effect.
- A linear vertical temperature distribution is assumed in the concrete deck at all times.
- AASHTO does not account for the effect of pre-existing transverse construction cracks in the concrete deck, whose effect tends to lessen the average temperature differential between the concrete deck and the steel beam.

The AASHTO LRFD (2012) provides a simple and general thermal gradient for composite bridges. However, by incorporating the aforementioned points in the selection of the maximum temperature differential, a more accurate thermal gradient can be obtained depending on the bridge properties. This accuracy will help the designers in better estimating and accounting for the effects of the thermal stresses in composite bridges in reaching an optimal design.

4.5 EFFECTS OF DECK TRANSVERSE CRACKS

4.5.1 Effects on the Vertical Temperature Distribution

In comparing the vertical temperature distribution between Position I (in the deck midway between the two cracks) and Position II (at the crack surface), it is apparent that the deck transverse cracks affect the temperature distribution only in June, given the already negligible temperature differential in December. Yet, a very high wind speed during the winter could lead to a negative gradient at the crack position due to air leakage through the cracks.

The variation in the temperature differentials between Position I and II ranges between 5.6 and 10.1 ˚F in June (June 4, 2010). The highest difference of 10.1 ˚F is reached at 21:00, as shown in Figure 4-25, during the cooling process of the bridge. In fact, the bridge will have a faster cooling process near the cracks due to losing heat faster by convection at the crack surface.

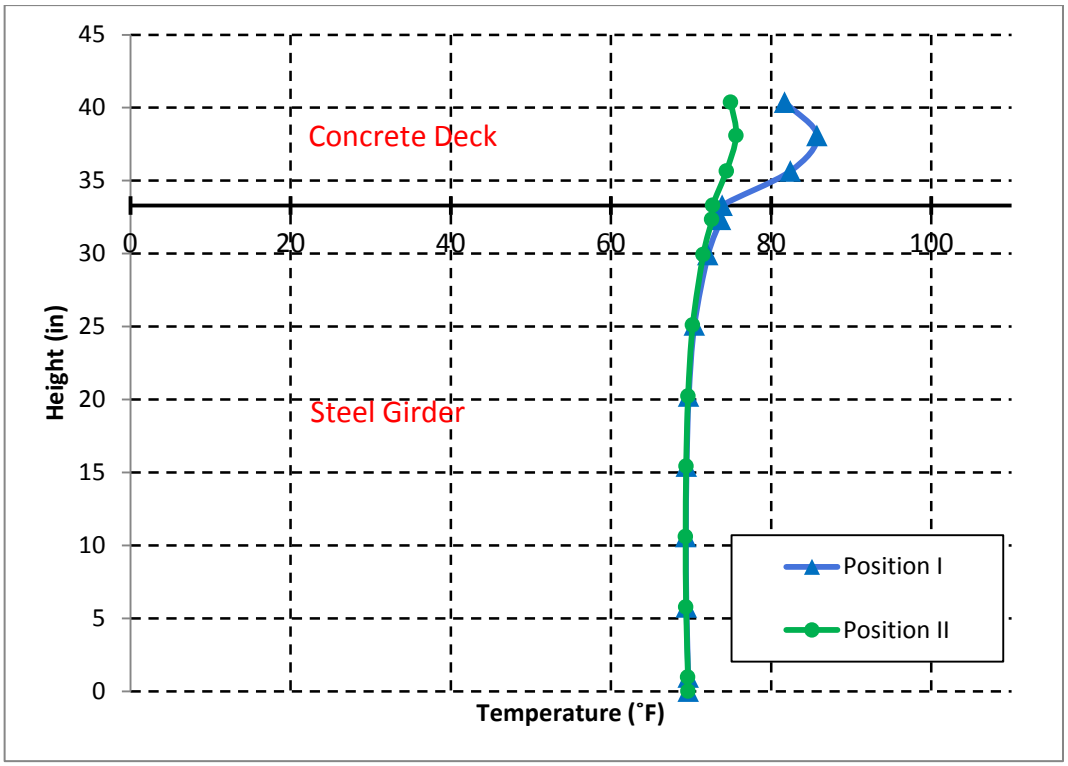

Figure 4-25 Vertical Temperature Distribution (21:00; June 4, 2010)

The vertical temperature distribution in the concrete deck at position I was nonlinear for the majority of the day, as discussed in Section 4.4.4. However, the thermal gradient at Position II has a much lower degree of nonlinearity due to air leakage through the cracks. The air flow appears to help the concrete deck surface at mid-depth to adjust its temperature to the transient conditions of the surrounding. Figures 4-26 and 4-27 provide examples of the vertical temperature distribution at 20:00 on June 4, 2010 for Positions I and II, respectively. It is apparent from Figure 4-26 the nonlinearity of the thermal gradient during the cooling process of the bridge when the concrete surface at mid-depth of the deck has the highest temperature. Yet, Figure 4-27 shows that the thermal gradient at Position II at 20:00 is roughly linear where the temperature at the mid-depth of the concrete deck is 11.3 ˚F less than the corresponding temperature at Position I.

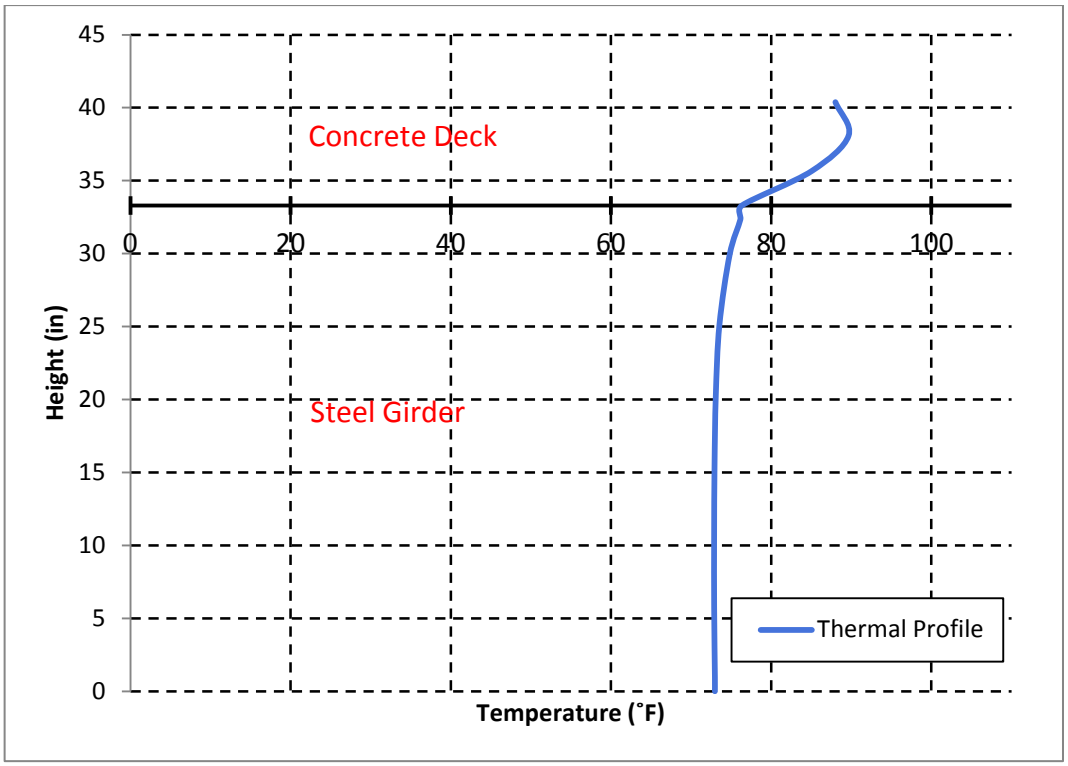

Figure 4-26 Vertical Temperature Distribution at Position I (20:00; June 4, 2010)

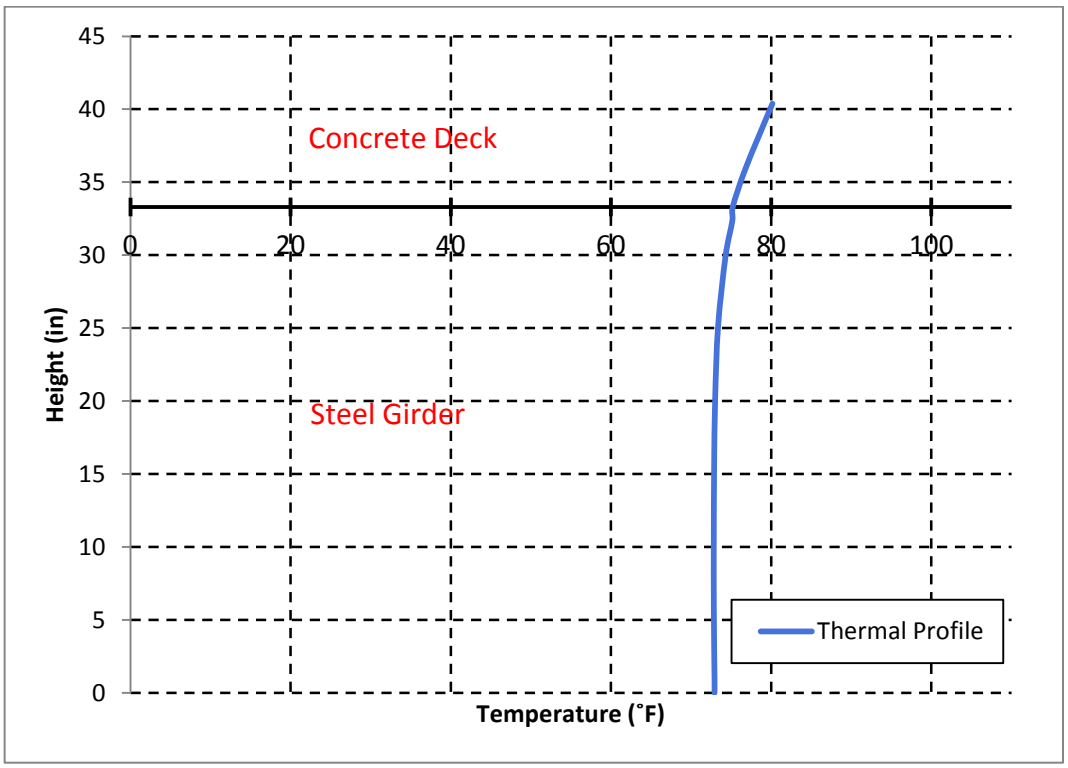

Figure 4-27 Vertical Temperature Distribution at Position II (20:00; June 4, 2010)

Finally, it is worth noting that the temperature in the concrete deck is higher at Position II at the surface of the crack in the morning after sunrise when the heating process of the bridge begins. The maximum temperature reverts to be at Position I at mid-depth of the deck between the two cracks starting at 10:00 on June 4, 2010. This can be related to the tangible increase in the wind speed at 10:00 which decrease the rate of heating at Position II, and also to the increase of solar radiation on the top of the concrete deck. Figure 4-28 illustrates by color contours the higher temperature at the crack surface in comparison to the middle of the concrete deck at 8:00 on June 4, 2010.

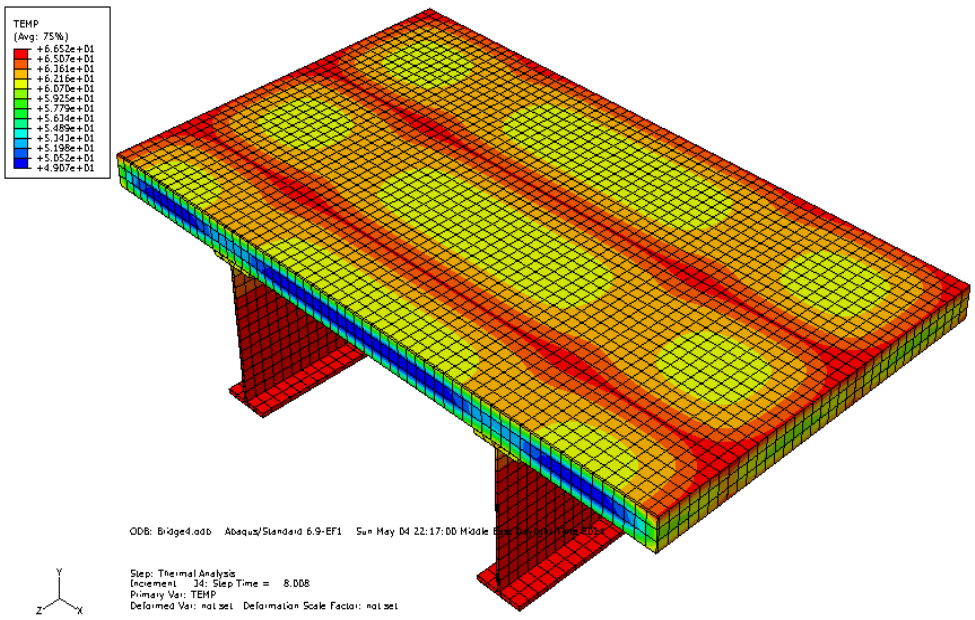

Figure 4-28 Temperature Distribution (8:00; June 4, 2010)

4.5.1 Effects on the Longitudinal Temperature Distribution

Various codes and researchers ignore the temperature differentials in the longitudinal direction of the bridge as they are negligible when compared with the vertical temperature distribution. The difference in the longitudinal temperature distribution

is not expected to exceed 5 ˚F, which constitutes less than 15% of the vertical temperature differential of 34 ˚F suggested by AASHTO (2012).

The analysis of the FE model results indicates a maximum temperature differential of 11.3 ˚F in the longitudinal direction of the bridge as discussed in Section 4.5.1. In fact, nonlinear longitudinal temperature distribution develops in the concrete bridge due to difference in the thermal profile between Positions I and II. The longitudinal temperature distribution is roughly uniform at times of maximum heating from 11:00 to 19:00 as illustrated in Figure 4-29. The only exception will be near the cracks' locations where nonlinear longitudinal temperature develops for a maximum distance of 5 inches from each crack side.

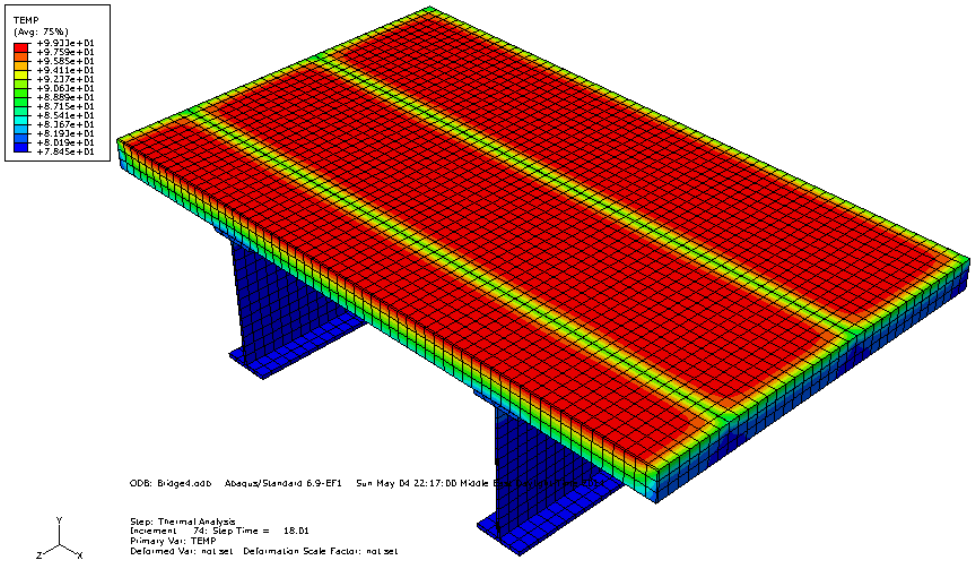

Figure 4-29 Temperature Distribution (18:00; June 4, 2010)

Figure 4-30 shows the temperature distribution in the bridge at 20:00 on June 4, 2010 when the maximum longitudinal temperature differential of 11.3 ˚F has been obtained. At 20:00, the vertical temperature differential is 16.8 ˚F. Therefore, the longitudinal temperature differential constitutes more than 67 % of the vertical temperature differential. Hence, the effect of the longitudinal thermal gradient on the

development of cracks and nonlinear strains requires further assessment and cannot be treated in a trivial manner.

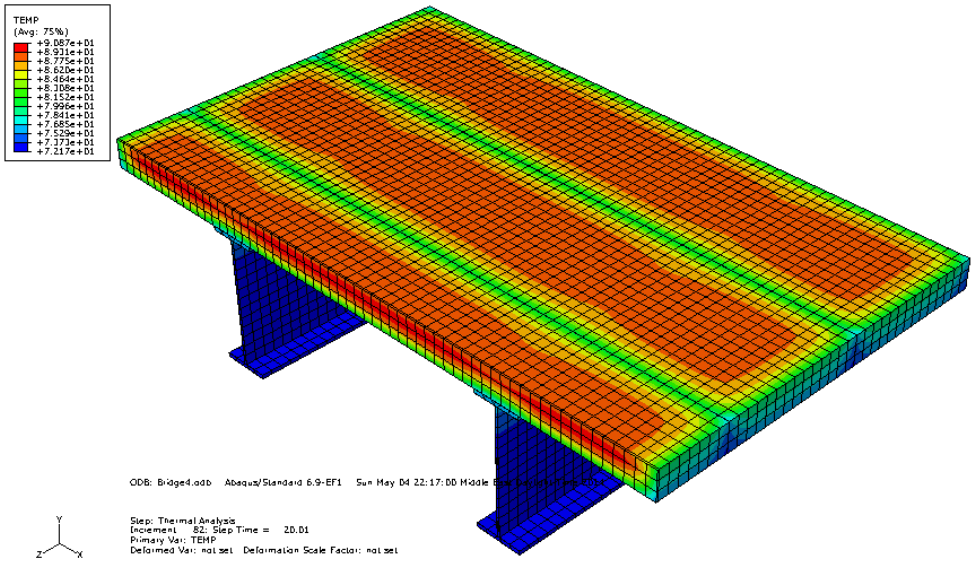

Figure 4-30 Temperature Distribution (20:00; June 4, 2010)

4.6 SUMMARY

The results of a 3D thermo-elastic finite element analysis model were presented in this chapter. Discussions included studying of the temperature distribution in a selected case study bridge and comparing the obtained vertical thermal gradient to that suggested by the AASHTO provisions. Also investigated were the effects of the deck pre-existing transverse construction cracks on the vertical and longitudinal temperature distributions.

The results indicate that the AASHTO provisions overestimate the temperature differential for the studied bridge, and do not include the nonlinear thermal gradient for the bridge which produces a nonlinear strain component that can be critical for the bridge design. In addition, the pre-service deck transverse cracks appear to have a

significant effect on both vertical and longitudinal temperature distributions in the bridge.

Chapter Five
Conclusions and Recommendations

5.1 Summary and Conclusions

Thermal stresses are known to cause considerable damage in composite bridges. Such thermal stresses arise from the non-uniform temperature distribution within the bridge cross-section. In fact, previous studies have indicated that composite bridges exposed to environmental conditions will have a uniform vertical temperature distribution in the steel girders, and a linear thermal gradient in the concrete deck. These studies have also indicated a uniform temperature distribution in the longitudinal direction of the bridge; however, they fall short of considering the existence of construction transverse cracks in the concrete deck and their effect on the temperature distribution in composite bridges.

The aim of this study was to investigate the effect of pre-existing transverse construction cracks in the concrete deck on the temperature distribution of composite steel-concrete bridges. To achieve this goal, first a literature review on the thermal profile, parameters affecting the thermal profile, and bridge deck cracking was carried out. Second, a 3D finite element model was developed for a selected case study bridge to simulate the thermal behavior of the bridge at a given geographical location and on two selected days in June and December. Third, the effect of transverse cracks on the temperature distribution within the bridge was analyzed. Finally, a comparison between the obtained thermal gradients and those proposed by previous studies and existing design codes was presented.

Based on the thermal-elastic finite element analysis results of the case study bridge in the area of Fargo, ND, the following conclusions were reached:

- For the used deck overhang and its shading properties, similar vertical temperature gradients were obtained in the exterior and interior steel girders.
- The assumption of zero initial temperature has no significant effect on the thermal gradient only when the bridge is exposed to solar radiation that accelerates the temperature convergence within the concrete deck.
- The temperature in the concrete deck reached a maximum value of 101.4 ˚F at 15:00 on June 4 at the top surface of the concrete deck.
- The ground-reflected solar radiation appears to affect the temperature distribution at the bottom surface of the concrete deck, and reduce the thermal gradient in the concrete deck.
- After sunset, and during the cooling process, the concrete is the warmest at mid-depth of the deck.
- The temperature in the steel girder reached a maximum value of 83.4 ˚F at 14:00 on June 4 at mid-depth of the steel web.
- The maximum positive vertical temperature differential between the concrete deck and steel girder reached a maximum value of 19.8 ˚F at 18:00 on June 4 in the middle of deck between the two cracks; however, the absolute maximum temperature differential reached a value of 20.2 ˚F at 11:00 at mid-depth of the concrete deck.
- The vertical thermal gradient is almost uniform for the entire day in December under normal environmental conditions.
- The AASHTO LRFD Bridge Design Specification (2012) is overly conservatively and overestimates the vertical thermal gradient, which leads to

significant error in assessing the thermal stresses in composite steel-concrete bridges.

- The finite element model thermo-elastic analysis results show a nonlinear vertical temperature distribution in the concrete deck when compared to the linear distribution proposed by AASHTO and other previously suggested models. This nonlinearity will create a nonlinear strain component that requires further assessment.
- The highest variation in the temperature differentials between the two positions at the middle of the concrete deck and at the crack surface reaches 10.1 ˚F at 21:00 on June 4 during the cooling process of the bridge.
- The concrete deck transverse cracks appear to decrease the degree of nonlinearity in the vertical temperature distribution near the crack surface due to air leakage through the cracks.
- The longitudinal temperature differential reached a maximum value of 11.3 ˚F at 20:00 on June 4. This longitudinal temperature differential constitutes more than 67% of the vertical temperature differential, and thus its impact on the bridge needs further assessment.

5.2 RECOMMENDED FUTURE WORK

During various research projects, questions arise when conducting the literature review and after examining the results. Many of these questions remain unanswered as for they are beyond the objective of the work.

The following topics could have impacts on understanding the temperature distribution in composite steel-concrete bridges and should be incorporated in future studies:

- The effects of the pre-existing construction transverse deck cracks on the stress distribution within the bridge and hence on the design of composite bridges.
- The effects of the nonlinear temperature distribution in the vertical and longitudinal directions of the bridge on the thermal stresses and deformations of the bridge.
- The effects of the longitudinal cracks on the temperature distribution in bridges.
- The effects of the deck transverse cracks under different environmental conditions such as sudden ice and snow on the bridge deck, and very high wind speed condition.

References

AASHTO. (1989b). *AASHTO guide specifications, Thermal effects in concrete bridge superstructures*. Washington, DC: American Association of State Highway and Transportation Officials.

AASHTO, LRFD. (2012). *LRFD bridge design specifications*. Washington, DC: American Association of State Highway and Transportation Officials.

Abaqus (2009). *Abaqus 6.9-EF documentation.* Rhode Island: Dassault Systemes Simulia Corp.

ASHRAE. (1959). Heating, ventilating, air conditioning guide. *American Society of Heating and Air conditioning Engineers, 37,* 52.

Berwanger, C. (1983). Transient thermal behavior of composite bridges. *Journal of Structural Engineering*, *109*(10), 2325-2339.

Chen, Q. (2008). *Effects of thermal loads on Texas steel bridges.* (Doctoral dissertation). Retrieved from ProQuest Dissertations and thesis database. (UMI No. 3320677)

Cheng, T. T. H., & Johnston, D. W. (1985). *Incidence assessment of transverse cracking in concrete bridge decks: Construction and material considerations*. (Report No. FHWA/NC/85-002, 1). Retrieved from http://www.ntis.gov/search/product.aspx?ABBR=PB88118260

Curtis, R. H., & White, H. (2007*). NYSDOT bridge deck task force evaluation of bridge deck cracking on NYSDOT bridges*. New York: New York State Department of Transportation.

Dilger, W. H., Ghali, A., Chan, M., Cheung, M. S., & Maes, M. A. (1983). Temperature stresses in composite box girder bridges. *Journal of Structural Engineering*, *109*(6), 1460-1478.

Duffie, J.A., & Beckman, W.A. (1991*). Solar engineering of thermal process* (2nd ed.). New York: John Wiley & Sons.

Elbadry, M.M., & Ghali, A. (1983). Temperature variations in concrete bridges. *Journal of Structural Engineering, 109*(10), 2355-2374.

Emanuel, J. H., & Hulsey, J. L. (1978). Temperature distributions in composite bridges. *Journal of the Structural Division, 104*(1), 65-78.

Emanuel, J. H., & Taylor, C. M. (1985). Length-Thermal stress relations for composite bridges. *Journal of Structural Engineering, 111*(4), 788-804.

Frosch, R., J. (2007). *Controlling bridge deck cracking in Indiana* (Issue No. 46). Indiana: U. S. Department of Transportation, Federal Highway Administration.

Fu, H. C., Ng, S. F., & Cheung, M. S.(1990). Thermal behavior of composite bridges. *Journal of Structural Engineering, 116*(12), 3302-3323.

Giussani, F. (2009). The effects of temperature variations on the long-term behaviour of composite steel–concrete beams. *Engineering Structures, 31*(10), 2392-2406.

Ibrahim, A. M. (1995). *Three-dimensional thermal analysis of curved concrete box girder bridges* (Master's thesis, Concordia University, Montreal). Retrieved from http://spectrum.library.concordia.ca/95/

Imbsen, R. A., Vandershaf, D. E., Schamber, R. A., & Nutt, R. V. (1985). *Thermal effects in concrete bridge superstructures (NCHRP Report No. 276).* Washington, DC: Transportation Research Board.

Kennedy, J. B., & Soliman, M. H. (1987). Temperature distribution in composite bridges. *Journal of Structural Engineering, 113*(3), 475-482.

Klein, L. E. (2006). *Finite element analysis of a composite bridge deck* (Doctoral dissertation, University of Southern Queensland). Retrieved from http://eprints.usq.edu.au/2477/1/KLEIN_Lindsay_2006.pdf

Kosel, H. C., & Michols, K. A. (1985). *Evaluation of concrete deck cracking for selected bridge deck structures of Ohio Turnpike*. Ohio: Construction Technology Laboratory, Ohio Department of Transportation.

Krauss, P. D., & Rogalla, E. A., (1996). *Transverse cracking in newly constructed bridge decks* (*NCHRP Report No. 380).* Washington, DC: Transportation Research Board.

Moorty, S., & Roeder, C. W. (1992). Temperature-dependent bridge movements. *Journal of Structural Engineering, 118*(4), 1090-1105.

NCDC. (n.d.). *Quality controlled local climatological data*. Retrieved from http://cdo.ncdc.noaa.gov/qclcd/QCLCD?prior=N.

NREL. (n.d.). *National solar radiation database*. Retrieved from http://rredc.nrel.gov/solar/old_data/nsrdb/1991-2010/hourly/siteonthefly.cgi?id=727530.

Noda, N., Hetnarski, R.B., & Tawingawa, Y. (2000). *Thermal stresses* (1st ed.). New York: Taylor & Francis.

PCA, (1970). *Final report – Durability of concrete bridge decks – A cooperative study*. State Highway Departments of California, Illinois, Kansas, Michigan, Minnesota, Missouri, New Jersey, Ohio, Texas, and Virginia: Portland Cement Association.

Ramey, G. E., Wolff, A. R., & Wright, R. L. (1997). Structural design actions to mitigate bridge deck cracking. *Practice Periodical on Structural Design and Construction, 2*(3), 118-124.

Ramey, G. E., & Wright, R. (1994). *Assessing and enhancing the durability/longevity performances of highway bridges (HRC Research*

Project 2-13506). Alabama: Auburn University. Retrieved from http://www.eng.auburn.edu/files/centers/hrc/94-03.pdf

Reynolds, J. C., & Emanuel, J. H. (1974). Thermal stresses and movements in bridges. *Journal of the Structural Division*, *100*(1). 63-79.

Tong, M., Tham, L.G., & Au, F. T. K. (2002). Extreme thermal loading on steel bridges in tropical region. *Journal of Bridge Engineering*, *7*(6), 357-366.

Zuk, W. (1961). Thermal and shrinkage stresses in composite beams. *ACI Journal Proceedings*, *58*(9), 1529-1558.

Appendix A

Environmental Conditions

Table A-1 Hourly Ambient Temperature and Wind Speed for the City of Fargo, ND

	June 4, 2010		December 23, 2010	
Time	Temperature (˚F)	Wind Speed (MPH)	Temperature (˚F)	Wind Speed (MPH)
1	61	10	19	7
2	60	7	18	7
3	57	5	18	8
4	59	3	18	7
5	57	0	18	7
6	59	3	18	7
7	62	8	19	7
8	65	13	19	7
9	69	8	20	6
10	74	13	19	9
11	78	18	21	13
12	79	20	22	13
13	79	20	22	13
14	80	25	23	9
15	80	24	23	9
16	80	23	23	9
17	79	22	24	7
18	76	11	24	8
19	74	10	24	9
20	70	7	23	10
21	67	3	23	9
22	64	5	23	7
23	59	0	24	6
24	58	5	24	7

Table A-2 Hourly Calculated Convection Heat Transfer Coefficient h_c on June 4, 2010

Time	June 4, 2010		
	Top Surface	Soffit Surface	Side Surface
	h_c (Btu/(h ft^2 ˚F))		
1	0.02665	0.02359	0.02543
2	0.02037	0.01731	0.01915
3	0.01618	0.01312	0.01496
4	0.01199	0.00894	0.01077
5	0.00571	0.00265	0.00449
6	0.01199	0.00894	0.01077
7	0.02246	0.01941	0.02124
8	0.03293	0.02988	0.03171
9	0.02246	0.01941	0.02124
10	0.03293	0.02988	0.03171
11	0.04340	0.04035	0.04218
12	0.04759	0.04453	0.04637
13	0.04759	0.04453	0.04637
14	0.05806	0.05500	0.05684
15	0.05597	0.05291	0.05474
16	0.05387	0.05081	0.05265
17	0.05178	0.04872	0.05056
18	0.02874	0.02569	0.02752
19	0.02665	0.02359	0.02543
20	0.02037	0.01731	0.01915
21	0.01199	0.00894	0.01077
22	0.01618	0.01312	0.01496
23	0.00571	0.00265	0.00449
24	0.01618	0.01312	0.01496

Table A-3 Hourly Calculated Convection Heat Transfer Coefficient h_c on December 23, 2010

Time	December 23, 2010		
	Top Surface	Soffit Surface	Side Surface
	h_c (Btu/(h ft^2 ˚F))		
1	0.02037	0.01731	0.01915
2	0.02037	0.01731	0.01915
3	0.02246	0.01941	0.02124
4	0.02037	0.01731	0.01915
5	0.02037	0.01731	0.01915
6	0.02037	0.01731	0.01915
7	0.02037	0.01731	0.01915
8	0.02037	0.01731	0.01915
9	0.01828	0.01522	0.01705
10	0.02456	0.02150	0.02333
11	0.03293	0.02988	0.03171
12	0.03293	0.02988	0.03171
13	0.03293	0.02988	0.03171
14	0.02456	0.02150	0.02333
15	0.02456	0.02150	0.02333
16	0.02456	0.02150	0.02333
17	0.02037	0.01731	0.01915
18	0.02246	0.01941	0.02124
19	0.02456	0.02150	0.02333
20	0.02665	0.02359	0.02543
21	0.02456	0.02150	0.02333
22	0.02037	0.01731	0.01915
23	0.01828	0.01522	0.01705
24	0.02037	0.01731	0.01915

Table A-4 Calculated Total Hourly Solar Radiation I_t on a Bridge Surface on June 4, 2010

Time	June 4, 2010			
	Top Surfaces*	Soffit Surfaces**	Outer Web***	Remaining Webs****
	I_t (Btu/in^2)			
1	0.00000	0.00000	0.00000	0.00000
2	0.00000	0.00000	0.00000	0.00000
3	0.00000	0.00000	0.00000	0.00000
4	0.00000	0.00000	0.00000	0.00000
5	0.00352	0.00106	0.00229	0.00053
6	0.05988	0.02642	0.04315	0.01321
7	0.14791	0.08031	0.08946	0.04015
8	0.40353	0.14441	0.14001	0.07221
9	0.70171	0.20711	0.18721	0.10355
10	0.99929	0.26170	0.22683	0.13085
11	1.26564	0.30326	0.25554	0.15163
12	1.47992	0.32933	0.27385	0.16466
13	1.61554	0.33672	0.27843	0.16836
14	1.66172	0.32545	0.27103	0.16273
15	1.61805	0.29727	0.25166	0.14864
16	1.48056	0.25360	0.22102	0.12680
17	1.25391	0.19760	0.17981	0.09880
18	0.95238	0.13455	0.13243	0.06727
19	0.59510	0.07150	0.08242	0.03575
20	0.21703	0.02043	0.03575	0.01021
21	0.00176	0.00035	0.00106	0.00018
22	0.00000	0.00000	0.00000	0.00000
23	0.00000	0.00000	0.00000	0.00000
24	0.00000	0.00000	0.00000	0.00000

* Top surface of the concrete deck

** Bottom surfaces of the concrete deck and the steel girders

*** The outer web surface (Exterior girder)

**** All the remaining webs except for ***

Table A-5 Calculated Total Hourly Solar Radiation I_t on a Bridge Surface on December 23, 2010

Time	December 23, 2010			
	Top Surfaces*	Soffit Surfaces**	Outer Web***	Remaining Webs****
	I_t (Btu/in^2)			
1	0.00000	0.00000	0.00000	0.00000
2	0.00000	0.00000	0.00000	0.00000
3	0.00000	0.00000	0.00000	0.00000
4	0.00000	0.00000	0.00000	0.00000
5	0.00000	0.00000	0.00000	0.00000
6	0.00000	0.00000	0.00000	0.00000
7	0.00000	0.00000	0.00000	0.00000
8	0.00000	0.00000	0.00000	0.00000
9	0.01409	0.00282	0.00845	0.00141
10	0.04227	0.00845	0.02536	0.00423
11	0.07221	0.01444	0.04332	0.00722
12	0.11447	0.02289	0.06868	0.01145
13	0.12328	0.02466	0.07397	0.01233
14	0.11271	0.02254	0.06763	0.01127
15	0.09686	0.01937	0.05812	0.00969
16	0.04755	0.00951	0.02853	0.00475
17	0.00881	0.00176	0.00528	0.00088
18	0.00000	0.00000	0.00000	0.00000
19	0.00000	0.00000	0.00000	0.00000
20	0.00000	0.00000	0.00000	0.00000
21	0.00000	0.00000	0.00000	0.00000
22	0.00000	0.00000	0.00000	0.00000
23	0.00000	0.00000	0.00000	0.00000
24	0.00000	0.00000	0.00000	0.00000

* Top surface of the concrete deck

** Bottom surfaces of the concrete deck and the steel girders

*** The outer web surface (Exterior girder)

**** All the remaining webs except for ***

Table A-6 Shading Length l_{sh} Calculation on June 4, 2010

	June 4, 2010					
Time	θ_z	θ_a	γ_s	$90+\gamma-\gamma_s$	l_{sh} (in)	$\%I_b$ on Web Side
1.00	-	-	-	-	-	-
2.00	-	-	-	-	-	-
3.00	-	-	-	-	-	-
4.00	-	-	-	-	-	-
5.00	88.50	1.50	57.40	147.40	1.90	0.94
6.00	82.50	7.50	64.70	154.70	12.01	0.64
7.00	73.00	17.00	75.00	165.00	46.07	0.00
8.00	63.00	27.00	85.30	175.30	242.52	0.00
9.00	52.80	37.20	96.40	186.40	-265.57	0.00
10.00	42.80	47.20	109.60	199.60	-125.55	0.00
11.00	33.80	56.20	126.80	216.80	-97.25	0.00
12.00	27.10	62.90	151.00	241.00	-87.14	0.00
13.00	24.70	65.30	182.40	272.40	-84.87	0.00
14.00	27.80	62.20	213.10	303.10	-88.30	0.00
15.00	35.00	55.00	236.10	326.10	-99.86	0.00
16.00	44.20	45.80	252.60	342.60	-134.11	0.00
17.00	54.20	35.80	265.30	355.30	-343.28	0.00
18.00	64.40	25.60	276.30	366.30	170.28	0.00
19.00	74.40	15.60	286.50	376.50	38.34	0.00
20.00	83.80	6.20	296.80	386.80	9.40	0.72
21.00	89.10	0.90	303.40	393.40	1.11	0.97
22.00	-	-	-	-	-	-
23.00	-	-	-	-	-	-
24.00	-	-	-	-	-	-

Table A-7 Shading Length l_{sh} Calculation on December 23, 2010

	December 23, 2010					
Time	θ_z	θ_a	γ_s	$90+\gamma-\gamma_s$	l_{sh} (in)	$\%I_b$ on Web Side
1.00	-	-	-	-	-	-
2.00	-	-	-	-	-	-
3.00	-	-	-	-	-	-
4.00	-	-	-	-	-	-
5.00	-	-	-	-	-	-
6.00	-	-	-	-	-	-
7.00	-	-	-	-	-	-
8.00	-	-	-	-	-	-
9.00	87.10	2.90	129.20	219.20	-3.13	0.00
10.00	80.80	9.20	139.80	229.80	-8.27	0.00
11.00	75.10	14.90	152.50	242.50	-11.70	0.00
12.00	71.60	18.40	166.40	256.40	-13.35	0.00
13.00	70.40	19.60	180.90	270.90	-13.89	0.00
14.00	71.90	18.10	195.30	285.30	-13.22	0.00
15.00	75.70	14.30	209.00	299.00	-11.37	0.00
16.00	81.60	8.40	221.70	311.70	-7.71	0.00
17.00	87.60	2.40	231.50	321.50	-2.63	0.00
18.00	-	-	-	-	-	-
19.00	-	-	-	-	-	-
20.00	-	-	-	-	-	-
21.00	-	-	-	-	-	-
22.00	-	-	-	-	-	-
23.00	-	-	-	-	-	-
24.00	-	-	-	-	-	-

Appendix B

Thermal Profiles

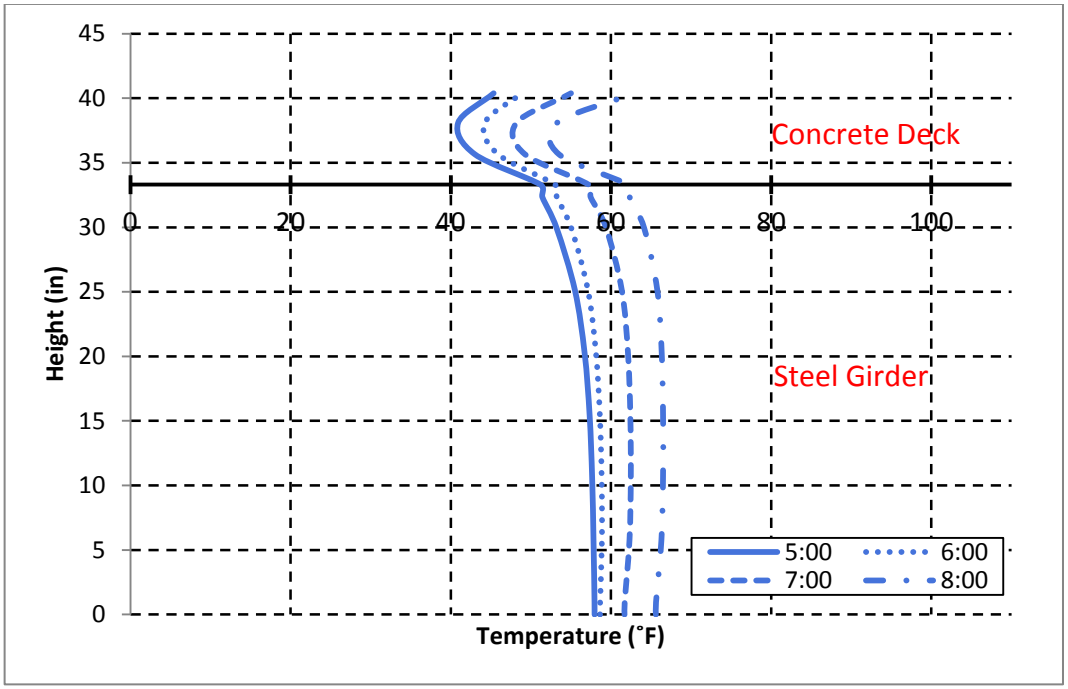

Figure B-1 Vertical Temperature Distribution at Position I (5:00-8:00; June 4, 2010)

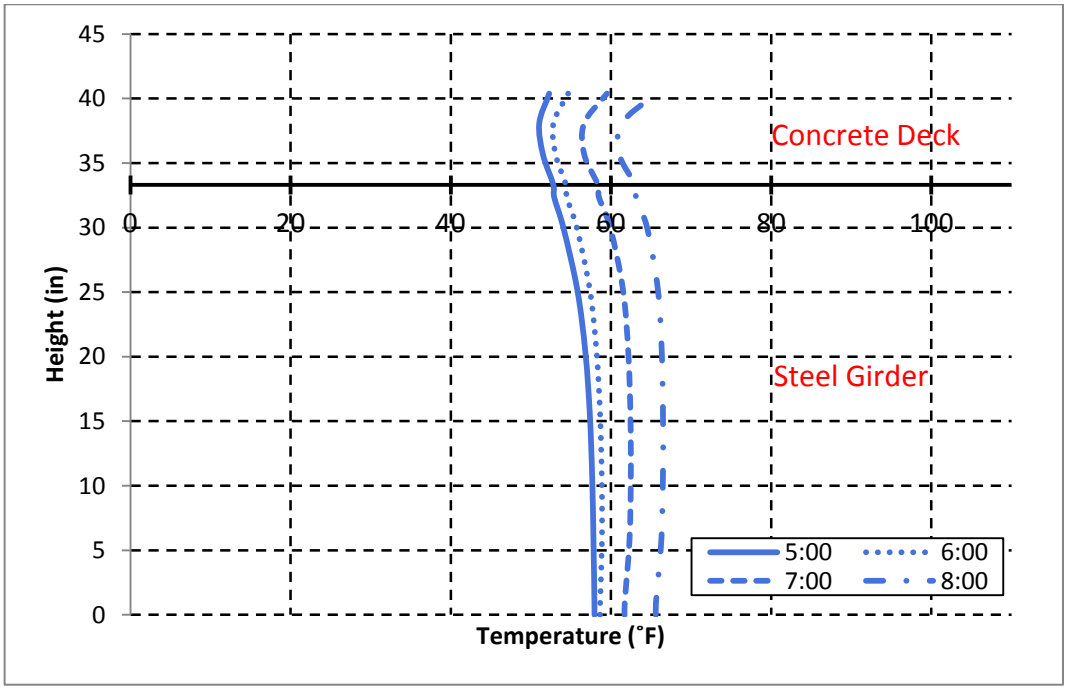

Figure B-2 Vertical Temperature Distribution at Position II (5:00-8:00; June 4, 2010)

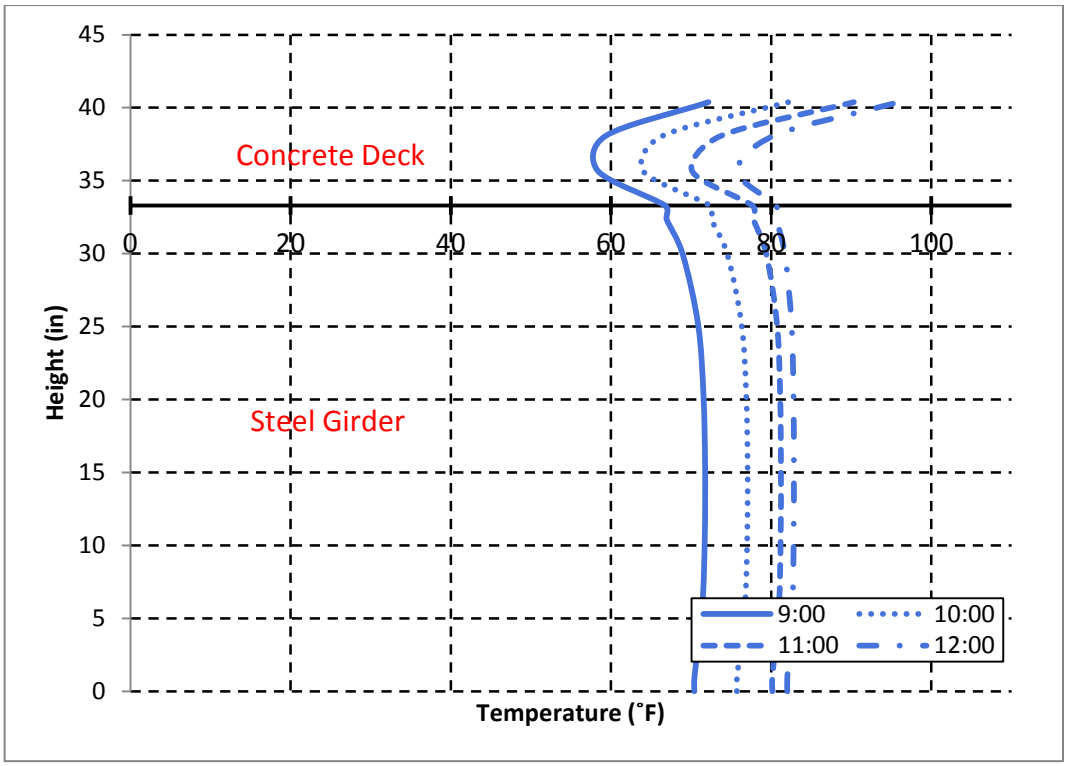

Figure B-3 Vertical Temperature Distribution at Position I (9:00-12:00; June 4, 2010)

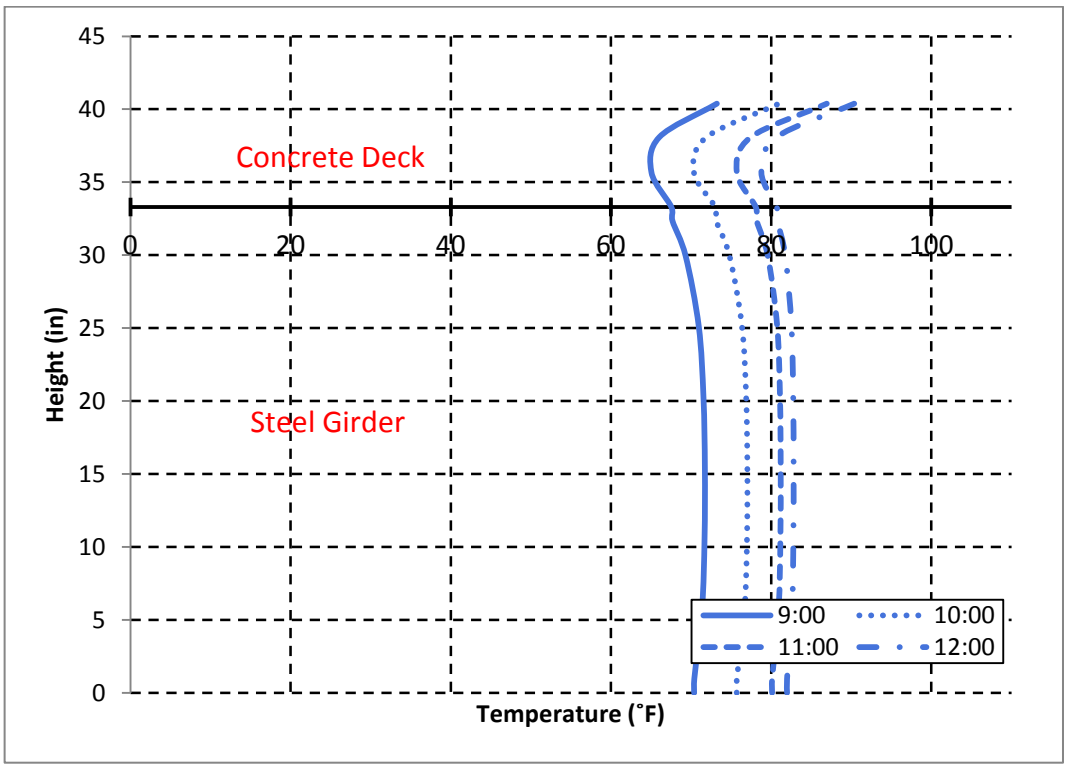

Figure B-4 Vertical Temperature Distribution at Position II (9:00-12:00; June 4, 2010)

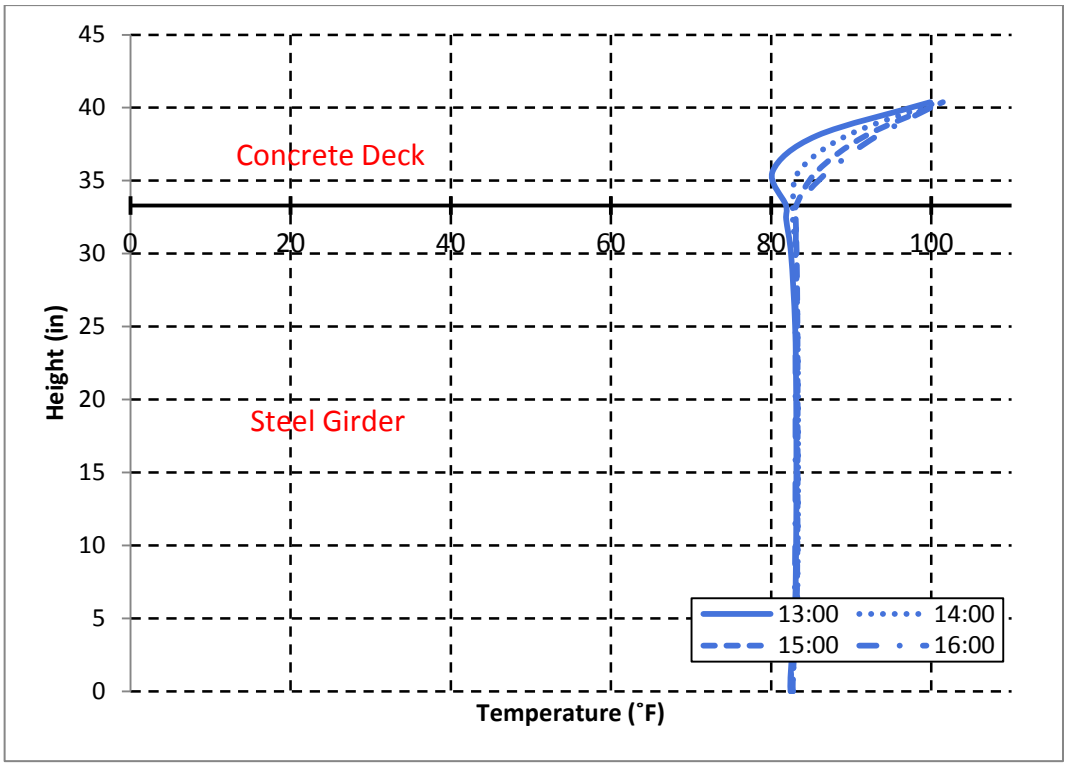

Figure B-5 Vertical Temperature Distribution at Position I (13:00-16:00; June 4, 2010)

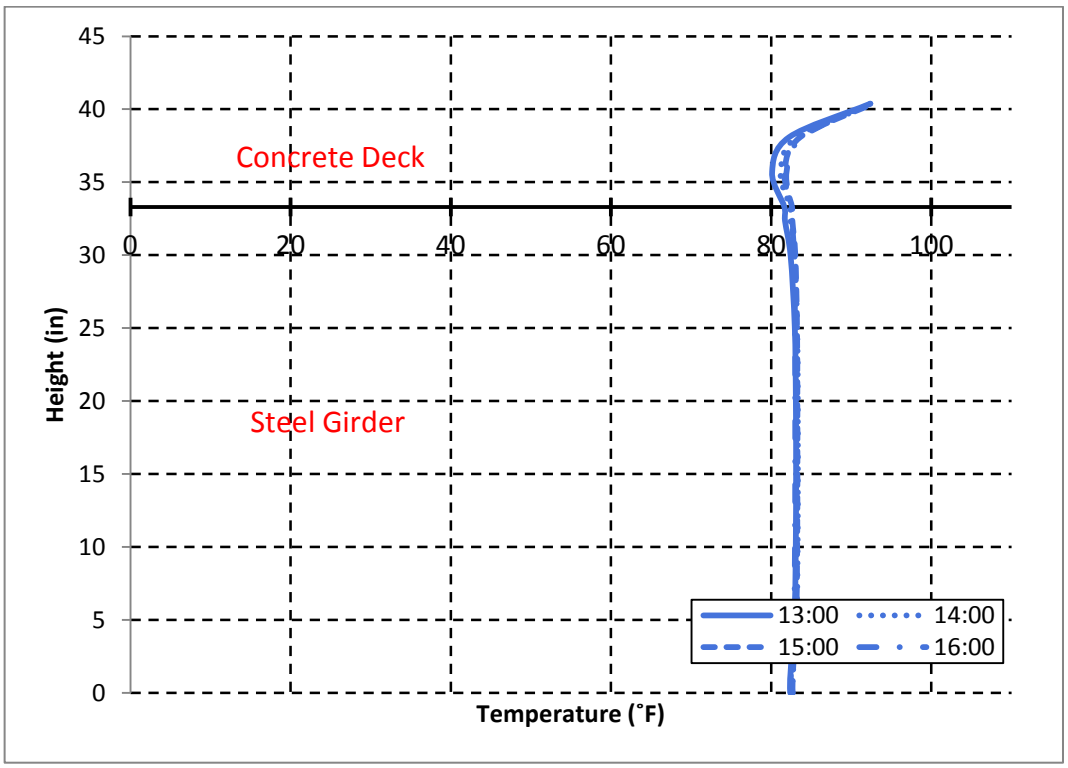

Figure B-6 Vertical Temperature Distribution at Position II (13:00-16:00; June 4, 2010)

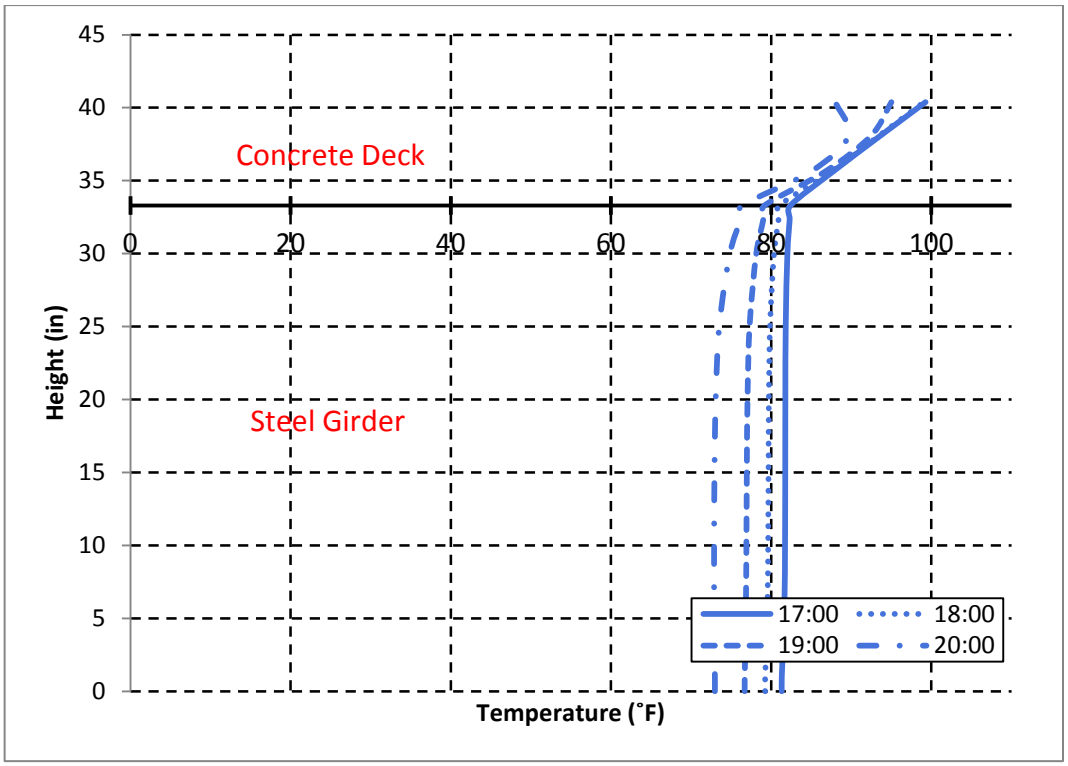

Figure B-7 Vertical Temperature Distribution at Position I (17:00-20:00; June 4, 2010)

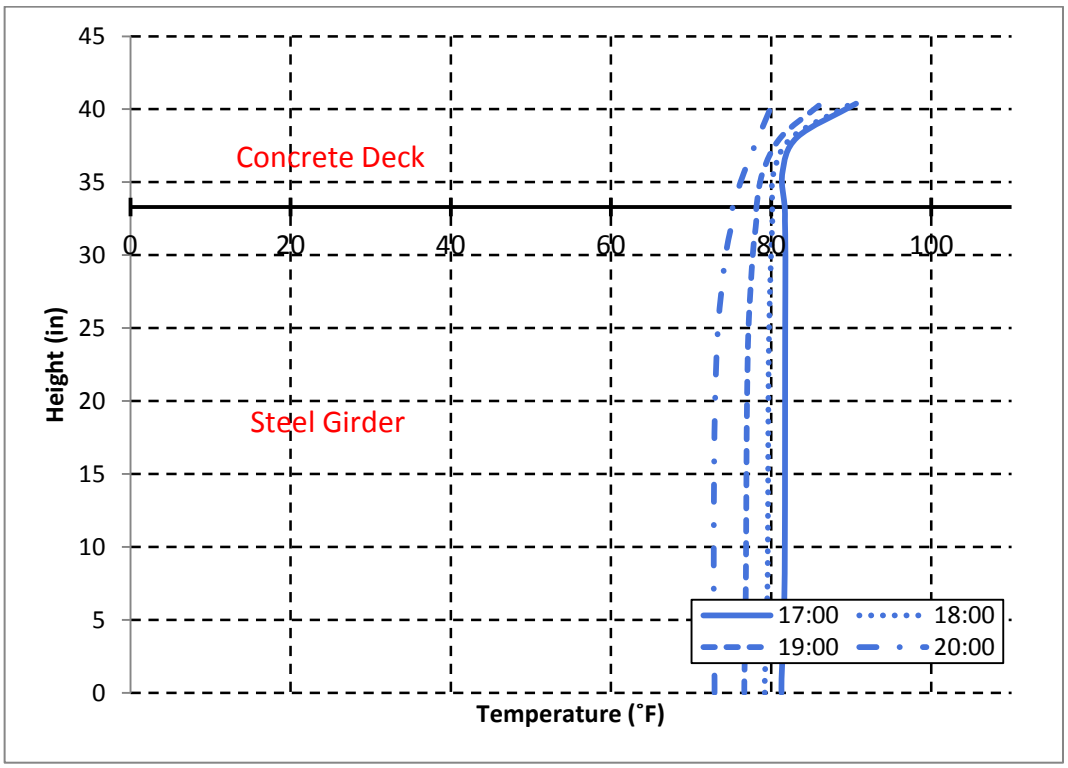

Figure B-8 Vertical Temperature Distribution at Position II (17:00-20:00; June 4, 2010)

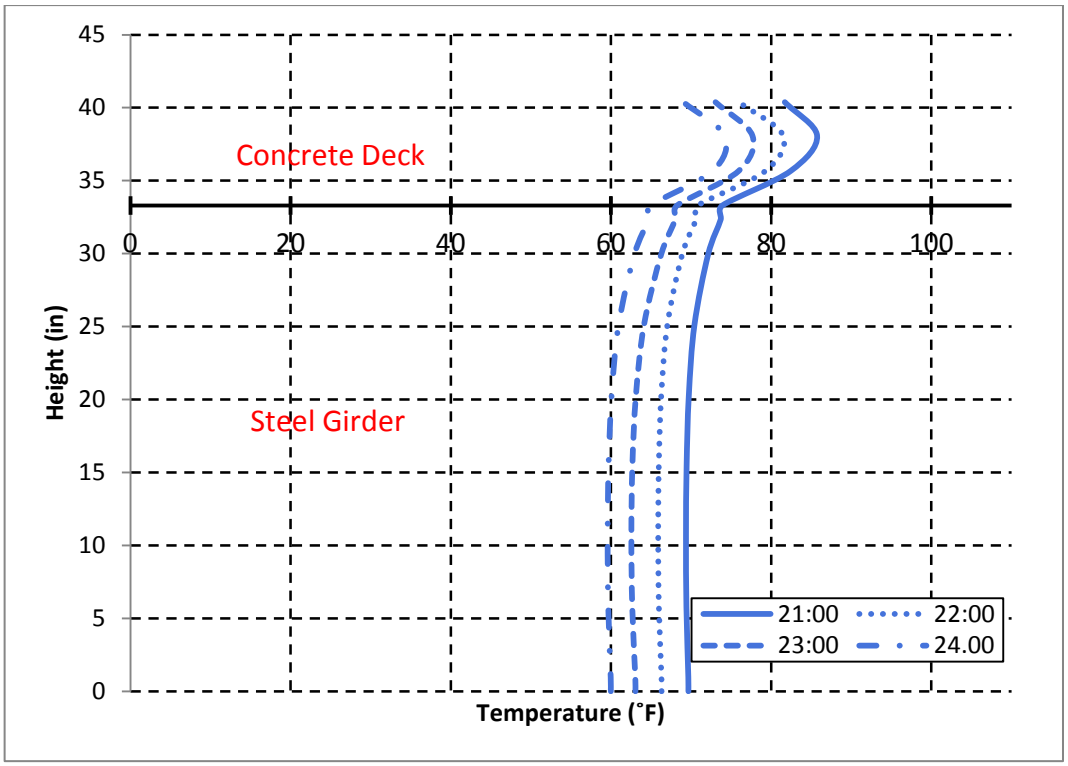

Figure B-9 Vertical Temperature Distribution at Position I (21:00-24:00; June 4, 2010)

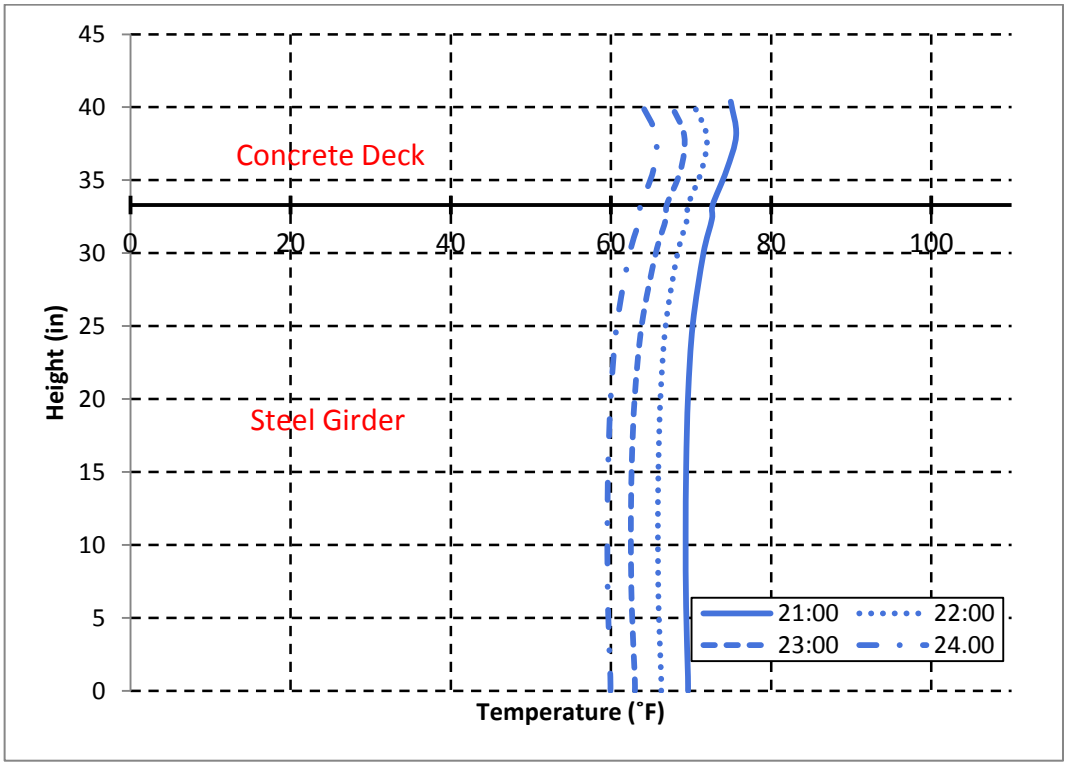

Figure B-10 Vertical Temperature Distribution at Position II (21:00-24:00; June 4, 2010)

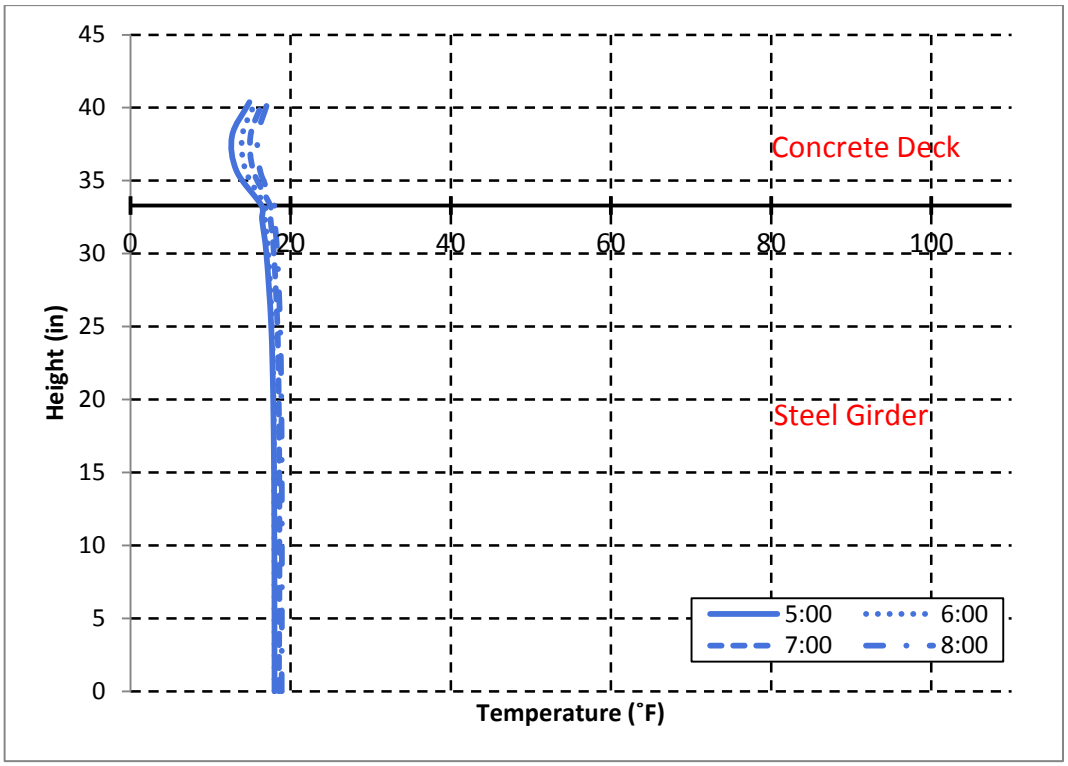

Figure B-11 Vertical Temperature Distribution at Position I (5:00-8:00; December 23, 2010)

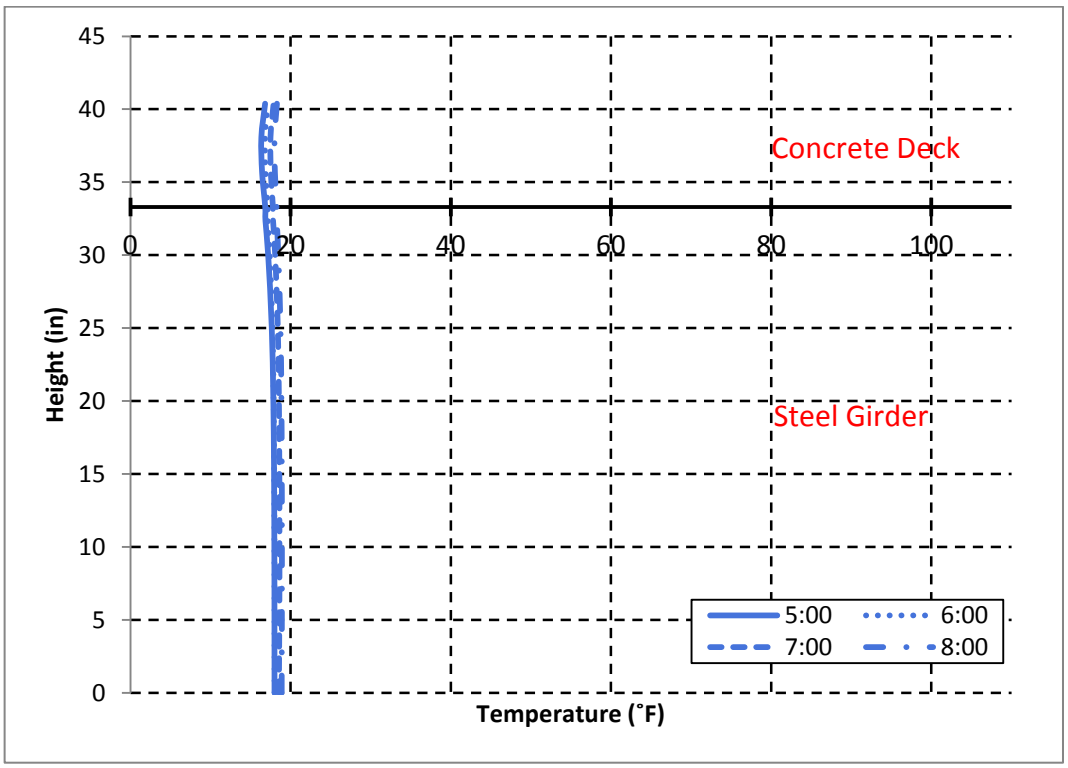

Figure B-12 Vertical Temperature Distribution at Position II (5:00-8:00; December 23, 2010)

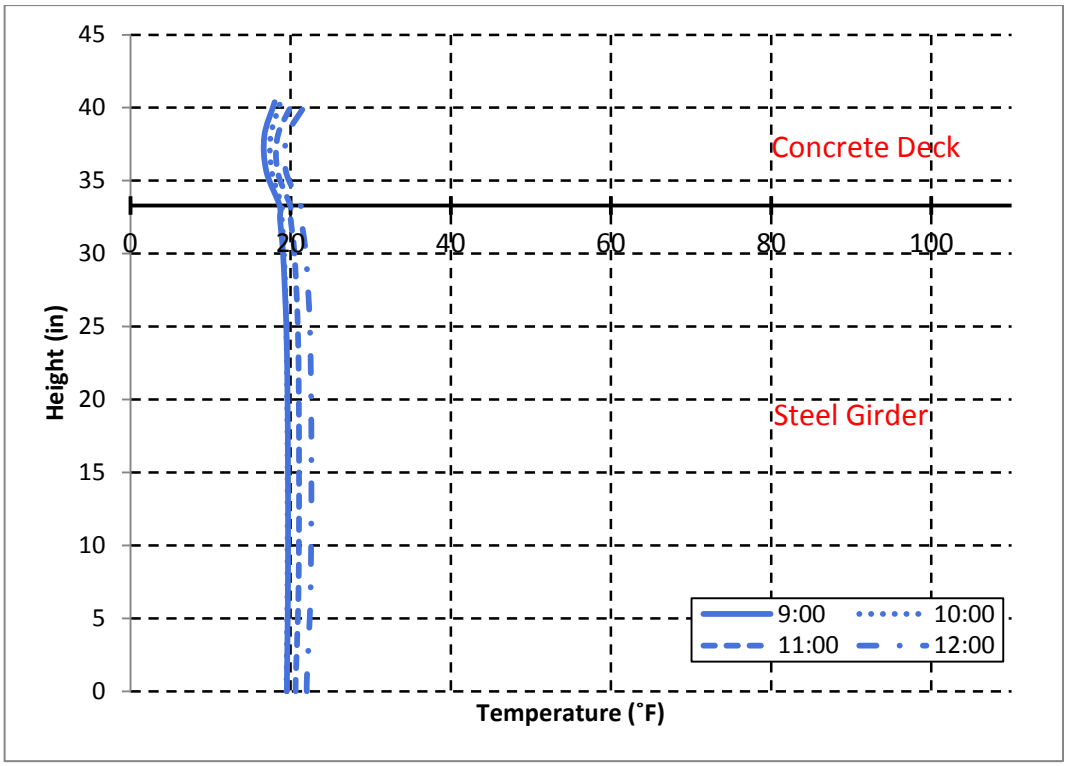

Figure B-13 Vertical Temperature Distribution at Position I (9:00-12:00; December 23, 2010)

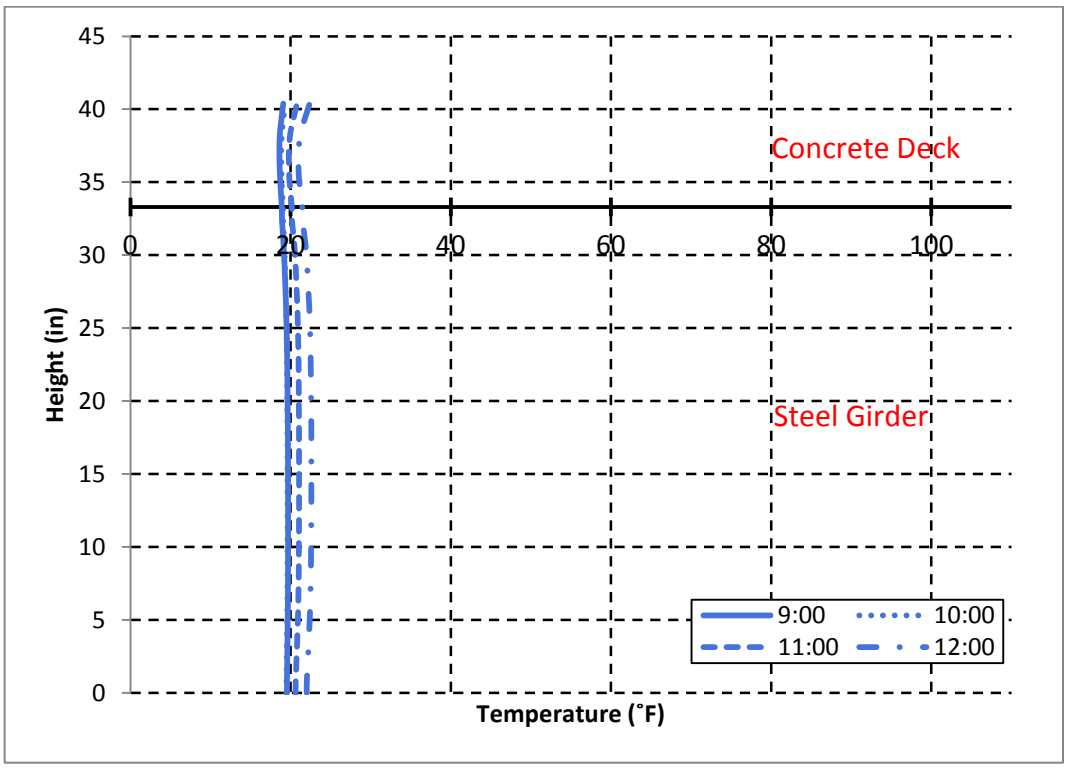

Figure B-14 Vertical Temperature Distribution at Position II (9:00-12:00; December 23, 2010)

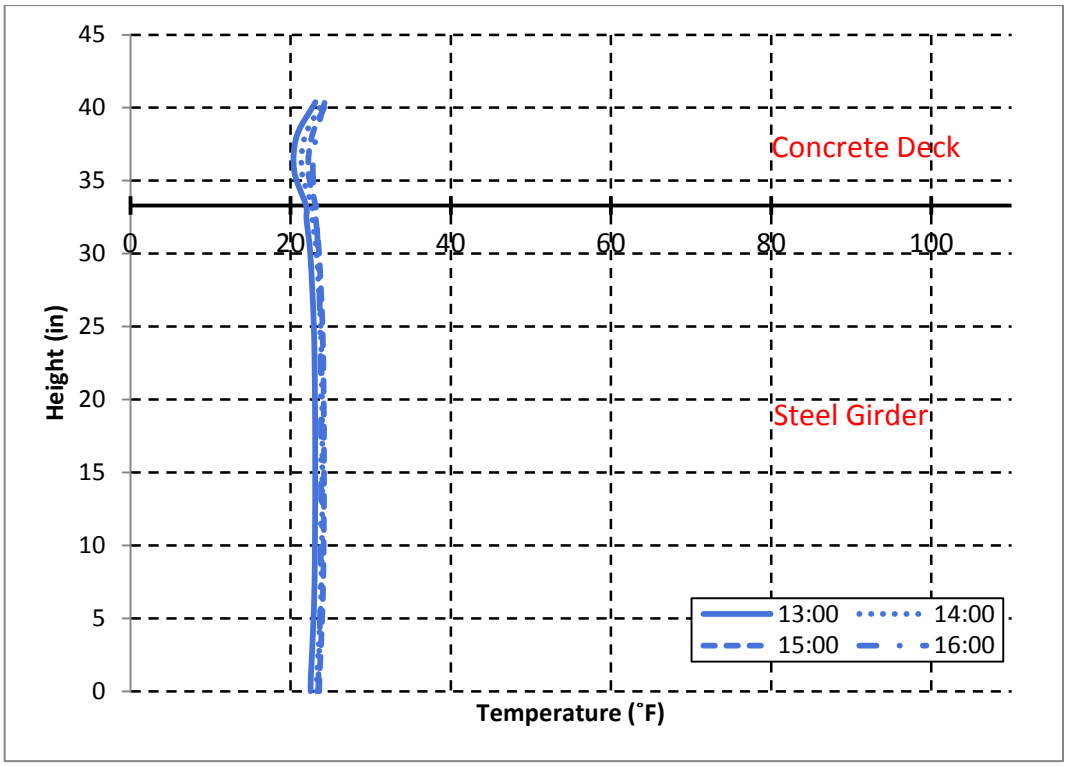

Figure B-15 Vertical Temperature Distribution at Position I (13:00-16:00; December 23, 2010)

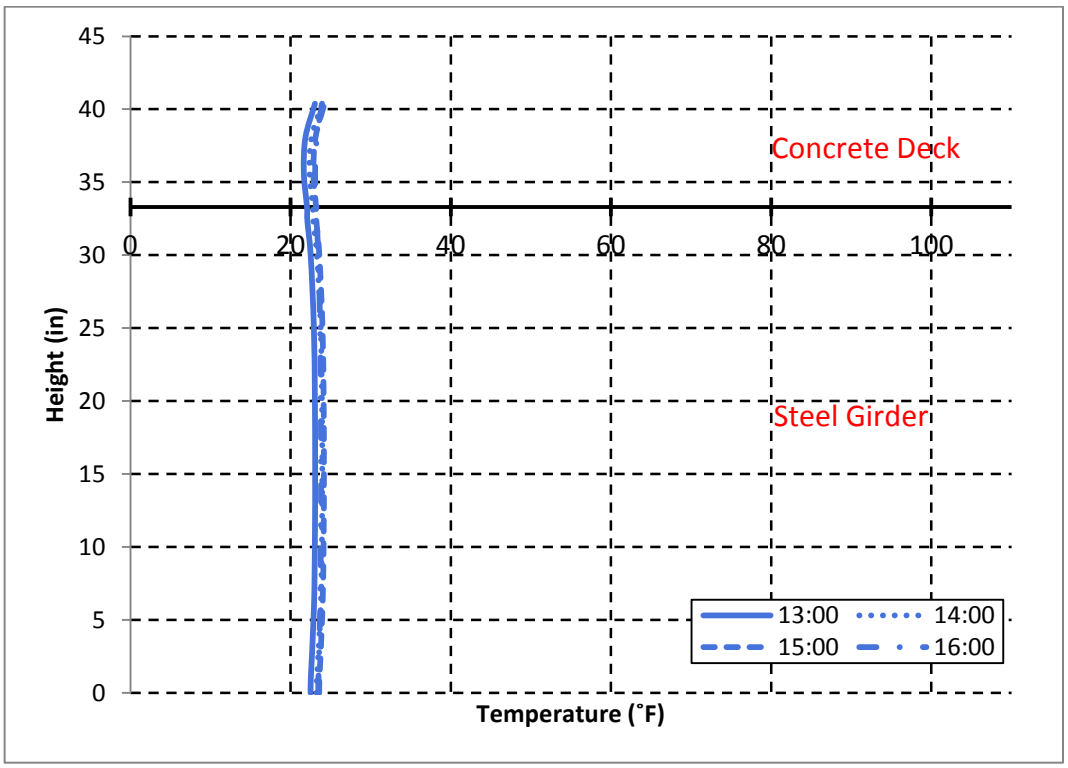

Figure B-16 Vertical Temperature Distribution at Position II (13:00-16:00; December 23, 2010)

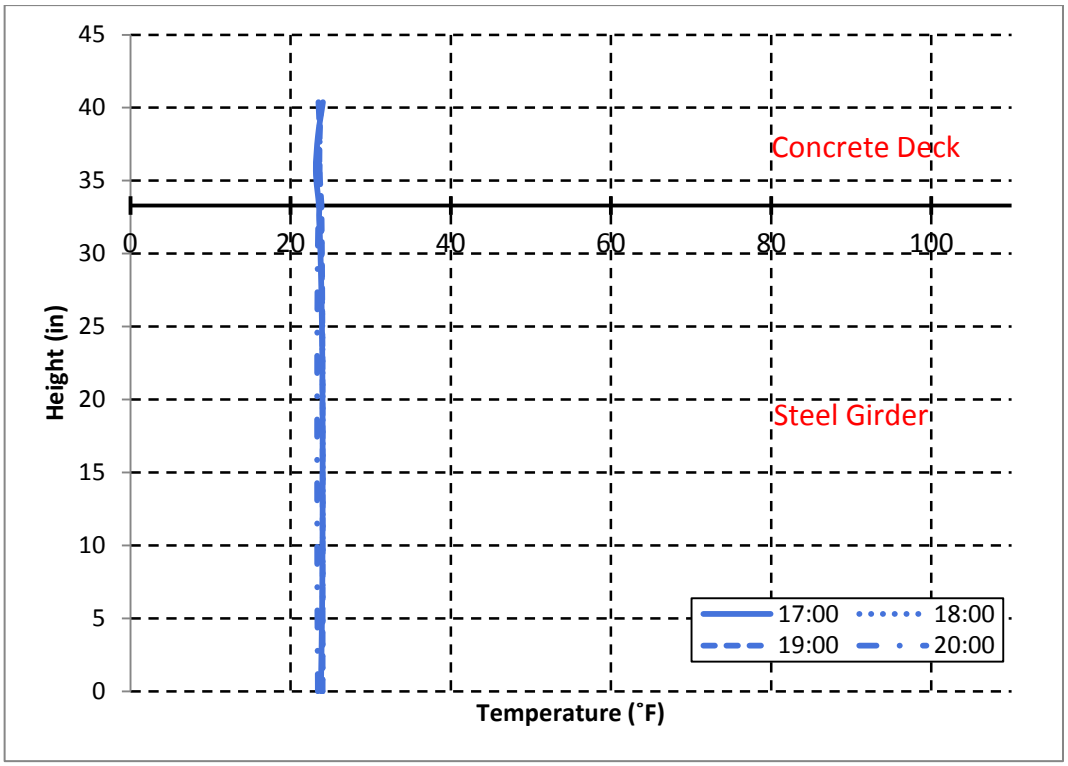

Figure B-17 Vertical Temperature Distribution at Position I (17:00-20:00; December 23, 2010)

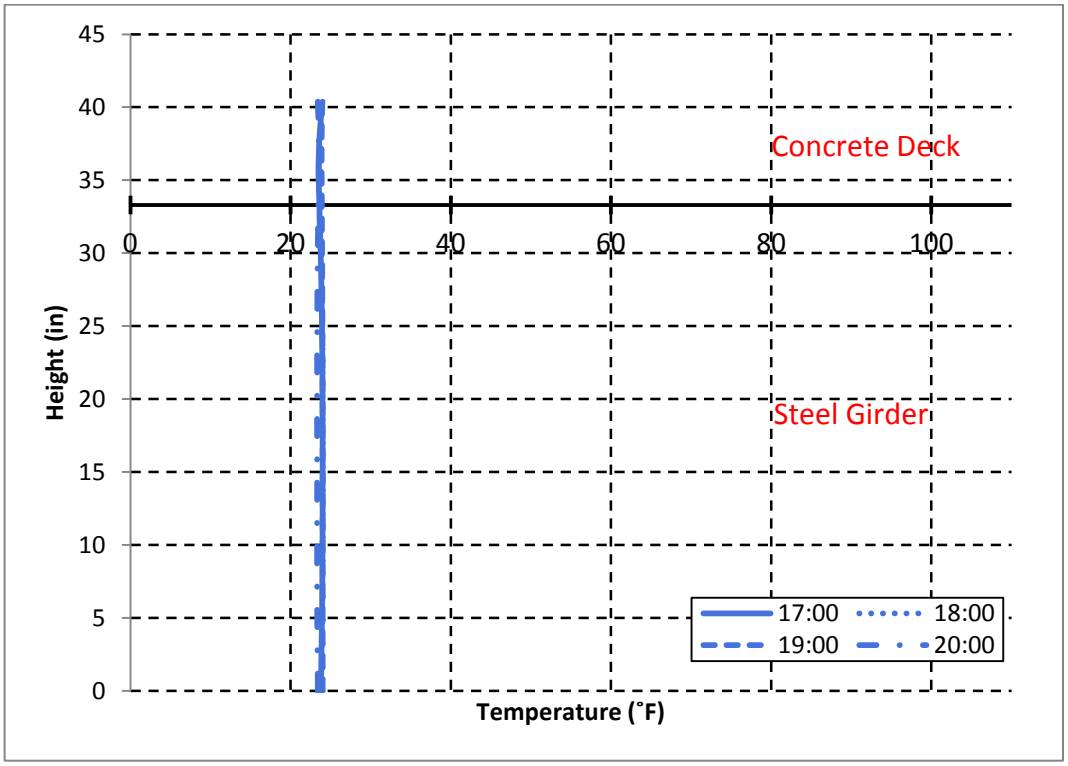

Figure B-18 Vertical Temperature Distribution at Position II (17:00-20:00; December 23, 2010)

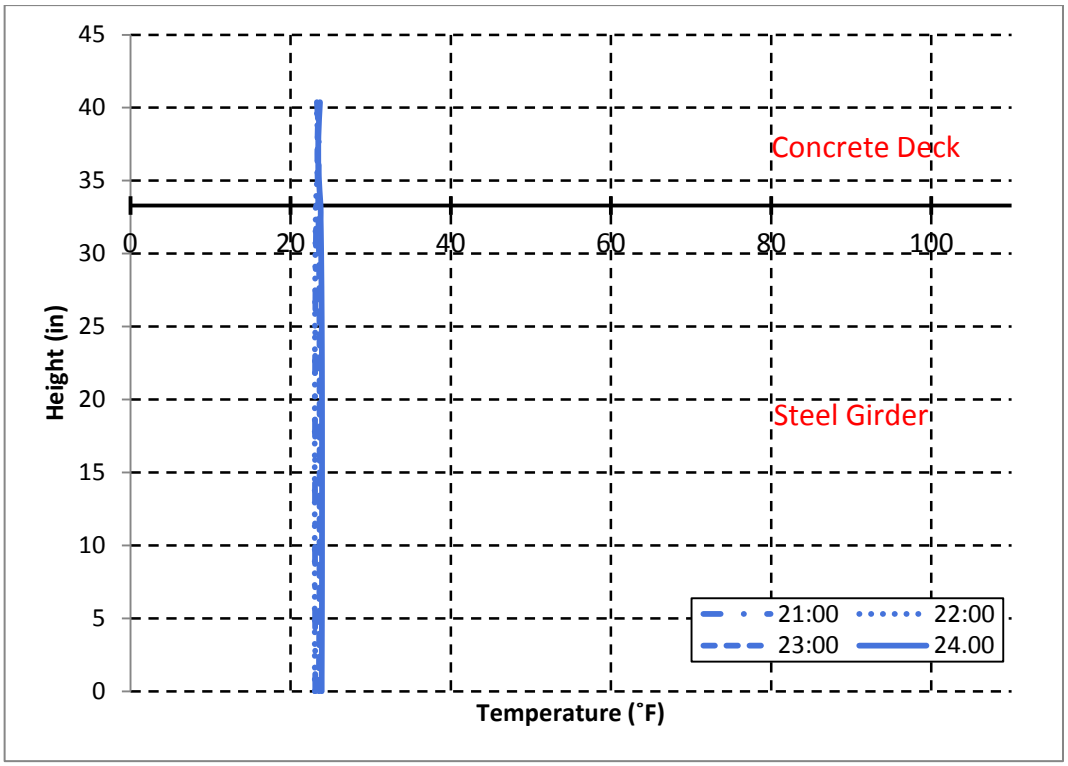

Figure B-19 Vertical Temperature Distribution at Position I (21:00-24:00; December 23, 2010)

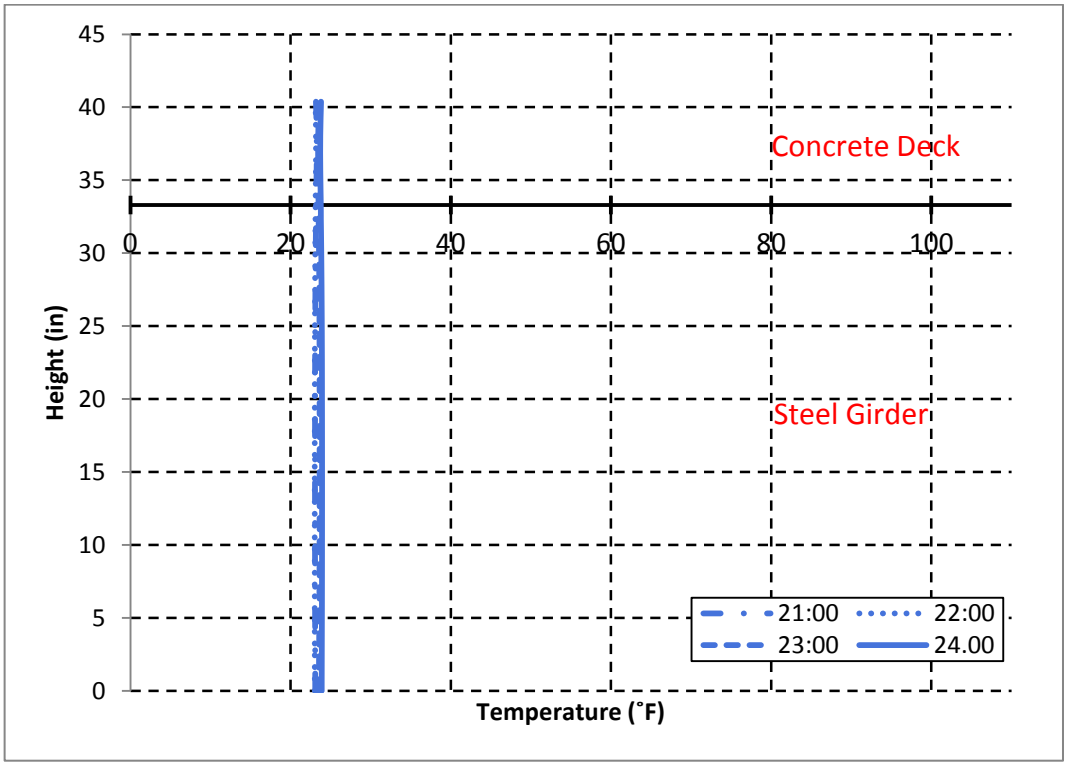

Figure B-20 Vertical Temperature Distribution at Position II (21:00-24:00; December 23, 2010)